General Disclaimer

One or more of the Following Statements may affect this Document

- This document has been reproduced from the best copy furnished by the organizational source. It is being released in the interest of making available as much information as possible.

- This document may contain data, which exceeds the sheet parameters. It was furnished in this condition by the organizational source and is the best copy available.

- This document may contain tone-on-tone or color graphs, charts and/or pictures, which have been reproduced in black and white.

- This document is paginated as submitted by the original source.

- Portions of this document are not fully legible due to the historical nature of some of the material. However, it is the best reproduction available from the original submission.

Produced by the NASA Center for Aerospace Information (CASI)

NASA CR-152467

(NASA-CR-152467) LARGE, HIGH RESOLUTION INTEGRATING TV SENSOR FOR ASTRONOMICAL APPLIATIONS Final Report, 1 Jan. 1975 - 31 Aug. 1976 (Princeton Univ., N.J.) 156 p HC A08/MF A01 CSCL 03A G3/89

N77-22020

Unclas 24405

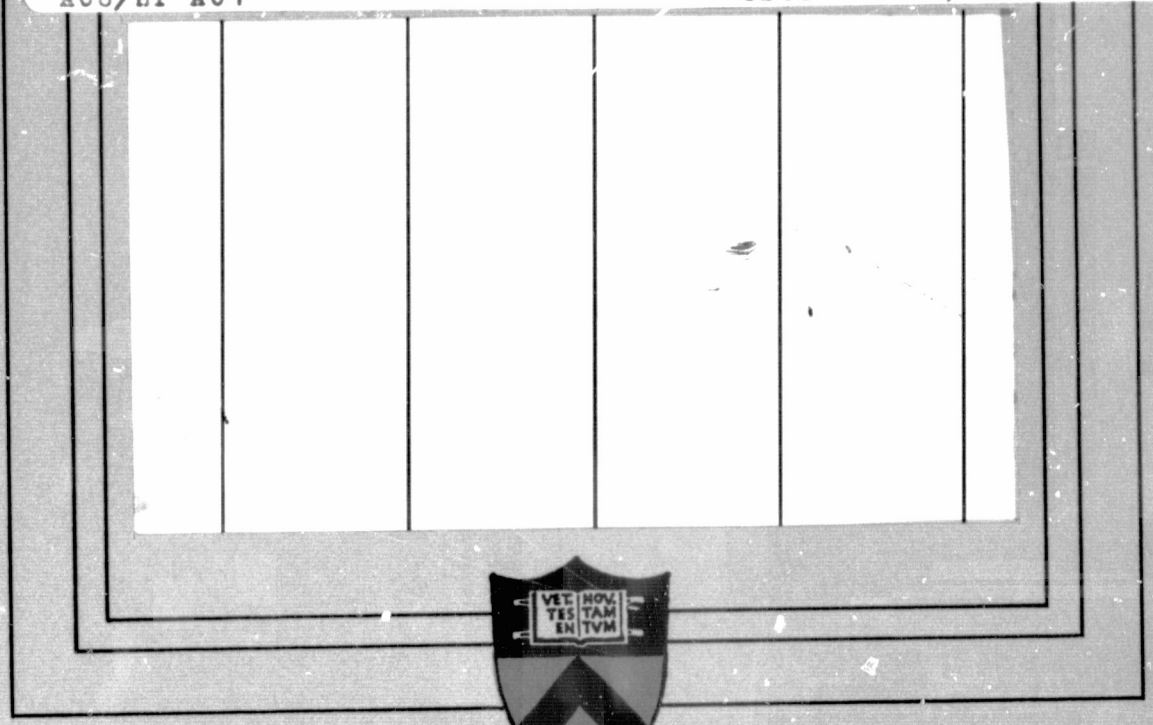

PRINCETON UNIVERSITY

PRINCETON UNIVERSITY
Department of Astrophysical Sciences

FINAL REPORT
NAS5-20833
January 1, 1975 - August 31, 1976

LARGE, HIGH RESOLUTION INTEGRATING TV SENSOR FOR ASTRONOMICAL APPLICATIONS

for

GODDARD SPACE FLIGHT CENTER
Greenbelt, Maryland 20771

January 10, 1977

Principal Investigator
Technical Director

Dr. Lyman Spitzer, Jr.
Mr. John L. Lowrance

OUTLINE OF FINAL REPORT ON CONTRACT NAS5-20833

Section 10 Introduction

20 Description of the 70 mm and 35 mm astronomy SEC tubes.

21 Schematic: Principles of Operation.

22 Typical Operating Conditions,

Mechanical Drawing of 70 mm tube,

Photograph of 70 mm tube.

23 Focus, Deflection, and Alignment Coils.

24 Sequential Operation and the Target Prepare Cycle.

30 70 mm Analog Test Set at Princeton.

Brief description:

Block Diagram.

Photos of head and electronics rack.

40 Characteristics of operable tubes delivered to Princeton.

41 Princeton Tube Census data (PR, window and pc type, condition of target, etc.)

42 MTF performance, on-axis.

43 MTF performance, off-axis.

44 Photometric performance of 35 mm tubes.

50 Problem areas and recommendations of further development.

- 51 Magnetic material in tubes.
- 52 Microphonics during readout.
- 53 Target anti-reflection coatings.
- 54 Target leakage.
- 55 Image section background.

60 Photocathode/window development.

70 Environmental.

80 Permanent Magnet Focus Assembly (PMA).

90 Astronomical Observing.

100 Appendices

- 101 Westinghouse data on gross tube starts, yield of operable tubes, etc.
- 102 Statement of Work, Schedule.
- 103 Referenced Publications.
- 104 Bibliography of Astronomical Papers.
- 105 Environmental tests, Sept. '74.
- 106 Computer Program for Photometric Noise Analysis.
- 107 Photodiode Spectral Response Curves.

Section 10 Introduction

In the mid-60's NASA recognized that televison type sensors would be very useful in space astronomy if they could be made to integrate for long periods of time and provide high spatial resolution and photometric accuracy without excessive sensor cooling. A study completed in 1965 concluded that a magnetically focused SEC tube made by Westinghouse had the best chance of meeting these requirements. This choice was based on the almost indefinite storage capability of the SEC's potassium chloride target which also exhibited a gain of approximately 100 to overcome readout noise.

Through a series of SR&T grants and contracts a magnetically focused SEC tube with a 35 mm (25 x 25 mm) format was developed for scientific photometric applications. This tube was flown in a Princeton sounding rocket ultraviolet echelle spectrograph payload and was used for a number of ground-based astronomical observations (see bibliography). It is currently being used as the data sensor in the Balloon Ultraviolet Stellar Spectrograph, (BUSS), a collaborative program between the Space Research Laboratory at Utrecht, Netherlands and the NASA Johnson Space Center. This 35 mm SEC tube is also the data sensor for the NCAR-High Altitude Observatory's Coronograph/Polarimeter for the Solar Maximum Mission satellite.

Anticipating the Space Telescope requirements, a 70 mm version of this tube was designed. This is the final report on the most recent contract to develop this tube to meet the ST f/24 Camera requirements, (NAS5-20833). In addition to providing an interim report on the status of the 70 mm SEC tube development, this report is being written in an effort to familiarize the reader with the SEC tube and its scientific application.

The ST f/24 camera requirements as determined by the Instrument Definition Team are given in Table I.

TABLE I

f/24 Field Camera Performance Requirements

Angular field-of-view	3 min x 3 min
Angular resolution	0.2 sec
Positional accuracy within FOV	1.0 sec rms
Stability of line-of-sight	± 0.03 sec
Overall wavelength range	115 nm - 800 nm
Spectral resolution	$5 < \lambda/\Delta\lambda < 100$ (21 filters)
Photometric dynamic range (overall)	(m_v 1.5 to m_v 23)/sec^2
Photometric dynamic range (per observation)	100
Minimum detectable energy	m_v 23/sec^2
Exposure time	10 ms - 1 hour (continuous)
Calibration stability	1% (Tungsten, Hydrogen)
Detector	
- format	2000 x 2000 pixels
- pixel size	25 x 25 microns
- dynamic range	100:1
- spatial frequency response	50% at 0.5 cycle/pixel (20 cycles/mm)
- capacity	1600 photoelectrons/pixel
- photometric reproducibility	1%
- photometric accuracy	2%

The 70 mm format tube does provide for 2000 x 2000 pixels that are 25 microns square as determined by the scan line spacing and video bandwidth. As discussed later in this report, photometric measurements made with the 35 mm SEC tubes show a dynamic range of at least 100 to 1, with a capacity of 1600 photoelectrons per 625 micron^2 pixel. The photometric reproducibility is better than 1%. The photometric accuracy in single exposures is approximately 4% in 50 x 50 micron size pixels and improves with stacking of multiple exposures. During the contract for continuing the development we expect to demonstrate equally good photometric performance with the 70 mm format SEC tube. The resolution of the 70 mm tube meets the criteria of 50% response at 20 cycles/mm in the central region of the format, and with the removal of the remaining magnetic parts presently used in the tube's fabrication we expect to achieve this spatial frequency response over almost all of the format. Figure 101 is a picture made with the 70 mm SEC tube.

The ST f/24 Camera has one requirement that is new relative to the 35 mm SEC tube that was developed. It must be sensitive in the red as well as the ultraviolet and visible spectrum. And this broad sensitivity must be achieved while still maintaining the tube background at a low level. Some red sensitive 35 mm tubes have been made with low background. However, the yield was quite low and the S-20 photocathodes on glass windows were not sensitive in the ultraviolet.

We have some encouraging interim results on this aspect of the program which are discussed in this report, but the problem is not yet solved. It may be necessary to choose between red and u.v. sensitivity and also tradeoff red sensitivity for low background.

Results of environmental tests of the 70 mm SEC tube are very encouraging and we anticipate no substantative problems in utilizing it in a flight camera system that will meet the Space Shuttle launch demands.

REPRODUCIBILITY OF THE
ORIGINAL PAGE IS POOR

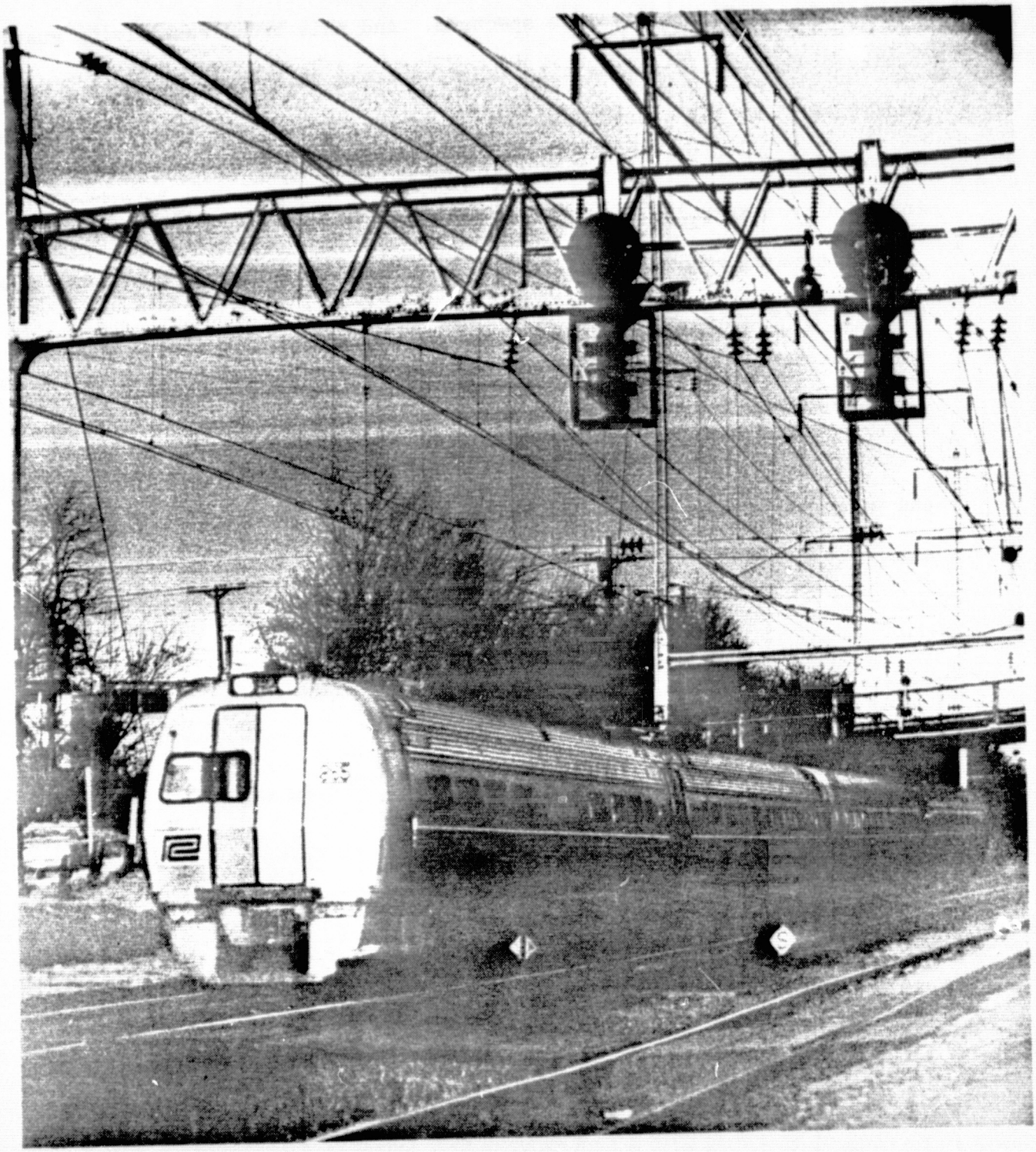

Figure 101

Section 21 SEC Tube Principles of Operation

The SEC type television camera tube has been described in detail in the literature.[1,2] It is similar to the earlier television camera tubes such as the Image Orthicon in its exposure mechanism and to the Vidicon in its readout mechanism.[3] The electron bombarded silicon target tubes (EBS) also referred to as SIT tubes, are similar in their principle of operation to the SEC tube.

Referring to Figure 211, photons are absorbed in a photocathode which is evaporated on the vacuum side of the window; in this case, magnesium fluoride. Photoelectrons emitted from the photocathode are accelerated by an 8000 volt electrostatic field, striking the target, also shown in Figure 211. An axial 80 gauss magnetic field focuses the photoelectrons at the target in one Larmor loop. A small percentage of the photoelectrons are backscattered or absorbed in the Al_2O_3 supporting substrate and the aluminum signal plate. After losing approximately 2000 volts getting through the Al_2O_3 and Al layers, the photoelectrons pass into the low density, (~ 1%), potassium chloride layer. Here they lose a large fraction of their energy creating secondary electrons, then passing through the KCl layer into the vacuum and strike the mesh or gun electrodes. The vacuum side of the low density KCl layer is polarized negatively with respect to the conductive signal plate by scanning it with a low energy electron beam and applying a positive potential to the signal plate. The secondary electrons move to the signal plate leaving a positive charge near the vacuum side of the KCl layer. This results in a charge pattern on the target that is the analog of the integrated optical image on the photocathode.

The electronic image is read out by scanning the target with a finely focused low energy electron beam. Electrons are deposited on the target as the KCl is restored by the scanning beam to a uniform voltage potential over

its surface. The electron signal flowing to the signal plate during readout is about 50 times the integrated photoelectron input to the target due to the multiplying action of the secondary emission process within the KCl layer. This "video" signal is amplified by a low noise amplifier. In this particular SEC tube the vacuum surface of the KCl is coated with a very thin layer of gold evaporated at a shallow angle to the surface. This layer serves to reduce any secondary emission from the electron beam scanning of the KCl during read-out, a source of trouble in the past and the reason for inserting a mesh very near the target called the suppressor mesh in the standard SEC tube. The suppresser mesh has the undesirable effect of lowering the voltage gradient near the target. This allows more scatter of the electron beam at the target and subsequently a reduction in resolution. This is the primary reason it was eliminated for this tube. Its closeness to the target also results in a high capacitance between the target and mesh, both of which vibrate causing a microphonic signal to be superimposed on the video signal. There were also problems of the target and mesh touching during severe vibration thereby causing physical damage to the KCl surface of the target.

In going to the gold coating one does pay a small price in that the target gain is reduced. This is probably a reduction in the transmission secondary emission (TSE) gain of the KCl layer.

The SEC target is a thin membrane of low thermal mass and very low lateral conductivity. It is subject to rupture during shock and vibration, burning of the surface from extremely strong inputs to the photocathode, and holes being made by small particles hitting the target. It is also susceptible to electrical breakdown across the layer if the vacuum surface is driven to a high voltage by secondary emission.

As discussed later in this report the 70 mm SEC target appears capable

of surviving the ST launch intact.

In the Apollo lunar mission a SEC camera was pointed at the sun, burning the target. We have never had this problem in the laboratory or in ground-based observing. We anticipate no problem in the ST application under normal usage. The f/24 camera will have a mechanical shutter and the television camera high voltage can be turned off.

Electrical damage is prevented by shifting the potential of the field mesh to near the target potential during exposure so that an excessive exposure cannot drive the target to a high potential by transmission secondary emission. During readout the field mesh is at a high voltage relative to the target but the gold coating retards secondary emission plus the electron beam only scans the surface once. Then the target is prepared for the next exposure, (see section 2.6). This avoids the runaway condition that can occur in continuous readout where the electron beam knocks off more secondary electrons than it deposits. This leaves the target more positive and on the next scan it repeats the process driving the KCl surface to an even higher potential The KCl eventually reaches the potential of the mesh under these circumstances, and breakdown may occur through the KCl. Fortunately this doesn't happen in sequential operation and is very unlikely in continuous operation with the gold coated targets.

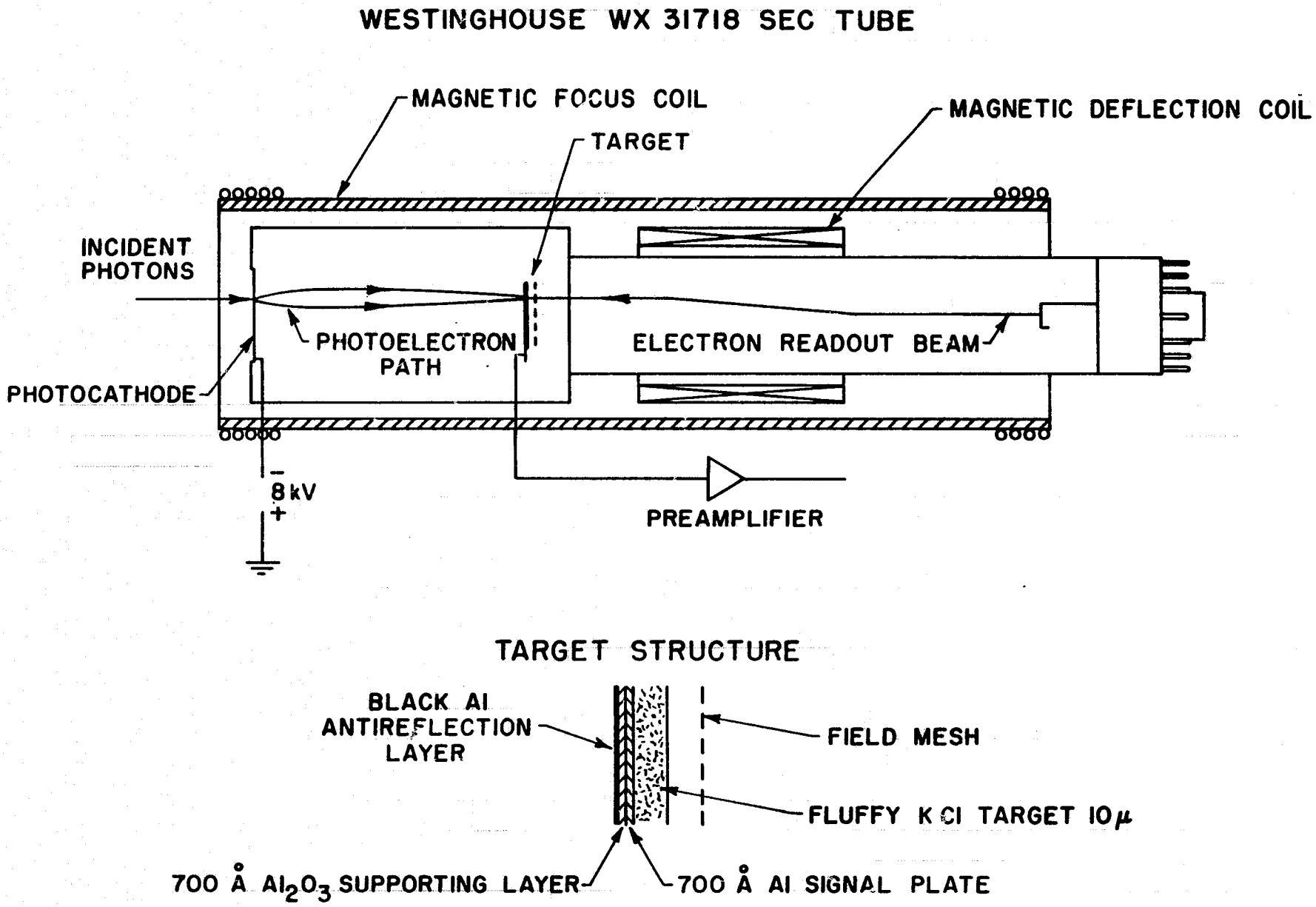
WESTINGHOUSE WX 31718 SEC TUBE
MAGNETIC FOCUS COIL
TARGET
MAGNETIC DEFLECTION COIL
INCIDENT PHOTONS
PHOTOELECTRON PATH
ELECTRON READOUT BEAM
PHOTOCATHODE
8 kV
PREAMPLIFIER
TARGET STRUCTURE
BLACK Al ANTIREFLECTION LAYER
FIELD MESH
FLUFFY KCl TARGET 10μ
700 Å Al_2O_3 SUPPORTING LAYER
700 Å Al SIGNAL PLATE

Figure 211

Section 22 Typical Operating Conditions

For the most demanding photometric applications, it is necessary to operate the SEC tubes in a slow scan readout mode. The reason for this is that the noise contributed by a preamplifier that is optimized for the best noise performance decreases as the scan rate is decreased. That is, the longer the preamplifier is allowed to examine the readout charge from each pixel the more accurate the charge measurement will be.

This noise reduction as the scan rate is reduced does not continue indefinitely. Below about 20 kHz analog bandwidth (25 microsecond pixel sample times) there is no further improvement (at least with present amplifiers and SEC tubes) and the noise performance actually degrades at still slower readout rates. In effect, there is a broad valley of optimum pixel readout times ranging from 50 to 5 microseconds per pixel.

The present Princeton equipment for SEC tube testing and for astronomical observing with SEC's, operates at a pixel readout period of 14 microseconds per pixel for an analog data bandwidth of 36 kHz. It requires 68 seconds to readout a 70 mm SEC target at that scan rate. In order to expedite tube and equipment adjustments a fast scan mode of one microsecond per pixel (500 kHz analog bandwidth) is also used, although the threshold performance is degraded by the less than optimum preamplifier noise performance at the fast scan rate. However the ability to examine the image on a slow scan monitor at the fast 5 second per frame rate, plus the once every 5 seconds opportunity to view the effect of such iterative adjustments as optical and image section focus, make the fast scan mode a very important feature which should be included in some form in any slow scan SEC tube equipment.

Tables 221 and 222 are actual slow scan operating conditions for some 35 mm and 70 mm SEC tubes of recent design. These tables not only show the

typical electrical parameters to be expected, but also show the range and variability one is liable to encounter. Bear in mind, however, that the SEC tube design is still evolving, and future tubes may differ in some ways from the patterns suggested in these tables.

Figure 221 is a cross-sectional drawing of the 70 mm tube as of June '76. Figure 222 is a photograph of an earlier but comparable 70 mm SEC tube.

Serial No.	PUO Tube	IG2 μ A	G 1 -V	Wall V	Mesh V	PC -V	A1 mA	A2 mA	T_{V^P}	T_{V^N}	$T_{V^{RO}}$	I_{A^F}	I_{mA^H}	Logbook
74-26-790	46	48.3	80.8	523.0	558.0	7450	+14.8	+9.91	13.9	15.0	15.2	0.9998	163	L6-193
74-35-375	47	40.	111	508.3	520.0	7250	+56.3	+20.	14.1	15.0	15.3	1.0001	153	L6-33
74-30-267	48													
75-05-264	49													
75-09-440	50	11.8	107	308.5*	335.9*	4150	+23.	0		14.9		0.7694*	159	L6-57,58
75-13-816	51	1.69	113	519.1	557.3	7150	+14.	+9.99	10.9	12.0	12.2	1.0001	154	L6-67
75-26-999	52	2.42	112	522.0	557	7075	+46.	+18.	13.9	15.0	15.1	0.9996	154	L6-107
75-26-001	53	70.8	60.1	334.2	359.3	7250	+45.	+17.6		15.0		0.9996	156	L6-109
75-39-002	54	16.6	60.9	516.9	559.7	7150	+13.	+9.95	10.8	11.9	12.1	0.9999	166	L6-161
75-44-440	55	2.	93.4	519.0	557.9	7150	+13.	+10.1		12.0		0.9997	165	L6-178
75-48-912	56	3.25	111	510.7	558.0	7450	+16.	+10.		14.8		1.0003	164	L6-201
76-04-820	57	11.2	50.5	532.9	558.0	6850	+43.	+30.	8.96	10.1	10.3	0.9999	158	L7-H.Y.Chiu
76-13-460	58													
76-13-780	59													
76-17-161	60													

I_F usually fixed at 1.0000 Amperes for 80.0 Gauss.

*Tube 50 operated at 62 Gauss because of PC voltage limitation.
Refer to Table 223 for caption definition

TABLE 221 35 mm . SEC PRINCETON OPERATING DATA

Serial No.	PUO Tube	IG2 μA	G1 -V	Wall V	Mesh V	PC -V	A1 mA	A2 mA	T_P V	T_N V	T_{RO} V	I_F A	I_H A	Logbook
72-22-220	101	80.0	68.0	338.5	605.0	8500	+6.60	-15.0		15.0		0.2420	134	L5-13
72-48-036	102	300.0	22.5	293.0	600.0	7900	-7.65	-12.4		15.0		0.2415	133	L5-14
73-30-653	103	280.	42.0	492.0	500.0	7200	+9.96	-9.45	9.00	10.0	10.3	0.7300	147	L5-25
73-30-650	104													
73-52-714	105													
74-39-995	106	62.0	78.7	495.4	530.4	7646	-15.0	-23.6		10.0		0.7164	159	L5-99
75-18-200	107	50.0	105.0	493.5	530.0	6100	+23.7	-19.4		12.0		0.7163	162	L5-127
75-22-722	108	46.0	76.7	495.1	530.4	6700	-25.1	-21.1		10.0		0.7162	164	L5-116

Notes: 1) Tubes 101 & 102: older focus coil; 80 Gauss.
2) Present test set focus coil.
3) Tubes 101-103, 106 & 107: absolute value of PC voltage in doubt.
4) Refer to Table 223 for caption definition.

TABLE 222 70 mm SEC PRINCETON OPERATING DATA

TABLE 223

Caption Legend for Tables 221 and 222

IG2 (μA)	Total electron gun emission less the minute fraction that forms the scanning beam. Measured in microamperes.
G1 (-V)	The electron gun control grid potential. Measured in minus Volts.
Wall (V)	The beam focus electrode potential. Measured in Volts.
Mesh (V)	The field mesh potential. Measured in Volts.
PC (-V)	Photocathode potential. Measured in minus Volts.
A1 (mA)	Alignment coil one current. Measured in milliamperes.
A2 (mA)	Alignment coil two current. Measured in milliamperes.
T_P (V)	Target bias potential during first phase of the prepare cycle. Measured in Volts.
T_N (V)	Target bias potential during expose and continuous scan modes. Measured in Volts.
T_{RO}(V)	Target bias potential during readout. Measured in Volts.
I_F (A)	Focus coil current. Measured in Amperes.
I_H (mA)	Electron gun heater current. Measured in milliamperes.

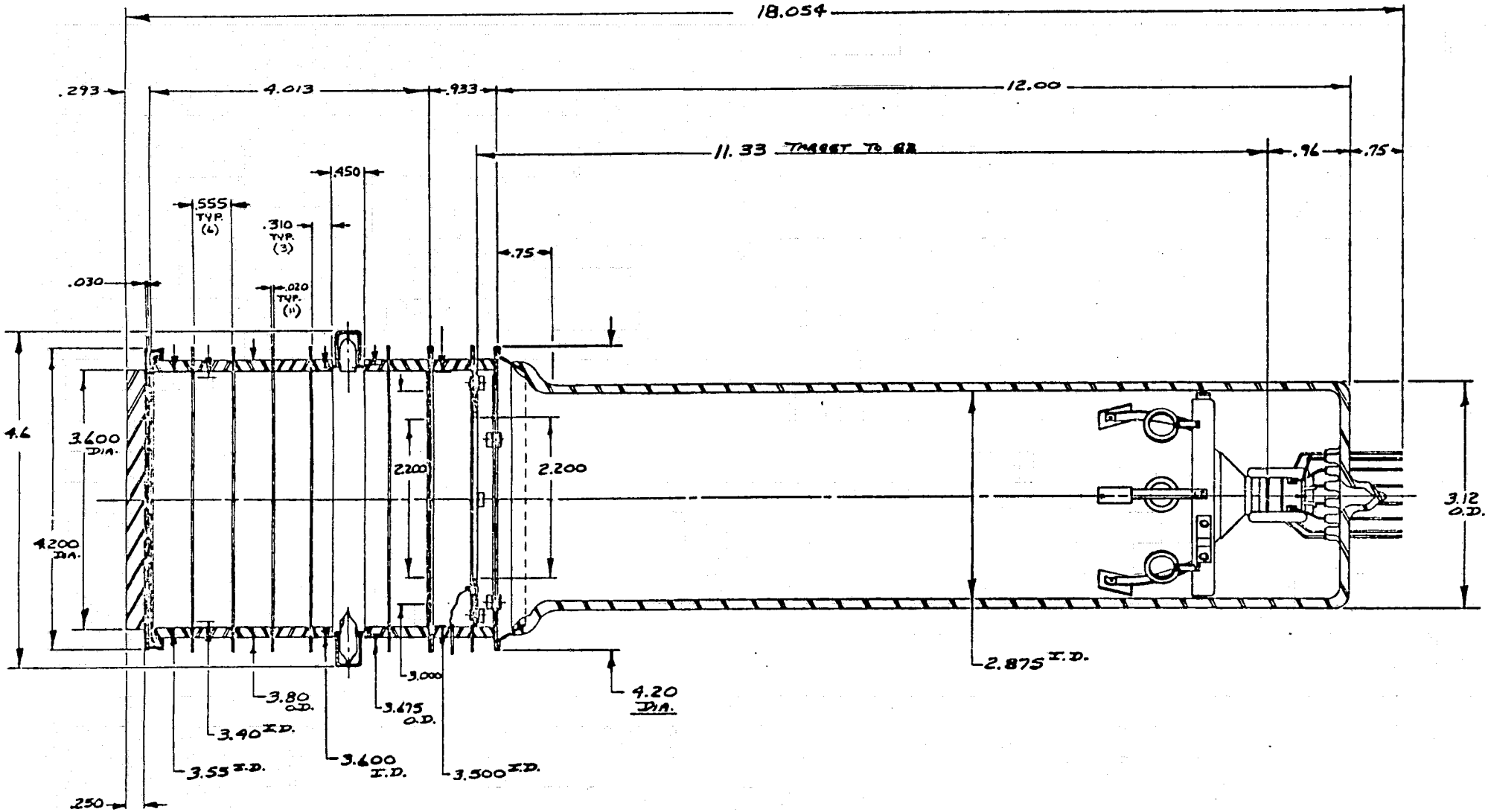
18.054
.293
4.013
.933
12.00
11.33 TARGET TO BB
.96
.75
.450
.555 TYP. (4)
.310 TYP. (3)
.020 TYP. (1)
.030
.75
4.6
3.600 DIA.
4.200 DIA.
2.200
2.200
3.12 O.D.
2.875 I.D.
3.000
3.80 O.D.
3.475 O.D.
4.20 DIA.
3.40 I.D.
3.55 I.D.
3.600 I.D.
3.500 I.D.
.250

Figure 221

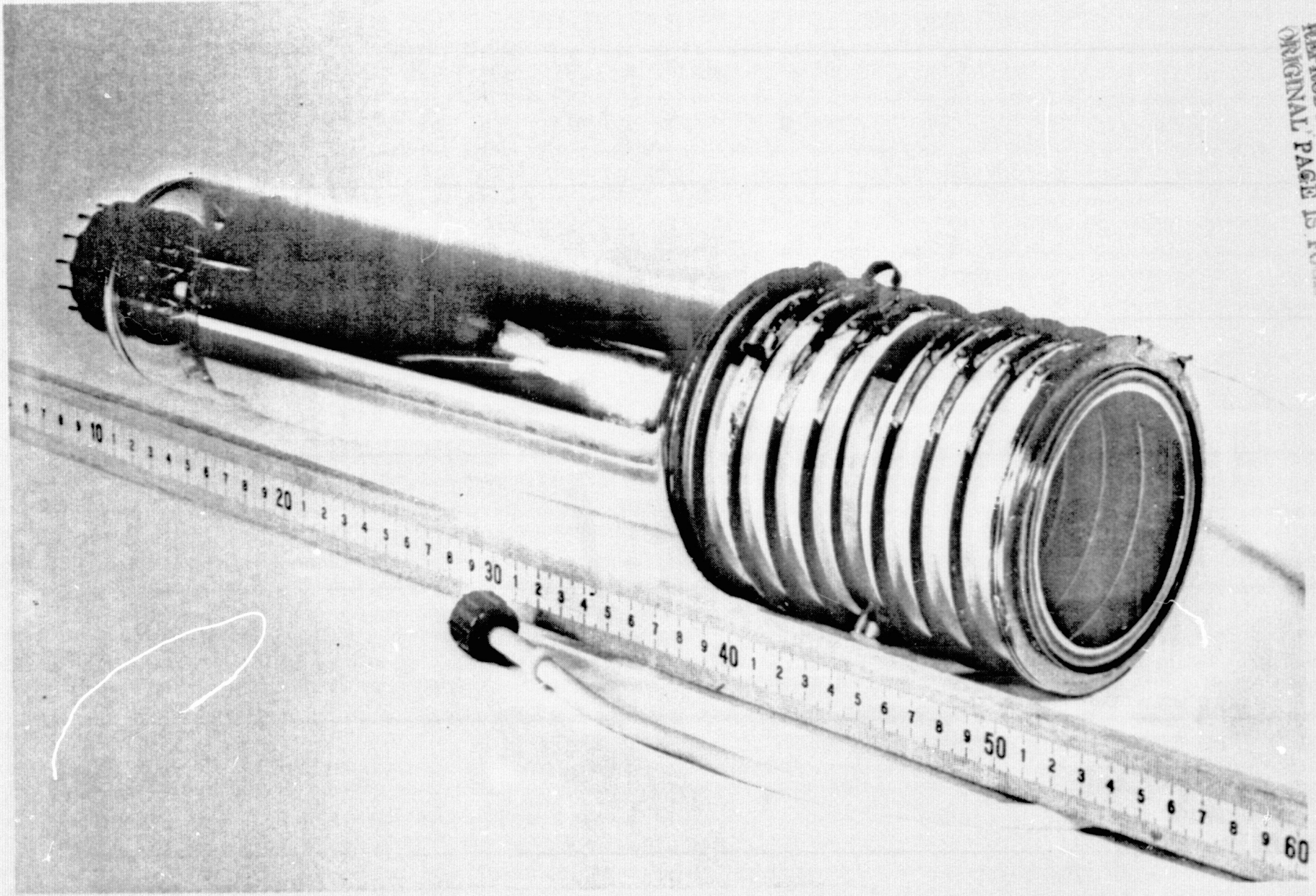

REPRODUCIBILITY OF THE
ORIGINAL PAGE IS POOR

Figure 222 Westinghouse WX-32193, 70 mm SEC Tube

Section 23 Focus, Deflection and Alignment Coils.

Focus Coil

The primary requirement for the 80 Gauss axial magnetic focus field required by the SEC tube is that the field lines be orthogonal to the photocathode and especially to the target.

The field intensity must be stable to within 0.03% to maintain the resolution performance.[4] However, long term changes in the magnetic focus field strength of the order of 10% can be accommodated by readjusting both the image and gun section electrode potentials to refocus the tube.

The crucial importance of orthogonality between the focus field and the target was demonstrated by Kamperman[5] who discovered that the off-axis twist induced in the focus field by winding the focus coil with too coarse a wire (which caused an excessive pitch to the helix of the windings) led to off-axis "waterfall" which is a condition of unstable read beam landing on the target. Kamperman and Princeton also found that the mechanical positioning of the SEC tube within the focus coil was critical with respect to the angular relationship between the tube and the focus coil axis. With a tube that was prone to "waterfall" it was necessary to carefully set the angular position of the tube to minimize the "waterfall". We believe that the optimum position was the one that had the target truly orthogonal to the focus field. We recommend that SEC camera head designs include provisions for adjusting for target to focus field orthogonality.

Focus coils made on the program at Princeton have had aluminum bobbins. The advantages of aluminum bobbins are good structural strength with light weight, excellent thermal conductivity, and good electrostatic shielding of the target electrode from the focus coil windings. As long as the deflection coils (which are inside the focus coil) have a magnetic return path in their

design for the deflection fields, the aluminum bobbins appear best. However, Ball Brothers Research Corp. has experimented with deflection coils without magnetic return shunts and they found that eddy current interaction between an aluminum bobbin and the deflection fields caused distortions of the readout beam scanning.

Deflection and Alignment Coils

Both the deflection coils and the focus coil (or focus permanent magnet assembly) must be considered as integral parts of the SEC tubes electro-optical design. It is not reasonable to specify tube performance without reference to a given coil assembly design.

At the present time, there is little rigorous data as to the specifications for SEC deflection coils. One parameter that can be measured is Beam Landing Error. This is the difference in volts in the minimum potential that will just cause the beam to land in the corners of the format as opposed to the center. Unfortunately it is very difficult to operate an SEC target at the near zero voltage required for this measurement. A special SEC tube with a metal target, usually known as a monoscope, is needed for this measurement.

The method used to date for judging deflection coils has been to try a few designs that the manufacturers considered promising. For both 35 mm and 70 mm SEC tubes the deflection coils made by Celco have been the most satisfactory. For the 35 mm tube, the Celco coil is No. C-1868-22 and No. B-1868-101 for the 70 mm tubes.

As furnished by Celco, both the 35 mm and the 70 mm deflection coils are equipped with a soft iron wire wrap which serves as the return path for the deflection fields. This soft iron shunt causes a depression in the axial magnetic focus field and also causes a radial component (a loss of orthogonality) near the edge of the target. Another, at least potential, disadvantage of the soft iron wrap is that any residual magnetism in the iron, and any variation in the permeability of the iron, can cause instabilities in the relationship between deflection coil current and read beam position on the target.

Of course, there are advantages in having the soft iron wrap, but most of them do not apply to the ST application. The two main advantages of soft iron wraps are higher deflection efficiency and confinement in the deflection fields; in particular, keeping the deflection fields out of the image section which is important only in continuous scan applications. Another possible advantage, at least from an analytical point of view, is that the soft iron wrap helps to

sharply define the beginning and end of the deflection zone in the readout beam electron optics.

In light of the above, Princeton removed the soft iron wrap from its Celco 35 mm deflection coil assembly in October 1975. The improvement in beam landing uniformity at an SEC target potential of 2 Volts was dramatic, as shown in Figure 231 The before and after oscilloscope traces (single tv lines) from top to bottom of Figure 231 are from lines 100, 512, and 950 out of the full frame of 1021 active scan lines. The bottom photos in Figure 231 are of the slow scan monitor screen. The SEC photocathode was uniformly illuminated for these tests. The improvement at the normal target bias for this tube (+12 Volts) was less evident but still noticeable. We concluded that the overall performance of the 35 mm system was improved by the removal of the soft iron wire wrap.

At the time of this report writing (August '76) experiments on Celco 70 mm deflection coils with and without soft iron wraps were underway at Ball Brothers Research Corporation under NAS5-24048. This work has indicated that the above mentioned removal of deflection coil magnetic shunts may lead to problems if the focus coil bobbin is aluminum. The focus coil bobbin in the reported Princeton experiment was brass.

Alignment coils do not offer a special problem with these SEC tubes, other than being certain that they are properly positional over the G2 aperture of the electron gun.

REPRODUCIBILITY OF THE
ORIGINAL PAGE IS POOR

Effect of Removal of Calco Iron Wire Wrap

TUBE 51 BEFORE @ $V_T = +2V$ AFTER

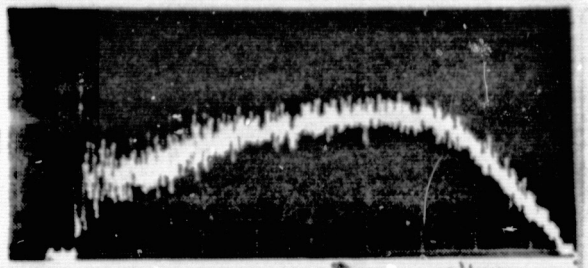

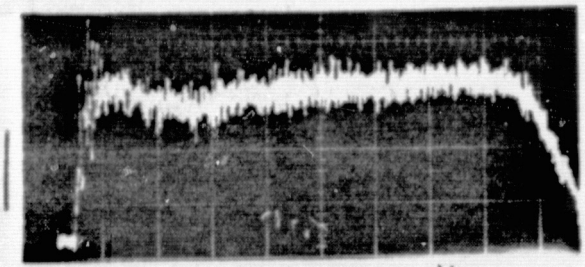

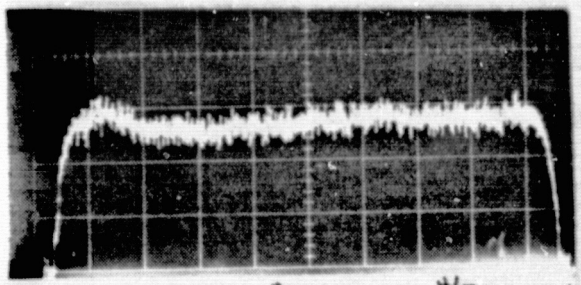

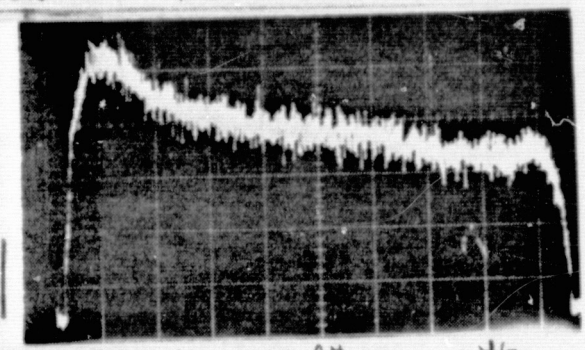

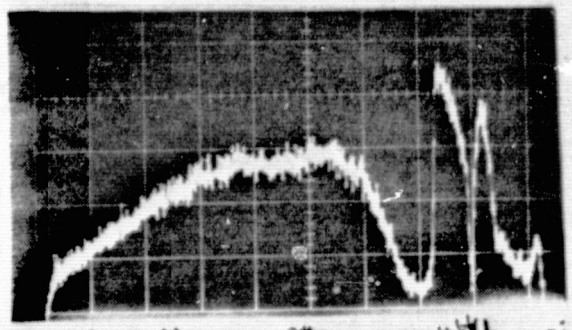

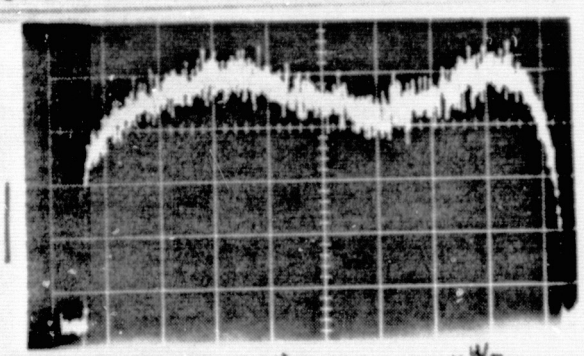

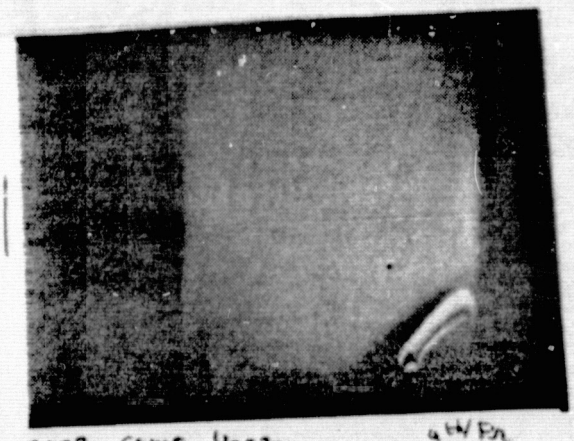

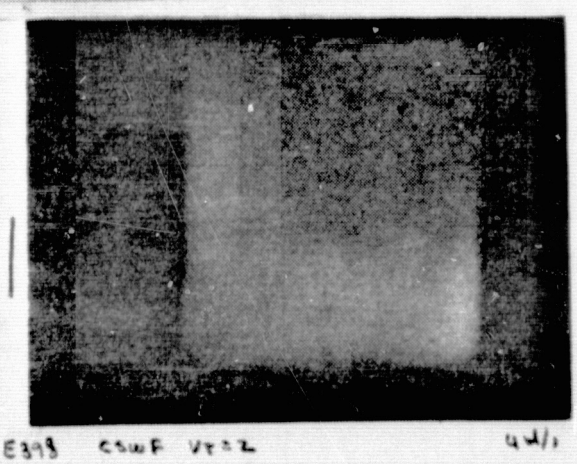

10-27-75

Figure 231

Section 24 Sequential Operation and the Target Prepare Cycle.

For the astronomy application, where exposure times of the order of minutes and hours are common, the SEC tube is operated in a manner quite different from that employed in broadcast television operation.

In normal TV operation the image section of the SEC tube is continuously writing an image into the SEC storage target while the reading electron gun is continuously reading out the image that has been integrated in the brief frame or field interval since the beam last scanned its present location.

In the sequential operating modes used in the astronomy application the SEC tube is cycled through five modes. They are: PREPARE, EXPOSE, HOLD, READY, and READOUT.

In the PREPARE mode any residual image is erased and the SEC storage target is normalized to make it suitable for a new exposure. During this mode four LED'S, designated as erase lights, are cycled to provide an even charge pattern on the target.

During the EXPOSE mode the photocathode and image section voltages are ON, integrating the incoming image into the SEC storage target. The field mesh voltage is ZERO, which limits the maximum target voltage excursion to the target bias level.

After an exposure the tube can be put into the HOLD mode where the photocathode and image section are OFF, the reading electron gun is OFF, and the field mesh voltage is LOW. The integrated image stored in the best SEC targets will not degrade perceptibly after an hour of storage. This mode is a safe standby mode.

The READY mode is the mode used prior to readout, to allow the wall, mesh, and target electrodes to be switched and settle to their readout levels.

During the READOUT mode the stored image is scanned out by the reading section's electron gun. During READOUT the photocathode voltage is OFF. It is safe to have a high field mesh potential during READOUT. The resultant high reading beam decelerating field contributes greatly to the high MTF and low beam pulling characteristics of suppressor meshless tubes.

REPRODUCIBILITY OF
ORIGINAL PAGE IS

The PREPARE mode is a sequence of operating states for the dual purpose of erasing any residual image including buried charge patterns within the target layer, and establishing the proper target conditions for the next exposure.

The details of the PREPARE cycles and other camera operating modes are given in Table 241. For further details on actually implementing this sequential operation please contact Princeton.

Another requirement of sequential tube operation is that of "target pulsing". This is a procedure in which the target bias is raised approximately 0.2 Volts above that used for the final PREPARE step and for the EXPOSE mode. If this were not done, the scanning electron beam would fail to land properly on those areas of the target that have received little or no exposure. The "target pulsing" bias insures that the scanning beam will land even in those portions of the target where the exposure was zero. Although "target pulsing" insures that threshold level signals will not be compressed or lost in the readout process, it does give the video signal a rather uneven black or "zero exposure" level.

In addition to the operating camera modes used in normal astronomy applications, the following modes are provided for test purposes: CONTINUOUS SCAN LOW MESH, CONTINUOUS SCAN HIGH MESH, FAST CONTINUOUS SCAN LOW MESH, AND FAST CONTINUOUS SCAN HIGH MESH.

The CONTINUOUS SCAN modes are used for test and setup of the camera system. The low mesh mode is a safe operating mode where the target cannot crossover (secondary emission of surface exceed 1) and be destroyed. In all the continuous scan modes the photocathode image section and gun section are both simultaneously on. When operating in the high mesh mode, care must be observed that the exposure is not so intense as to cause the target to crossover, although that is virtually impossible with the present gold coated targets.

The fast continuous modes are fourteen times faster than the normal scan rates. They are useful for quickly optimizing some camera parameters.

TABLE 241

SEQUENTIAL OPERATION AND THE TARGET PREPARE CYCLE

Modes	Beam	Heater	Photo-Cathode	Scan Size	Scan Rate	Target Voltage	Mesh Voltage	Erase Lights
Prepare I								
Frames								
0-4	On	On	On	Over	Slow	Prepare	Low	On
5	On	On	Off	Over	Slow	Prepare	Low	Off
6	On	On	Off	Full	Slow	Prepare	Low	Off
7	Off	On	Off	Full	Slow	Normal	High	Off
8-11	On	On	Off	Full	Slow	Normal	High	Off
Return to Hold	Off		Off	Zero	Slow	Normal	Low	Off
Prepare II								
Frames								
0-4	High	On	On	Over	Fast	Prepare	Low	High
5	High	On	Off	Over	Fast	Prepare	Low	Off
6	High	On	Off	Full	Fast	Prepare	Low	Off
7-14	Off	On	Off	Full	Fast	Normal	High	Off
15-17	High	On	Off	Full	Fast	Normal	High	Off
18	On	On	Off	Full	Slow	Normal	High	Off
Return to Hold	Off		Off	Zero	Slow	Normal	Low	Off
Exposure	Off		On	Zero	Slow	Normal	Zero	Off
Hold	Off		Off	Zero	Slow	Normal	Low	Off
Ready	Off	On	Off	Full	Slow	"Pulsed"	High	Off
Readout	On	On	Off	Full	Slow	"Pulsed"	High	Off
Continuous Scan Low	On	On	On	Full	Slow	Normal	Low	Off
Continuous Scan High	On	On	On	Full	Slow	Normal	High	Off
Fast Cont. Scan Low	High	On	On	Over	Fast	Normal	Low	Off
Fast Cont. Scan High	High	On	On	Over	Fast	Normal	High	Off

REPRODUCIBILITY OF THE
ORIGINAL PAGE IS POOR

Section 30 The 70 mm Analog Test Set at Princeton.

The test set used at Princeton for testing 70 mm SEC tubes in an integrated collection of equipment that has evolved almost continuously since the Westinghouse Aerospace Division (Baltimore) delivered the original apparatus in 1967.

Figure 301 is the Overall Block Diagram of the 70 mm analog test set. Figure 302 is the Block Diagram for the 70 mm Camera Head.

Figures 303 - 306 are photographs of the equipment. The control panel can be seen in the middle of the main electronics rack shown in Figure 303. Here, pushbuttons are used to activate the various PREPARE cycles (as discussed in section 24) and the various camera states such as HOLD and EXPOSE.

The two rectangular metal boxes in Figure 304 , the right side view of the camera head, are two preamplifiers used for the two scan rates employed. The upper preamplifier is the narrowband ($\sim$ 40 kHz) preamplifier used for the slow scan modes, while the lower unit is the wideband ($\sim$ 800 kHz) used for the fast scan modes.

The entire SEC assembly, which includes the focus coil and preamplifier, is mounted on ball bearing rods and is motor driven axially for optically focusing the camera.

The electronic content of the camera head has been minimized, only those functions that must necessarily be physically close to the SEC tube are located in the camera head.

When this equipment was formerly used for 35 mm tubes, the deflection amplifiers were located in the main electronics rack. However the long (35 meters) cables between the main electronics rack and the camera head proved unsatisfactory for the more demanding deflection requirements of the 70 mm tube. Accordingly, an additional one-half rack of electronics, Figure 306, connected with the camera head by 3 meter length cables, is used to house the 70 mm deflection amplifiers and their power supplies. The high voltage power supply for the image section is also located there. Refer to Figure 301.

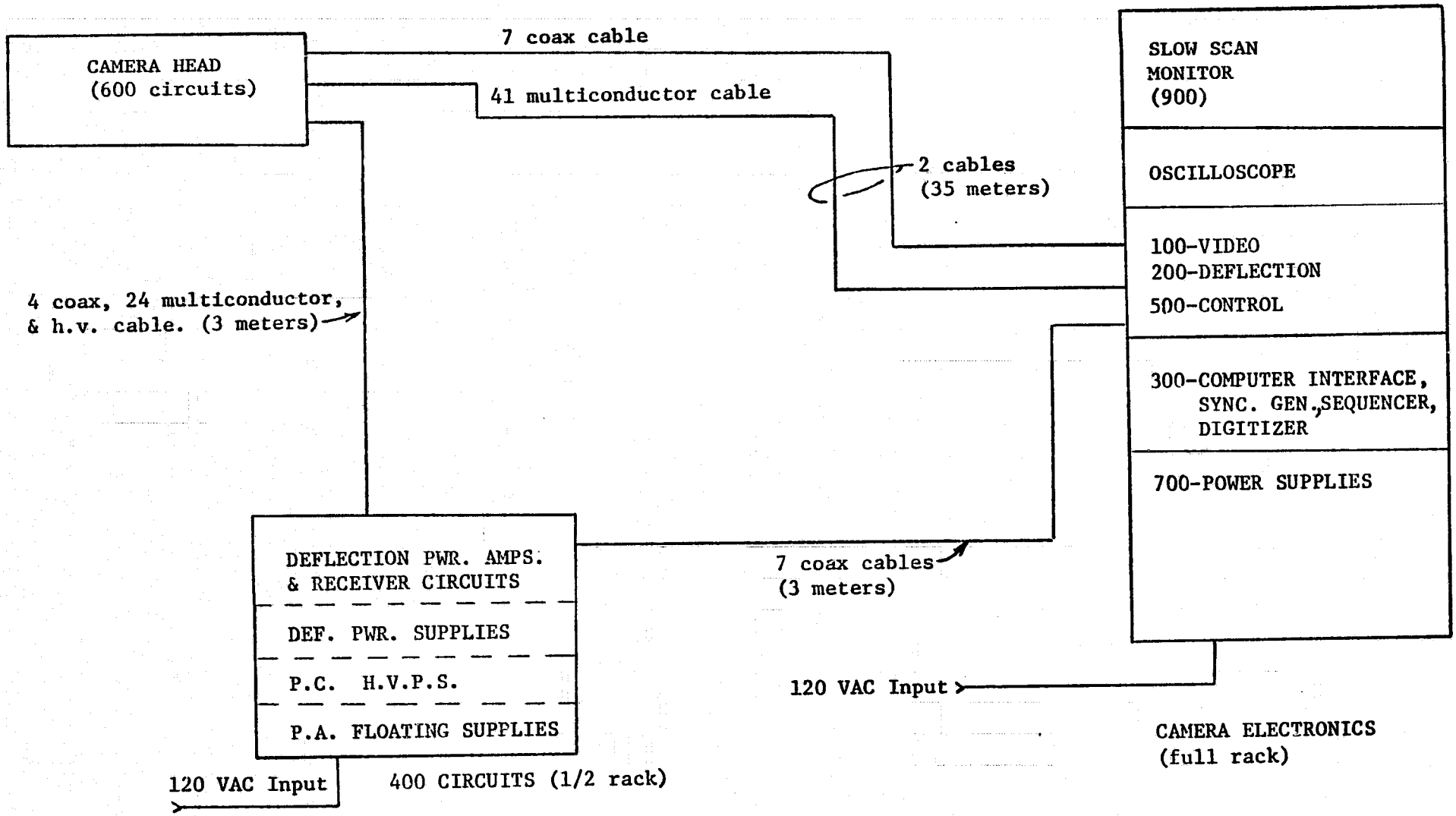

70 MM TEST SET - ANALOG CAMERA - OVERALL BLOCK DIAGRAM

Figure 301

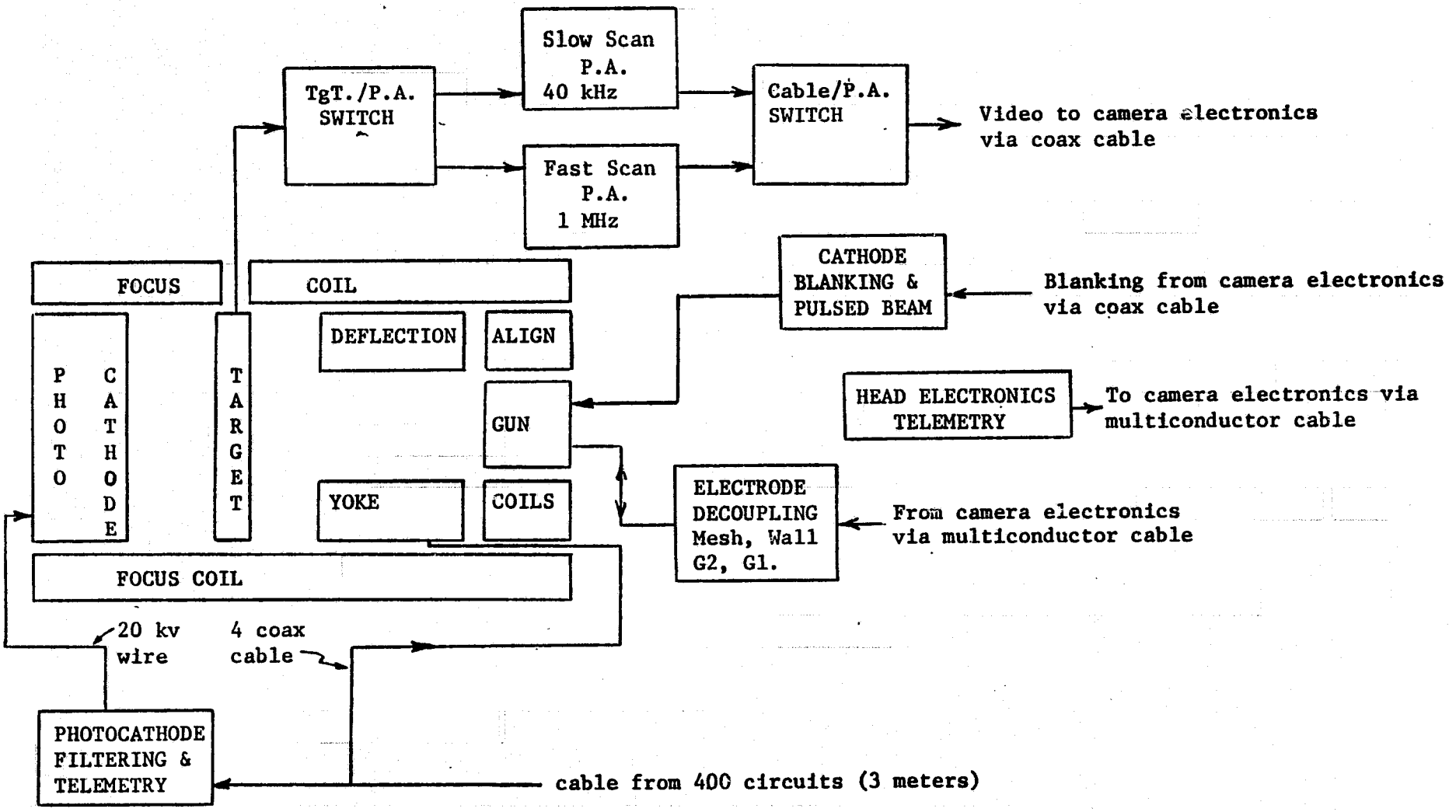

70 MM TEST SET - CAMERA HEAD - BLOCK DIAGRAM

Figure 302

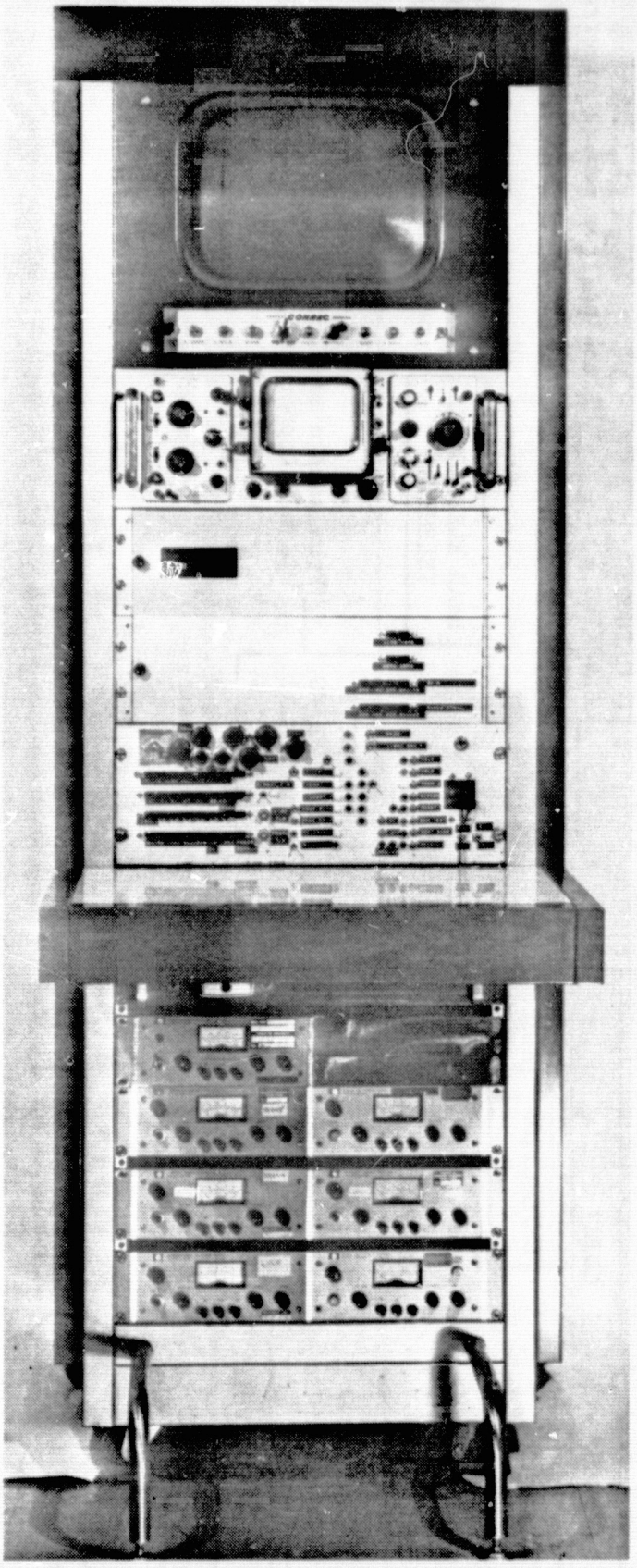

Figure 303

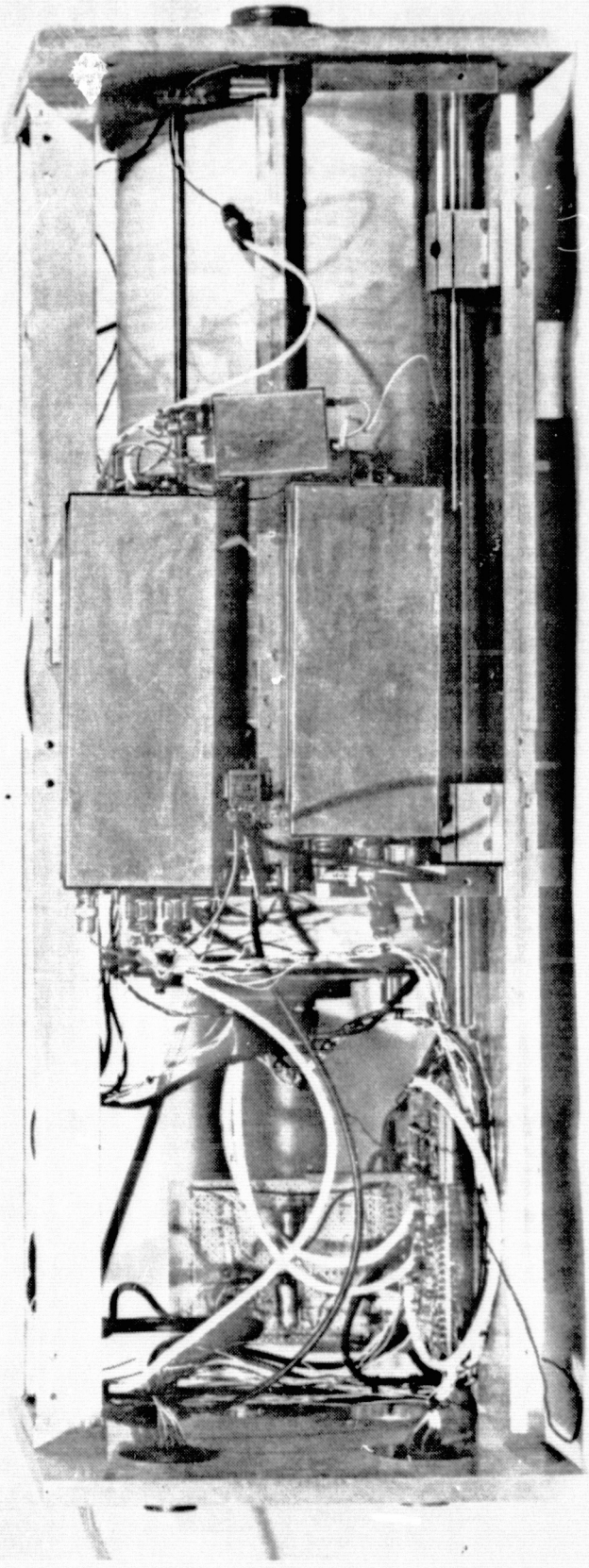

Figure 304

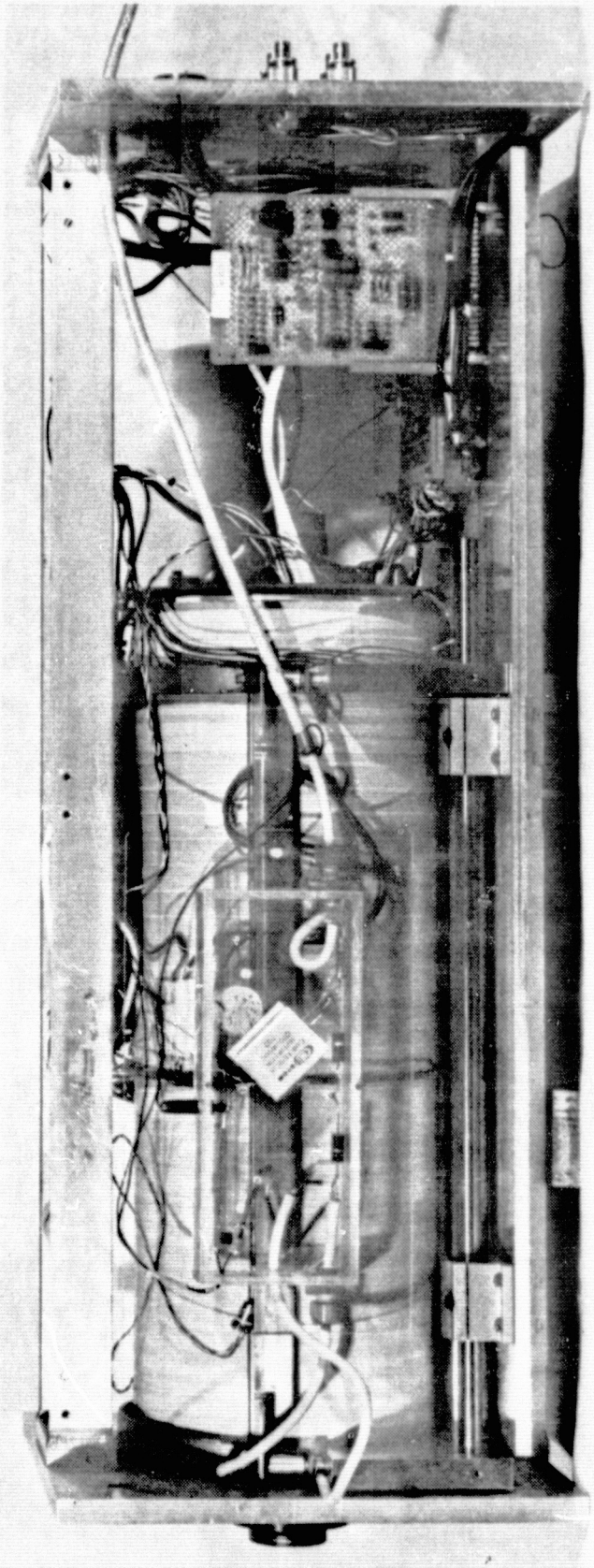

Figure 305

REPRODUCIBILITY OF THE
ORIGINAL PAGE IS POOR

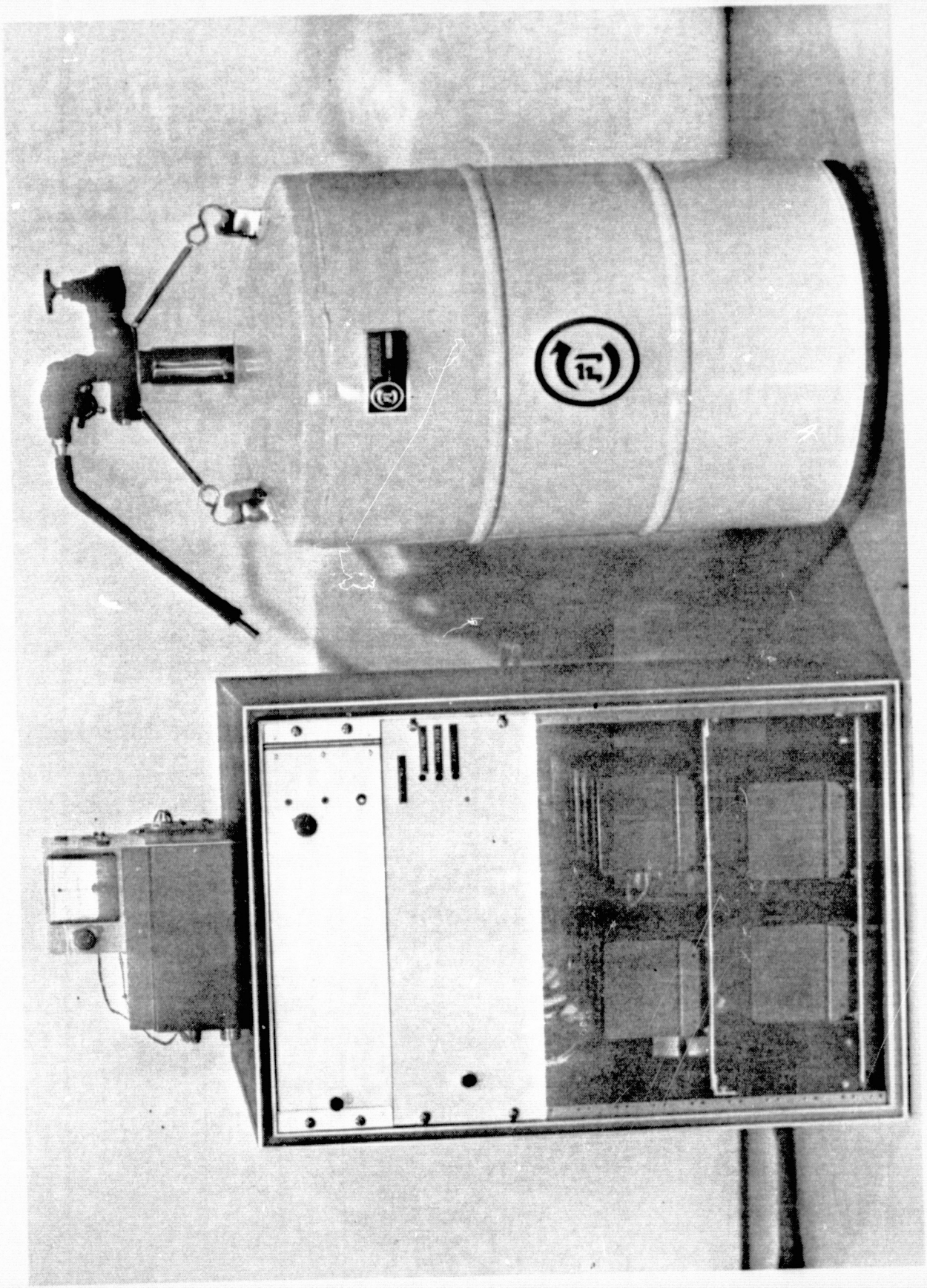

Figure 306

Section 41 Princeton SEC Tube Census Data

The SEC tube census summarizes pertinent data on the single sheet on all of the operable tubes that were delivered to, or evaluated by, Princeton during this contract. Both 35 mm (two digit PUO numbers) and 70 mm (three digit PUO numbers) SEC tubes are included. In order to present so much data in a compact format it was necessary to resort to codes and abbreviations for both column headings and data entries. The following pages are the guide for interpreting the census data given in Table 411 which follows the census guide.

SEC TUBE CENSUS GUIDE

COLUMN HEADING ABBREVIATIONS AND ENTRY INTERPRETATIONS:

PUO: Serial number assigned by Princeton to all delivered tubes. 1-99 are for 35 mm tubes and 101-199 are for 70 mm tubes.

W SER NO.: The serial number assigned to the tube by Westinghouse.

DEL.: The date the tube was delivered to Princeton (month/year).

WINDOW: The Image Section/Photocathode window material:

7056:	Corning 7056 glass
7056/PD:	with Palladium undercoat
MGFL:	Magnesium Fluoride (MgF_2)
MGFL/PD:	MgF_2 with Palladium undercoat
****/T:	with Tungsten undercoat
****/X:	with 'X' undercoat

PC: Photocathode:

S20:	S-20 (Na KCs SB) tri-alkali
CSK:	Cesium bi-alkali (Cs K Sb)
CST:	Cesium Telluride (C Te)
NAK:	Sodium bi-alkali (Na K Sb)

PR: Photoresponse in microamperes/lumen (when new).

TGT: Target:

STD:	Standard ($\sim 1/pe/\mu^2$)
HIC:	High capacity (~ 2 pe/μ^2)
MGO:	Magnesium Oxide (MgO)
ALO:	Aluminum Oxide (Al_2O_3)
EBS:	Silicon diode array

AR: Target Antireflection coating (usually aluminum black):

0:	none
5:	one-half of target coated
10:	all of target coated

AU: Grazing incidence gold target coating:

0:	none
18:	applied from two directions 180° apart
36:	applied from all angles, 360° rotary evaporator

TS: Target Support ("ring"):

CR:	Ceramic
GL:	Glass
KV:	Kovar
MY:	Molybdenum

NST: New Status (status of tube when new):

OPR:	Operational tube
LIM:	Limited operation tube
IMS:	Intact Mechanical Sample
MS*:	Mechanical Sample without (V) vacuum, (T) target, or (W) window.

NCON: New condition (condition of tube when new):

Refer to condition codes list. Up to three conditions (the three most significant) are shown.

CST: Current Status (present status of tube):

Refer to new status (NST) for codes.

CC: Current condition of tube.

A condition code is shown here only if there has been degradation of the tube since it was delivered.

CAUSE: Cause of degradation (if any):

S&H:	Shipping and handling
RAN:	Random
EVT:	Environmental testing
? :	Not known
NOD:	No degradation

COMMENTS AND DATA REFERENCES:

(data references refer to logbook or notebook pages, or tube dossier).

LOCATION: Present location of tube:

P:	Princeton
G:	GSFC
W:	Westinghouse
O:	Other
?:	Not known

CONDITION CODES:

Image section background:

(Exposure time that fills target with image section background)

6B:	10^6_5 seconds	(300 hrs.)
5B:	10^5_4 seconds	(30 hrs.)
4B:	10^4_3 seconds	(3 hrs.)
3B:	10^3_2 seconds	(17 min.)
2B:	10^2 seconds	(2 min.)
1B:	10 seconds	
0B:	Image section high voltage breakdown.	

Target Leakage:

(Storage time that fills target with target leakage.)

7L:	10^7_6 seconds	(300 hrs.)
6L:	10^6_5 seconds	(300 hrs.)
5L:	10^5_4 seconds	(30 hrs.)
4L:	10^4_3 seconds	(3 hrs.)
3L:	10^3_2 seconds	(17 min.)
2L	10^2 seconds	(2 min.)
1L:	10 seconds	
0L:	1 second	

Target condition:

9T:	uneven target layer
8T:	thin target, read beam penetrates
7T:	blemishes and small holes
6T:	holes
5T:	large holes (over 150 um)
4T:	very large holes (over 1 mm)
3T:	leaky tgt. electrode
2T:	open/shorted target
1T:	torn target (over 3 mm holes)
0T:	no target (over 50% gone)

Gun condition:

5G	low emission
4G	split or very low emission
3G	zero emission
2G	triode electrode leakage
1G	open/shorted triode electrode
0G	open heater

PR (Photoresponse):

5P:	PR	below	200 ua/lm
4P:	PR	below	100 ua/lm
3P:	PR	below	30 ua/lm
2P:	PR	below	10 ua/lm
1P:	PR	below	1 ua/lm
0P:	PR	below	0.1 ua/lm

Interelectrode Leakage and gas in gun:

5I:	some signal attributable to gun gas
4I:	strong signal attributable to gun gas
3I:	ion currents prevent slow scan operation
2I:	electrode leakage over 10 nm in wall or mesh
1I:	severe electrical leakage or breakdown

Tube envelope:

5E:	seal cracks or other potential failure seeds
4E:	gassy, possibly leaker
3E:	leaky, gas effects noted
2E:	to air
1E:	cracked and to air
0E:	smashed

Shading:

9S:	over	1.4:1	shading from target
8S:	over	1.4:1	shading from PC
7S:	over	1.4:1	signal shading
6S:	over	2:1	shading from target
5S:	over	2:1	shading from PC
4S:	over	2:1	signal shading
3S:	over	3:1	shading from PC
2S:	over	3:1	shading from target
1S:	over	3:1	signal shading

Target Gain:

7M:	25-50u fixed pattern over four percent
6M:	" " " " " ten percent
5M:	average target gain less than 100
4M:	" " " " " 50
3M:	" " " " " 20
2M:	" " " " " 10

DEFAULT CONFIGURATIONS:

	70 mm	35 mm
Image section envelope:	Ceramic	Glass
Target support:	Ceramic	Kovar
Gun limiting aperture:	15 μ	15 μ

SEC TUBE CENSUS AS OF SEP 13 1976

PUO	W SER NO.	DEL.	WINDOW	PC	PR	TGT:AR	AU	TS	NST	NCON	CST	CC	CAUSE	COMMENTS AND DATA REFERENCES.	LOCATION
108	75-22-722	?875	7056	S20	18	STD	0	18 CR	LIM	3B4.5L	LIM		NOD	UNSTABLE GUN FOCUS:L5-119-122;79,80;SEC-338,9	P
107	75-18-200	0575	7056	S20	84	STD	0	18 CR	LIM	2.5B4L	LIM		NOD	LIKE 108;L5-46-47,81-82,96,TLS;GREEN HALL PIX	P
106	74-39-995	0375	7056	CSK	70	STD	0	18 CR	LIM	1S5L5B	LIM		NOD	TGT THIN AT EDGE;L5-40,100;BELONGS TO WESTINGHOUSE	O
105	73-52-714	1273	MGFL	S20	19	STD	?	18 ?	LIM	3P	IMS	OP	?	SMALL WINDOW & IMAGE SECTION FRONT; PC DIED	P
104	73-30-650	1173	MGFL	?	?	?	?	? ?	IMS	2T	?			SMALL WINDOW & IMAGE SECTION FRONT, TGT ELEC OPEN	?
103	73-30-653	1173	7056	CSK	15	STD	10	18 GL	LIM	1S3P	?			SEVERE PORTHOLE SHADING, HAS GLASS TGT SUPPORT	?
102	72-48-036	0373	7056	S20	15	STD	10	18 CR	LIM	1S	LIM		NOD	VERY POOR CORNER LANDING,L5-17; GLASS IMAGE SECTION	P
101	72-22-200	1172	7056	S20	?	STD	10	? ?	?	?	?	?		GLASS IMAGE SECTION	?
55	75-44-440	1275	FIBER O	S20	136	STD	0	36 KV	LIM	1.5B	LIM		NOD	FIBER OPTIC; HIGH BACKGROUND;LG-178-180	P
54	75-39-002	1075	MGFL/5P	S20	80	STD	0	18 KV	LIM	2B	LIM		NOD	HALF OF WINDOW HAS PD UNDERCOAT;L6-160-168	P
53	75-26-001	0775	7056	CSK	47	STD	0	18 KV	LIM	1I	LIM		NOD	MESH BREAKDOWN AT 360V.PC RESISTIVE, NO PD L6-109	P
52	75-26-999	0775	7056/PD	CSK	28	STD	0	18 KV	LIM	3L3B	LIM		NOD	BOSS/LOAN;OPEN BUTTON LAST ACC RING L6-106,205	P
51	75-13-816	0375	7056/PD	CSK	33	HIC	0	18 KV	LIM	4.5L	MST	OT	S&H	PHOTOMETRIC TUBE,LOST TGT ON RETURN FROM OBS RUN;L6	P
50	75-09-440	0375	7056/PD	CSK	36	HIC	0	18 KV	LIM	0B	LIM		NOD	IMAGE SECTION BREAKDOWN AT 4KV;L6-57,58	P
49	75-05-264	0375	7056/PD	CSK	38	HIC	?0	18 KV	?	?	?			NO PUO DATA ON FILE, WEST. REPORTED CROSSOVER	P
48	74-30-267	0375	MGFL/?	CST	?	?	?	? ?	?	?	?	?		NO DATA ON FILE; WESTINGHOUSE TUBE	W
47	74-35-375	0874	7056/PD	S20	127	STD	0	18 KV	LIM	3B	LIM	4I	RAN	PHOTOMETRIC TUBE, GETTING GASSY, L6-29, 33, 37, 59	P
46	74-26-790		7056/PD	CSK	15	STD	5	18 KV							P
45	74-17-307		7056/PD	CSK		STD	05	18 KV							P
44	74-17-280		7056/PD	CSK	18	STD	5	18 KV							P
109	76-13-829	0576	?	?	?	STD	0	36 CR	LIM	2L1I5T	MST	OT	EVT	Mesh-Wall: 1/2 Megohm. Wrinkled target. Vibration test tube.	G?
110	76-17-170	0676	?	?	?	STD	0	36 CR	LIM	21	?	?	?	Mesh-Wall: 10 Megohm. Vibration test tube.	G?
111	76-17-944	0776	7056/PD	CSK	40	STD	0	36 CR	LIM	9T2S	?	?	?	Vibration test tube.	G?

Table 411

Section 42 On-Axis MTF Performance

Table 421 lists the best percent modulation at 20 cycles per mm obtained with square wave test patterns for various 35 mm and 70 mm tubes evaluated under this contract.

These measurements were made with a COMPON 135 mm enlarger lens operating at f/11, 3:1 magnification, and narrow band (~ 100 nm) green light. The results are not corrected for lens MTF and the lens MTF is not known but is assumed to be better than 80% at 20 cycles per mm under the very favorable wavelength and focal ratio employed. In 1967 Princeton had a comparable lens MTF tested (an EL-NIKKOR 63 mm, 6.3:1 magnification, broad band light) and that lens measured over 90% MTF at f/5.6 without the benefit of narrowband light.

Figure 421 shows a typical SWAR curve for these tubes.

TABLE 421

MEASURED ON-AXIS SWAR AT 20 CYCLES/MM

Tube	% Modulation 20 cycles/mm		Date Measured	Log Book Entry
111		57%	7-13-76	L5-169/170
110		49%	7-6-76	L5-167/168
109		52%	7-2-76	L5-163
108		48%	2-11-76	L5-121
107		58%	3-15-76	L5-155
106		45%	12-9-76	L5-98
103	87%	16 c/mm	11-16-73	L5-27
101		53%	3-19-73	L5-12A
52*	39%	16 c/mm	6-17-75	L6-108
51*	50%	20 c/mm	6-12-75	L6-78B
46*	39%	18 c/mm	1-30-76	L6-197
43*	60%	18 c/mm	6-11-74	L4-188

* 35 mm tubes

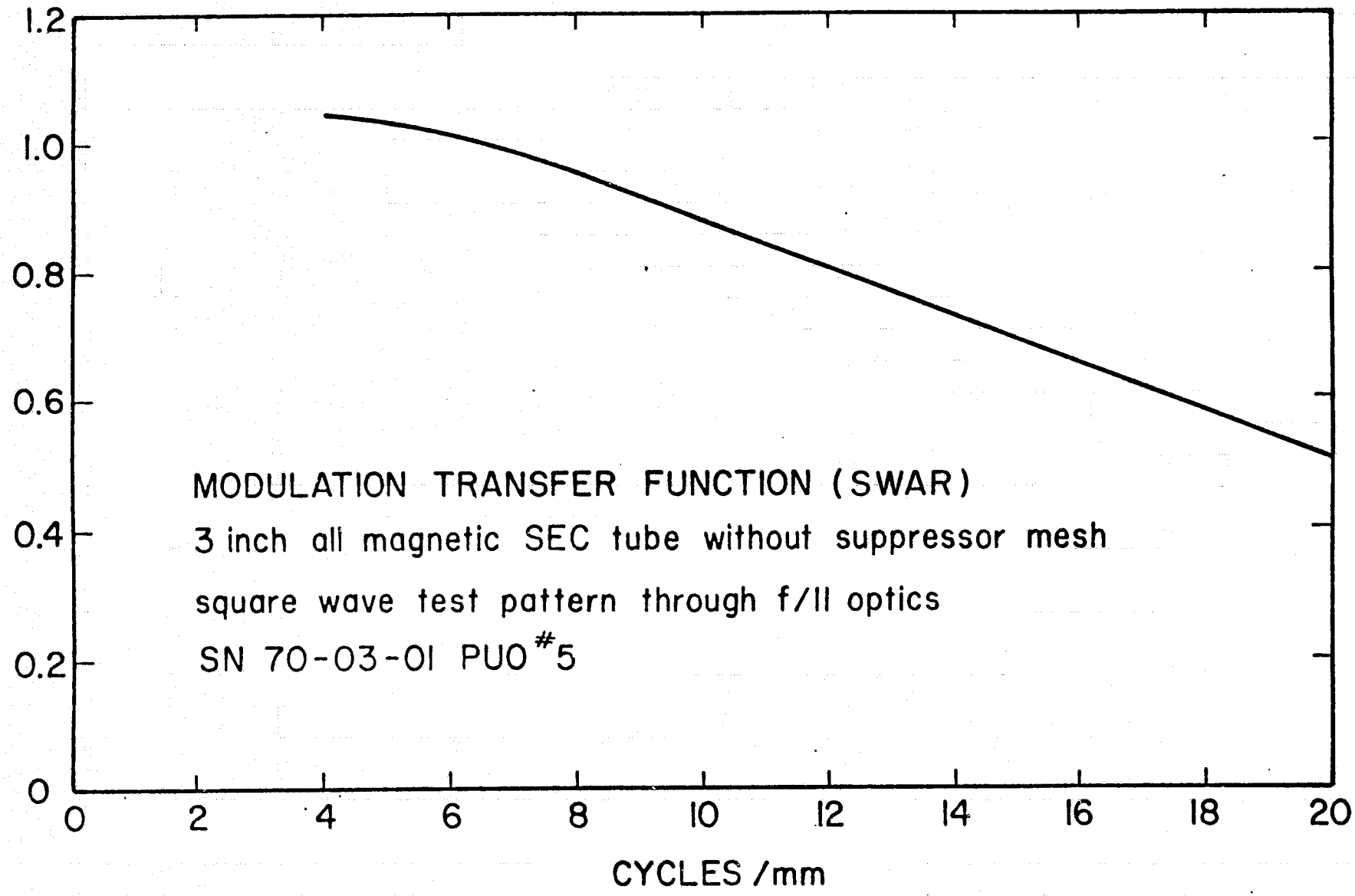

Figure 421 Typical Modulation Transfer Function (SWAR)

REPRODUCIBILITY OF THE
ORIGINAL PAGE IS POOR

Section 43 Off-Axis MTF Performance.

Figure 431 shows the best obtainable MTF data from tube 108 (delivered August 1975). These data were taken at the various points over the image format as indicated by the sketch in the right side of the Figure. For each data point the photocathode voltage was adjusted to maximize the MTF response. Therefore, the first order effects of the curvature of the image section focal surface have been nullified in the Figure 431 data.

The general scatter of the data of Figures 431-434 is partly attributable to the statistical difficulty of measuring high frequency MTF data on these sensors by measuring the video amplitude on an oscilloscope. There just are not enough photoevents in each pixel to give a clean reading. The best solution to the problem, the solution that works in both axes, is to use a computer to average the correct pixels together (vertically or horizontally as required) from the digitized video signal in order to measure the MTF. This solution will be implemented in the Princeton Parametric Test Set. An interim solution is to use slant-line type test patterns when measuring MTF. Although at high frequencies this technique is limited to only nearly vertical axis measurements, it does provide an automatic pixel averaging effect. We intend to use this technique for future MTF measurements at least until the Parametric Test Set is on-line.

Figure 431 shows that MTF responses of about 50% at a nominal 20 c/mm (2000 elements per target width) can be obtained over a central square region of 40 to 50 mm diagonal. Beyond that, the best obtainable MTF drops rather rapidly as the edge of the target is approached. Since all the currently available tubes have targets with known deficiencies near the edge, we do not know at this time how much of the off-axis MTF loss is attributable to the target.

Figure 432 shows the effect of the focal surface curvature at three locations: on-axis, 17 mm and 22 mm off-axis. This focal surface curvature is attributed to the magnetic field disturbance caused by the Kovar photocathode window flange.

Note that there is a 450 Volt difference between the optimum focus conditions at 22 mm off-axis and on-axis. Note also that a compromise focus voltage is not satisfactory. If the image section is focused at 17 mm off-axis (8200V), there is a significant loss of response at both 22 mm and on-axis.

Only the relative response measurements of Figure 432 are meaningful. The low maximum absolute responses, (about 35 to 40 percent versus over 50 percent in Figure 431) are attributed to the unstable gun focus properties of this particular tube. This problem was discovered part way through the image section measurements, and in light of the shortage of good tubes and the test time invested, the experiment was concluded with the same tube taking care to optimize the gun focus for each measurement.

Figure 433 expresses the curvature by plotting the voltage to focus the image section at various points over the format against the radial distance off-axis for each point. The available data are limited to a 50 mm diameter circle centered within the 50 by 56 mm format.

An attempt was made to correct for the magnetic field distortion caused by the Kovar photocathode window flange by introducing a compensating non-uniformity in the electric field of the image section. The standard electric field employed is a uniform, (parallel equipotential) accelerating field from the photocathode to the target. This field condition is reinforced by ring electrodes spaced at equal intervals along the axial dimension of the image section. If equal potential steps (voltage increments) are applied to these electrodes (the usual condition) they serve to reinforce the uniform electric field between photocathode and target. To compensate for the off-axis intensification of the axial magnetic field caused by the Kovar flange, the voltage step between the photocathode and the first ring electrode was made greater than the equal voltage steps between the other ring electrodes. This was done by increasing the value of the resistor between the photocathode and the first ring, while leaving the resistor values between the other rings at the usual value of 20 megohms.

A first resistor value of 30 megohms was found to reduce the image section focal surface curvature, as determined by observing the changes in photocathode voltage required to focus points on-axis, 17 and 22 mm off-axis. Next a 40 megohm first resistor was tried, and that proved to be about optimum for flattening the focal surface over a 44 mm diameter circle. Figure 434 shows the image section focus properties at our three reference test positions of on-axis, 17 and 22 mm off-axis. Again, the absolute response values have been depressed by the gun characteristics, but the relative responses indicate the image section properties under test.

Problems with target nonuniformity prevent meaningful experimental work beyond a 50 mm circle with the present tubes. However, we would speculate that the electric field compensation of the Kovar magnetic disturbance would not be a fully satisfactory solution over the entire 70 mm format.

Figure 435 is a plot of the S distortion in tube 108 (which we believe is representative of the current design in this respect). The data in Figure 435 are the horizontal displacements of a vertical line down the center of the format.

The total peak-to-peak displacement is about 24 pixels (0.6 mm) or about 1% of the format height of 50 mm. Figure 435 includes both data for the standard uniform electric field case and for the optimum electric field compensating electric field case of Figure 434. The effect of the compensating field on S distortion appears to be insignificant.

Overall rotation of the image associated with the non-uniform compensating electric field was largely removed by rotating the test pattern prior to taking the data of Figure 435. The rotation of the non-uniform (40 megohm) electric field case versus the standard uniform field case was found to be about five degrees.

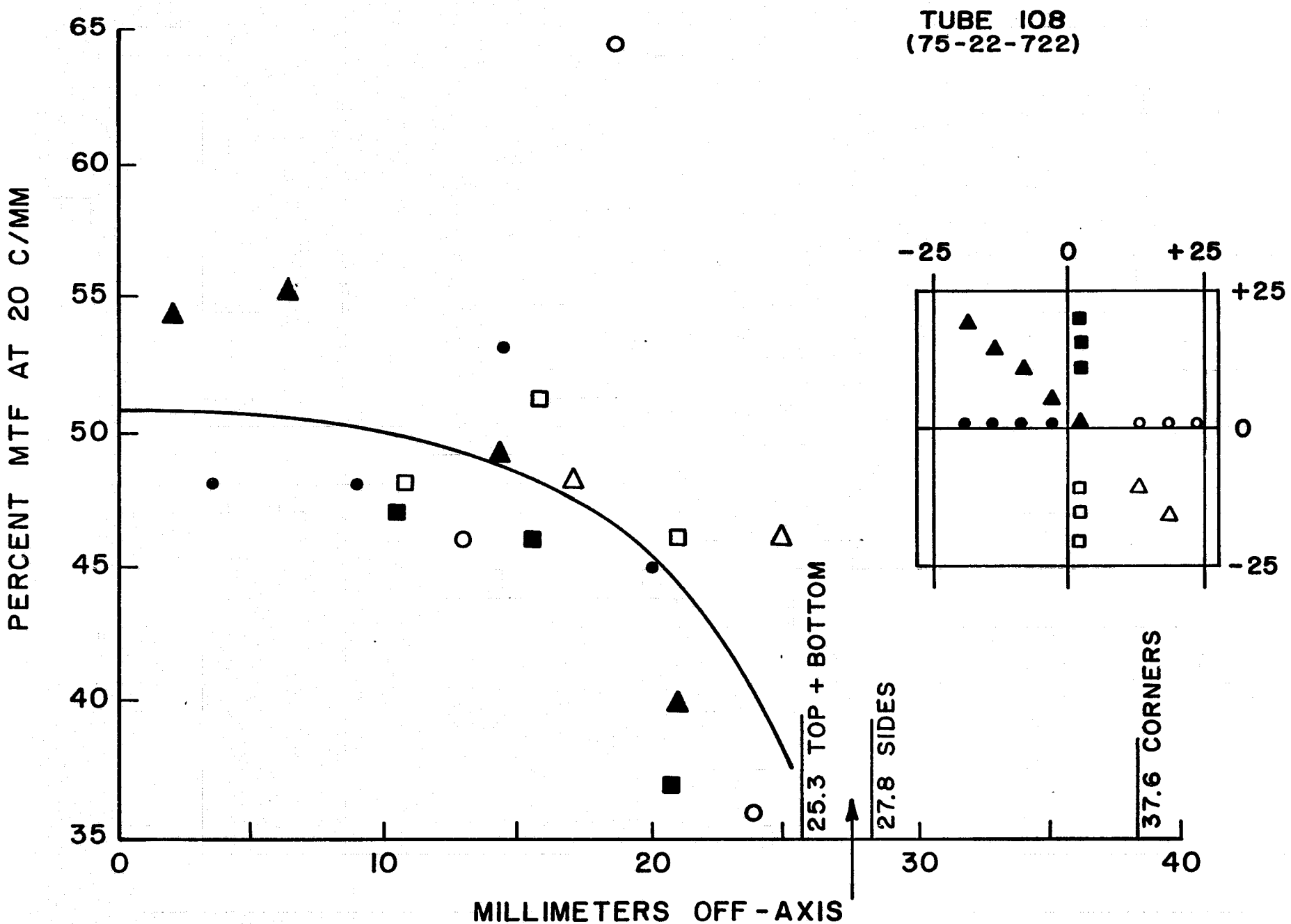
TUBE 108
(75-22-722)
PERCENT MTF AT 20 C/MM
65
60
55
50
45
40
35
0
10
20
30
40
MILLIMETERS OFF-AXIS
25.3 TOP + BOTTOM
27.8 SIDES
37.6 CORNERS
-25
0
+25
+25
0
-25

Figure 431

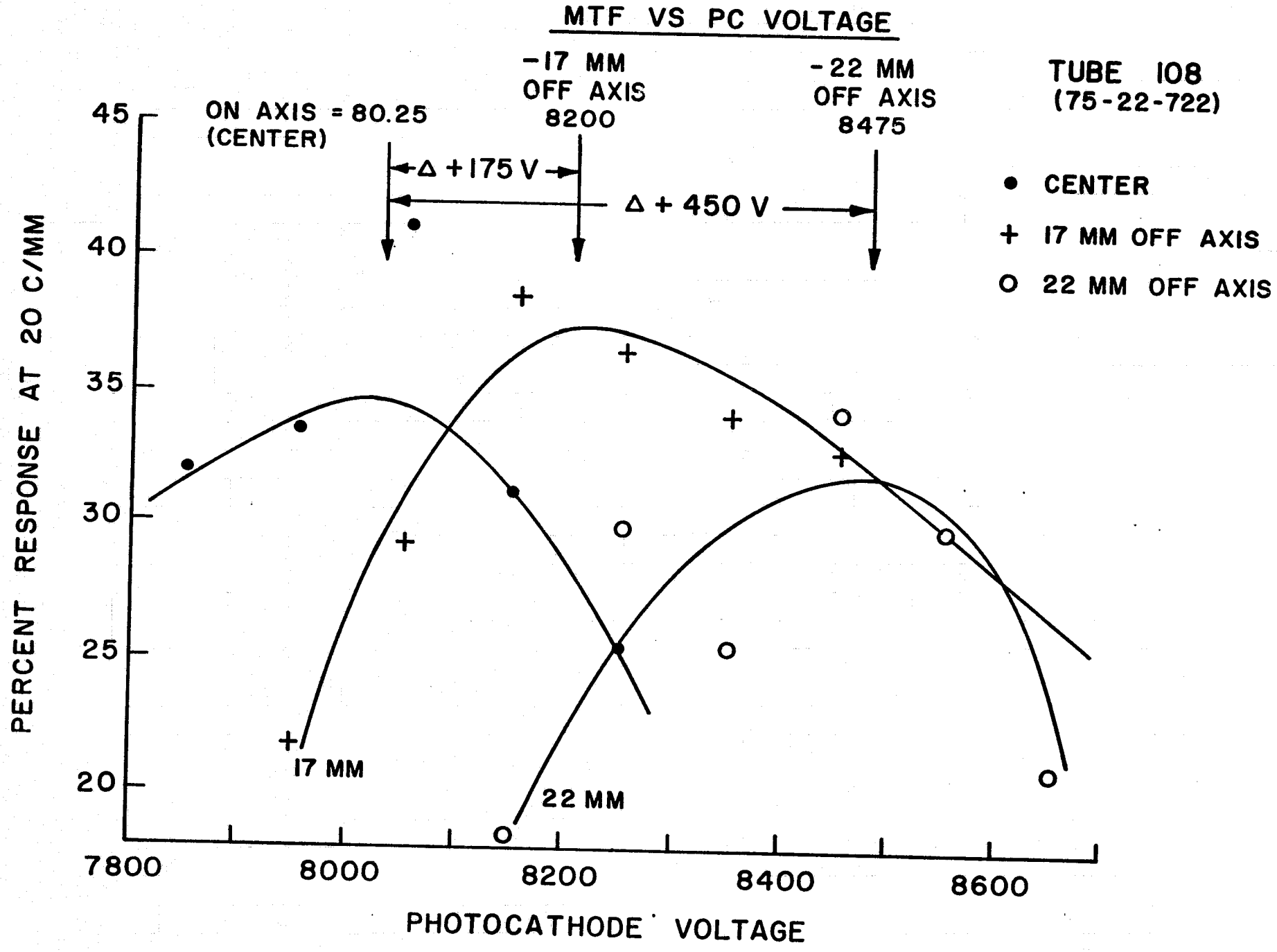
MTF VS PC VOLTAGE
TUBE 108
(75-22-722)
-17 MM
OFF AXIS
8200
-22 MM
OFF AXIS
8475
ON AXIS = 80.25
(CENTER)
Δ +175 V
Δ + 450 V
CENTER
17 MM OFF AXIS
22 MM OFF AXIS
PERCENT RESPONSE AT 20 C/MM
45
40
35
30
25
20
17 MM
22 MM
7800
8000
8200
8400
8600
PHOTOCATHODE VOLTAGE

Figure 432

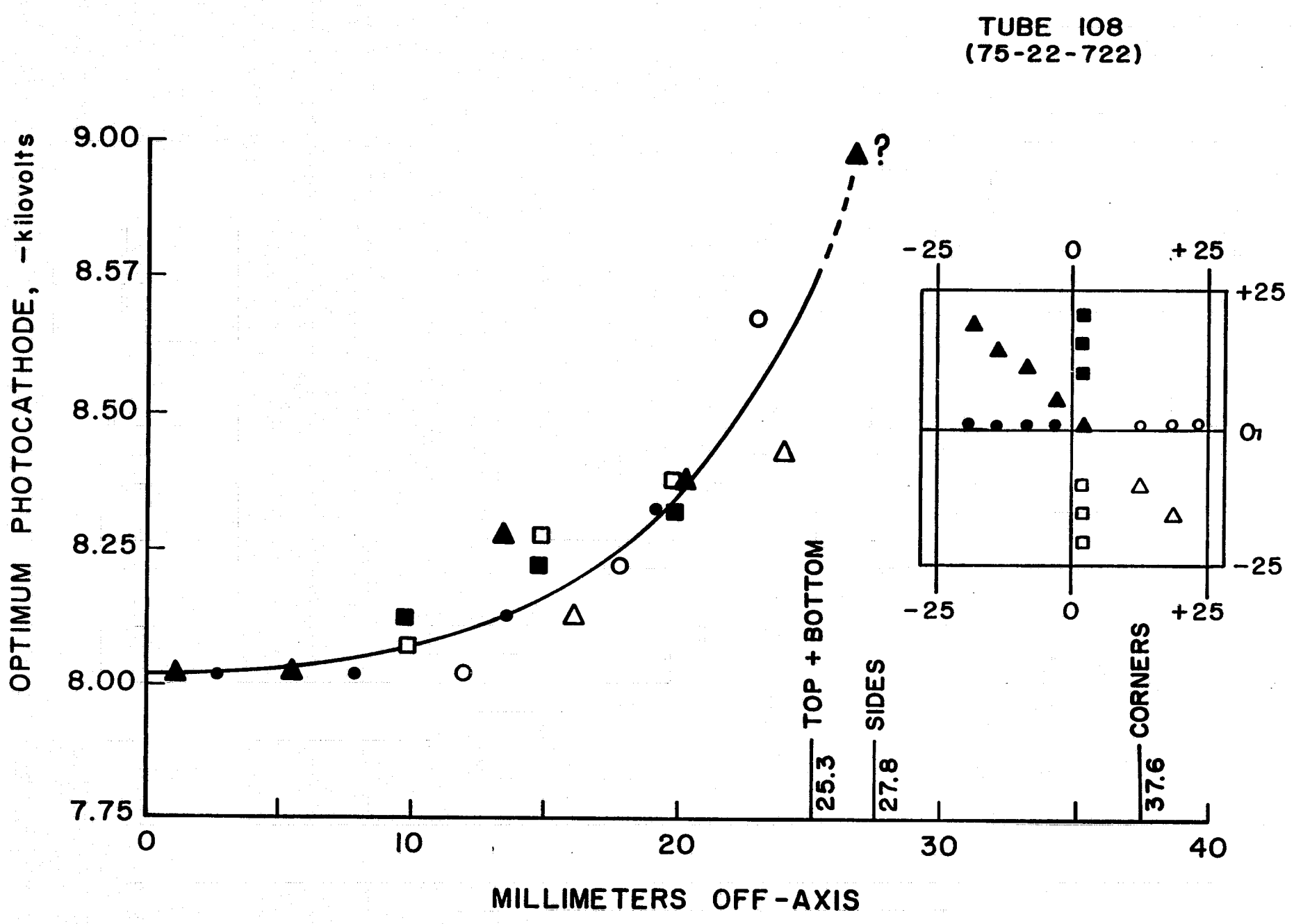
TUBE 108
(75-22-722)
OPTIMUM PHOTOCATHODE, -kilovolts
9.00
8.57
8.50
8.25
8.00
7.75
0
10
20
30
40
MILLIMETERS OFF-AXIS
TOP + BOTTOM
25.3
SIDES
27.8
CORNERS
37.6
-25
0
+25
+25
0
-25

Figure 433

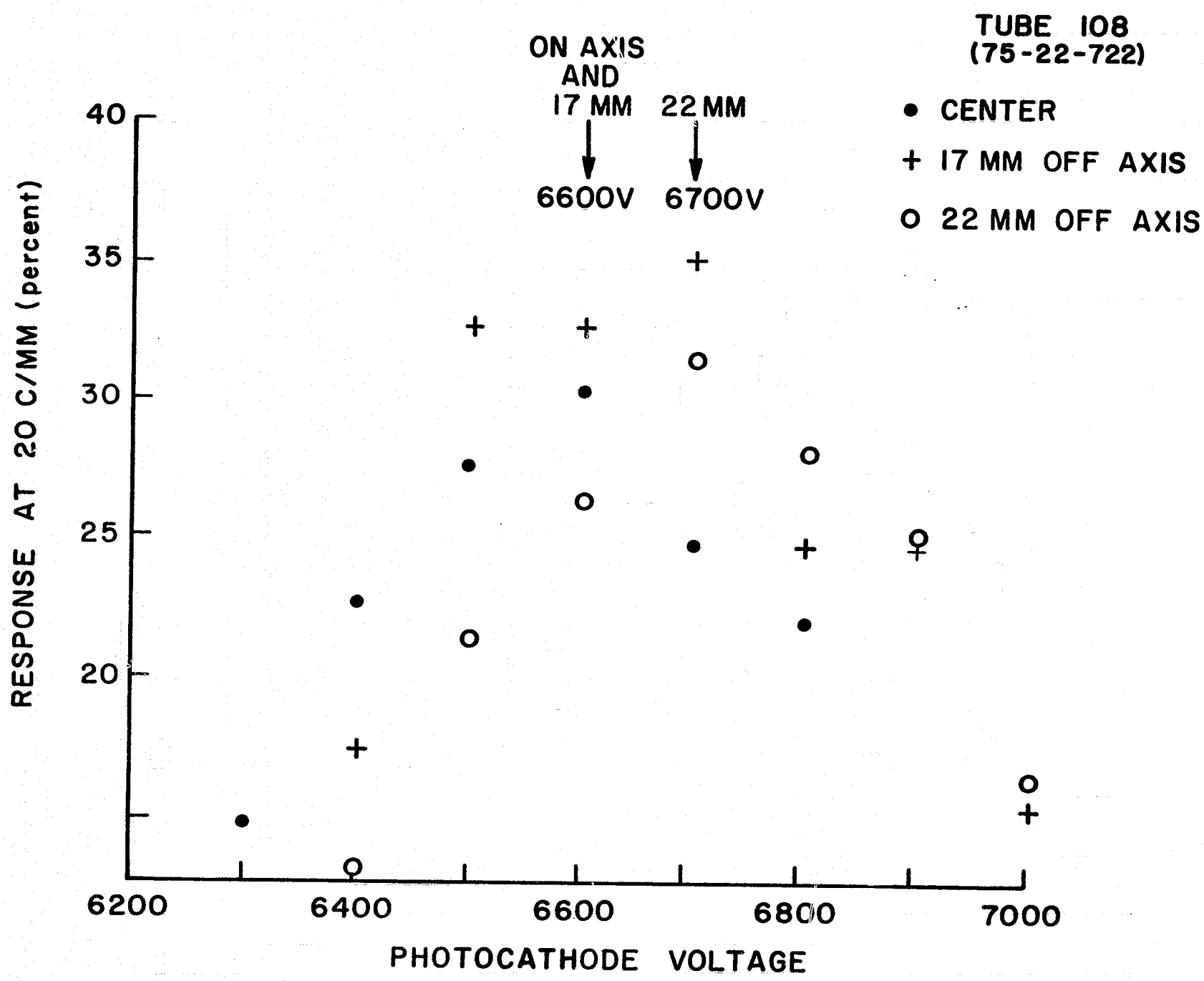
TUBE 108
(75-22-722)
ON AXIS
AND
17 MM 22 MM
6600V 6700V
• CENTER
+ 17 MM OFF AXIS
o 22 MM OFF AXIS
RESPONSE AT 20 C/MM (percent)
40
35
30
25
20
6200
6400
6600
6800
7000
PHOTOCATHODE VOLTAGE

Figure 4.34

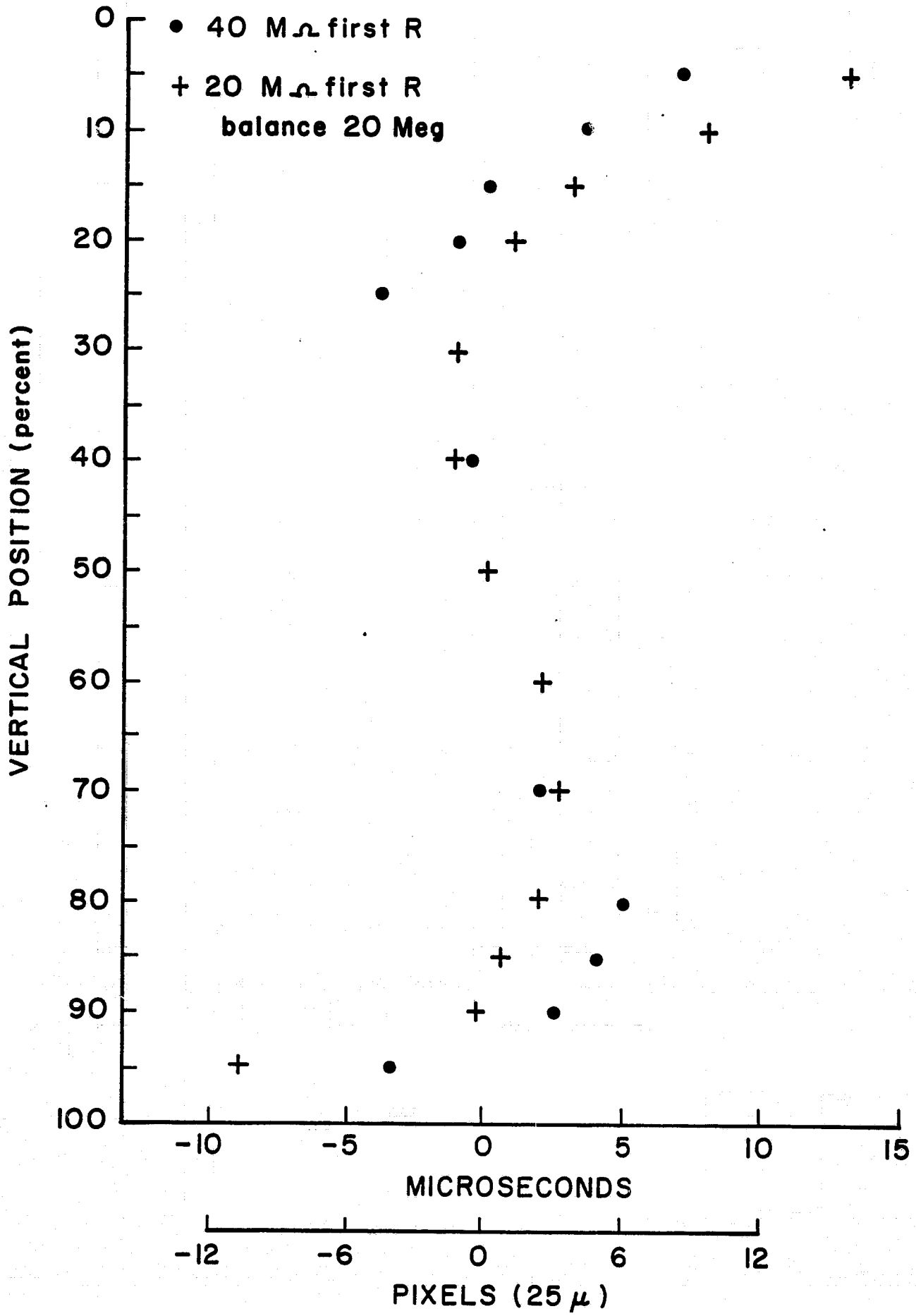
• 40 MΩ first R
+ 20 MΩ first R
balance 20 Meg
VERTICAL POSITION (percent)
0
10
20
30
40
50
60
70
80
90
100
-10
-5
0
5
10
15
MICROSECONDS
-12
-6
0
6
12
PIXELS (25 μ)

Figure 435

Section 44 Photometric Performance of 35 mm Tubes.

Photometric data for three 35 mm SEC tubes are listed in Table 441. The data are for a 100 by 100 pixel patch near the center of each tube. The first column shows the exposure level, calibrated[16] in photoelectrons emitted from the photocathode in a 25 micron square area. The response of the tube to the various exposures is listed in column two; the units are arbitrary but the same for the three tubes. The third and fourth columns show the signal-to-noise[16] ratios for 25 and 50 micron pixels, respectively. The response curves for these tubes are shown in Figure 441. The solid curves are the fits of the two parameter function:

$$E = A \tan \frac{R}{B}$$

to the data. Here E is the exposure, R the tube's response, and A and B the parameters of the fit. This function is linear for low and moderate exposures, and turns over into saturation at high exposures. The tangent function provides an excellent fit to the response curve of tube 57, a good fit to that of tube 51, and a moderate fit to that of tube 46. Note that tube 46 is non-linear at low and moderate exposures. The linearity of target response seems to be a characteristic which can vary from tube to tube. However, non-linearity is easily calibrated out.

The signal-to-noise curves for the three tubes are shown in Figure 442. The solid circles represent the signal-to-noise ratio for 50 micron pixels, the open circles that for 25 micron pixels. For exposures up to a few hundred photoelectrons per 25 micron pixel, the curves for all three tubes are similar. In this region, the signal-to-noise ratio is approximately half that expected from photon statistics alone. At high exposure levels, saturation effects in the targets cause the signal-to-noise ratio to reach a maximum and then decrease. In tube 51, which has a high capacity target, saturation effects are unimportant for exposures up to 1000 photoelectrons per 25 micron pixel. In contrast, the

much lower capacity tube 57 has passed its peak and started to decrease by that exposure level.

The "dynamic range" of these tubes depends upon the use to which they are put. For detection of faint objects, a signal-to-noise ratio of 3 may suffice; all of these tubes then have dynamic ranges greater than 100 for 25 micron pixels. For surface photometry, 5% accuracy, or better, may be required; the dynamic range for 50 micron pixels then varies from 2 to 10 for the tubes. In general, there is no single value for the "dynamic range" of any sensor.

Measurements of photometric variations across the face of a 35 mm SEC tube are listed in Table 442. Listed are the response and signal-to-noise ratios for 25 and 50 micron pixels as a function of relative exposure for each of four patches on tube 57. Patch 1 is near the center of the left edge of the tube; patch 3 is at the center of the tube; patch 2 is midway between patches 1 and 3; and patch 4 is midway between patch 3 and the right side of the tube. The response curves for the four patches are shown in Figure 443. All these curves are similar in shape to within the errors, and the principal difference between them is a gain shift caused by shading in the photocathode/target response. Figure 444 shows the signal-to-noise curves for 50 micron pixels, in the four patches. Again, the four curves have similar shapes. The patch near the edge of the tube has the best signal-to-noise ratio, however, the reduced resolution there smooths the noise somewhat.

Adding independent exposures of the same image together should improve the signal-to-noise ratio. Table 443 lists the data on multiple frame statistics for the three tubes. For each tube and exposure level investigated, the number of frames added and the associated signal-to-noise ratio for 50 micron pixels are tabulated. Figure 445 shows the data at three exposure levels in tube 57. The filled circles show the percentage noise measured in each of the multiple

frame summations. These points do not fall as the square root of the number of frames summed, as would be expected if the noise is totally random in nature. We thus propose a two component model for the noise. One component is random noise whose amplitude decreases with the number of frames added, and the other is persistent noise whose amplitude is constant. The total noise is thus:

$$\sigma = (C^2 + \frac{D^2}{N})^{1/2}$$

where σ is the total noise, N is the number of frames added, C is the persistent noise component, and D is the random noise component. Fits of this function to the data are the solid curves in Figure 445. The good fit of the solid curves to the filled circles supports this two component model of the noise. The random noise components alone, that is $D/\sqrt{N}$, are the dashed curves in Figure 445.

A simple method to correct the data for the persistent noise component is to subtract the mean of a large number of frames. Since the random noise decreases as $1/\sqrt{N}$, if N is large the noise is dominated by the persistent component. Thus, the subtraction removes the persistent component and leaves only the random component. The open circles in Figure 445 show the noise measurements in such subtracted frames. These open circles fit the dashed curves well, supporting the two component model for the observed noise. In another test, we have measured the mean and standard deviation of individual pixels over 16 frames. Since these are single pixel measurements, they are free of any fixed pattern noise component. These measurements agree almost exactly with the open circles on Figure 445. Thus it appears feasible to eliminate the persistent noise component from the data, obtaining the noise performance indicated by the dashed curves in Figure 445. Note that except in the non-linear region, these curves are approximately 1.6 times the noise in an ideal detector (the triangles in Figure 445).

Two identical series of photometric measurements were performed on Tube 46 to measure the reproducibility of the photoresponse. The two series were performed a week apart, with the camera turned off in the interim. The results are listed in Table 444. The first column shows the exposure level in photoelectrons per 25 micron pixel; the next two columns contain the tube's response for the two series, in digital counts(an arbitrary unit); the final column has the difference in digital counts between the two measurements. The RMS difference between the two sets of measurements is 9.7 digital counts, which corresponds to 11 photoelectrons. The two response curves are shown in Figure 446. The squares are those of the 1-15-76 measurement, the circles those of 1-22-76. There are no differences between the curves which are significant. The response measurement was repeated on 11-30-76; the triangles show the results of that measurement. Due to various changes in laboratory techniques and camera hardware, it was impossible to reproduce the absolute flux levels exactly. Thus the results were scaled in both axes before being put on Figure 446. However, it is clear that the shape of the response curve has not changed over the 10.5 month interval.

TABLE 441

PHOTOMETRY FOR THREE SEC TUBES

		Exposure pe/(25μ)^2	Response digital counts	Signal/Noise 25μ	50μ
		5	3	0.8	1.3
		10	8	1.4	2.4
		20	19	2.5	4.2
		39	45	3.5	5.7
Tube	51	78	95	6.6	10.4
		156	199	9.1	14.4
		313	388	11.9	20.8
		625	704	14.9	27.7
		1250	1182	15.7	31.5
		2500	1539	15.9	31.9
		5	2	0.9	2.0
		10	5	1.8	4.2
		20	10	3.3	6.5
		39	26	4.7	9.2
Tube	46	78	67	6.8	11.8
		156	166	8.7	15.0
		313	362	12.4	21.5
		625	621	13.7	28.1
		1250	902	13.0	29.4
		2500	1369	7.8	18.4
		6	9	0.5	1.1
		12	7	1.2	2.5
		23	12	2.5	5.1
		47	26	4.1	8.2
		94	65	5.7	10.5
		99	76	5.5	10.7
		198	160	7.6	15.6
Tube	57	395	310	8.8	19.2
		790	543	9.2	21.2
		1580	823	6.5	16.8
		1860	849	6.7	17.2
		3719	1071	3.1	8.4
		7439	1165	2.1	5.7
		14877	1224	1.4	3.8
		29755	1258	1.0	2.5

TABLE 442

PHOTOMETRY AT FOUR DIFFERENT POSITIONS ON TUBE 57

Relative Exposure	Response	S/N 25μ	S/N 50μ	Response	S/N 25μ	S/N 50μ	Response	S/N 25μ	S/N 50μ	Response	S/N 25μ	S/N 50μ
0.5	15.8	0.24	0.41	9.34	0.69	1.28	4.25	0.11	0.22	0.41	0.60	1.21
1.0	17.4	0.71	1.29	13.1	1.36	2.61	4.82	0.36	0.71	-1.30	1.17	2.36
2.0	27.7	2.82	4.84	20.7	2.23	4.08	9.72	1.79	3.40	4.58	2.14	4.24
4.0	50.1	3.39	5.58	32.9	3.91	6.81	19.6	3.72	6.49	8.18	4.28	8.09
8.0	73.4	6.00	10.0	65.5	7.90	13.7	46.8	6.95	12.2	38.6	7.07	12.6
16.0	162.8	11.2	17.9	139.2	10.9	18.3	102.2	9.34	16.9	88.9	9.51	16.5
32.0	319.4	17.0	26.5	269.2	15.0	24.2	207.2	12.4	21.6	192.2	12.3	22.0
64.0	616.4	19.8	32.1	512.7	18.3	29.5	387.8	15.5	27.0	363.0	14.2	25.2
128.0	1082.7	18.8	30.7	884.8	14.1	23.1	649.3	13.6	25.3	607.0	13.6	24.5
256.0	1651.3	11.9	21.4	1241.8	6.90	12.9	908.8	5.13	12.1	854.9	5.47	10.8
512	1903.3	12.1	16.8	1394.5	8.24	14.9	1030.5	4.63	12.9	947.2	5.36	11.4

TABLE 443

MULTIPLE FRAME STATISTICS

Tube	Exposure pe/(25μ)^2	Number of Frames Added / Signal-to-Noise Ratio (50μ pixels)									
51	313	1 / 20.8	2 / 24.6	4 / 28.2	6 / 29.3	7 / 30.3	8 / 30.2	9 / 31.0	11 / 31.2	13 / 31.5	15 / 31.8
46	156	1 / 15.0	2 / 18.0	4 / 21.0	8 / 22.6	12 / 23.4	16 / 24.0				
46	313	1 / 21.5	2 / 25.1	4 / 28.4	8 / 33.0	12 / 33.7	16 / 34.3				
46	1250	1 / 29.4	2 / 30.7	4 / 32.2	8 / 37.6	12 / 38.0	16 / 41.0				
57	99	1 / 10.7	2 / 13.7	4 / 15.7	6 / 16.6	8 / 18.7	10 / 19.9	12 / 20.6	14 / 21.1	15 / 21.8	
57	395	1 / 19.2	2 / 25.5	4 / 29.0	6 / 30.4	8 / 32.3	10 / 32.8	12 / 33.3	14 / 33.3	15 / 33.6	
57	1860	1 / 17.2	2 / 20.7	4 / 20.7	6 / 23.3	8 / 23.7	10 / 24.0	12 / 24.5	14 / 24.0	15 / 23.9	
57	7439	1 / 5.7	2 / 7.3	3 / 7.4	4 / 6.7	5 / 6.9	6 / 7.6				

TABLE 444

REPRODUCIBILITY OF PHOTORESPONSE

Exposure pe/(25μ)^2	Signal 1/15/76	Signal 1/22/76	Difference
5	1.1	6.3	5.1
10	2.3	7.0	4.7
20	9.8	13.4	3.7
39	30.6	24.9	-5.7
78	75.3	68.2	-7.1
156	180.0	180.2	0.2
313	392.0	395.9	3.9
625	691.6	673.2	-18.4
1250	1060.5	1049.8	-10.7
2500	1368.7	1350.6	-18.1

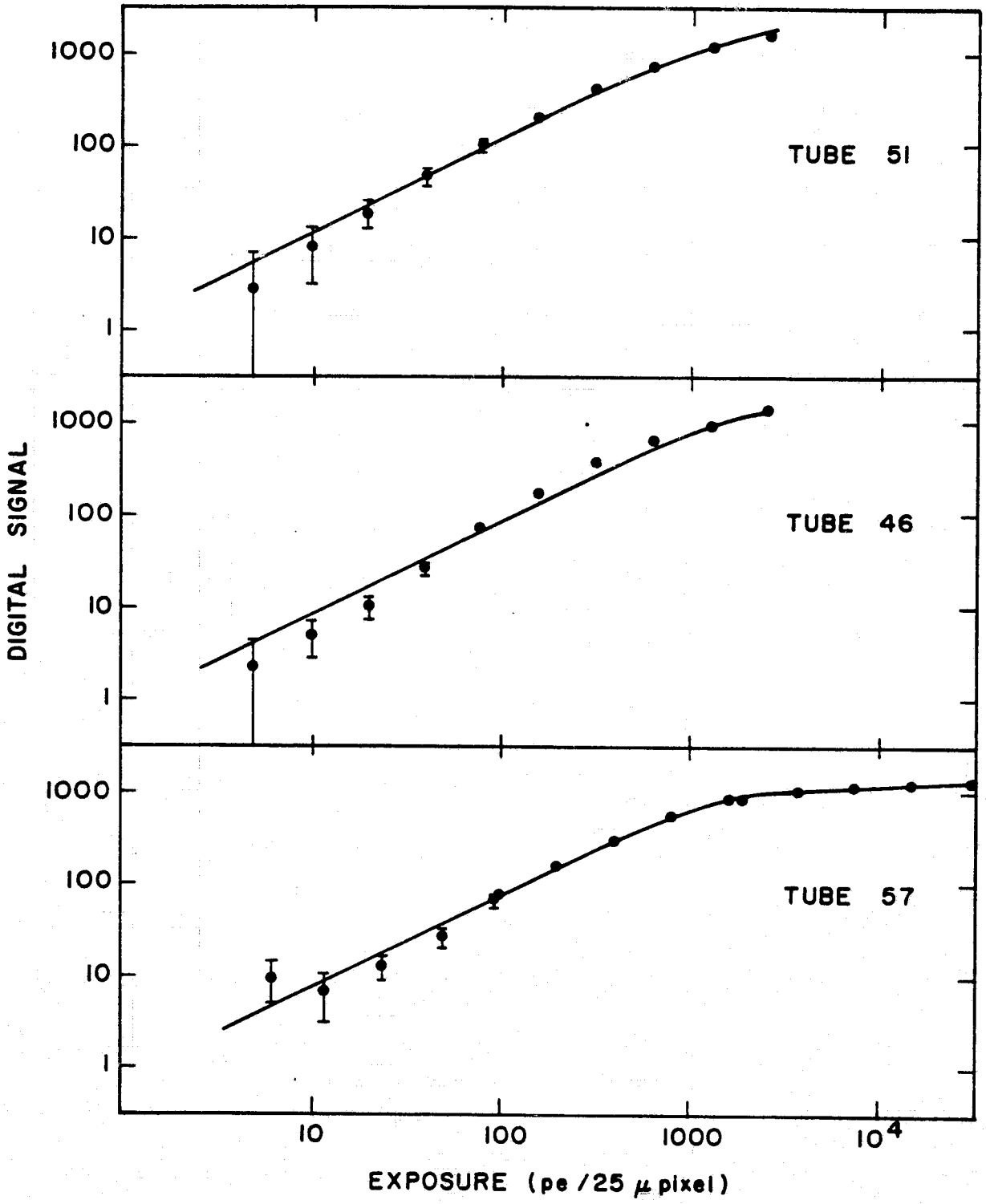

Figure 441

Response curves for three 35 mm SEC tubes. Solid curves are fits of the function $E = A \tan \frac{R}{B}$ to data.

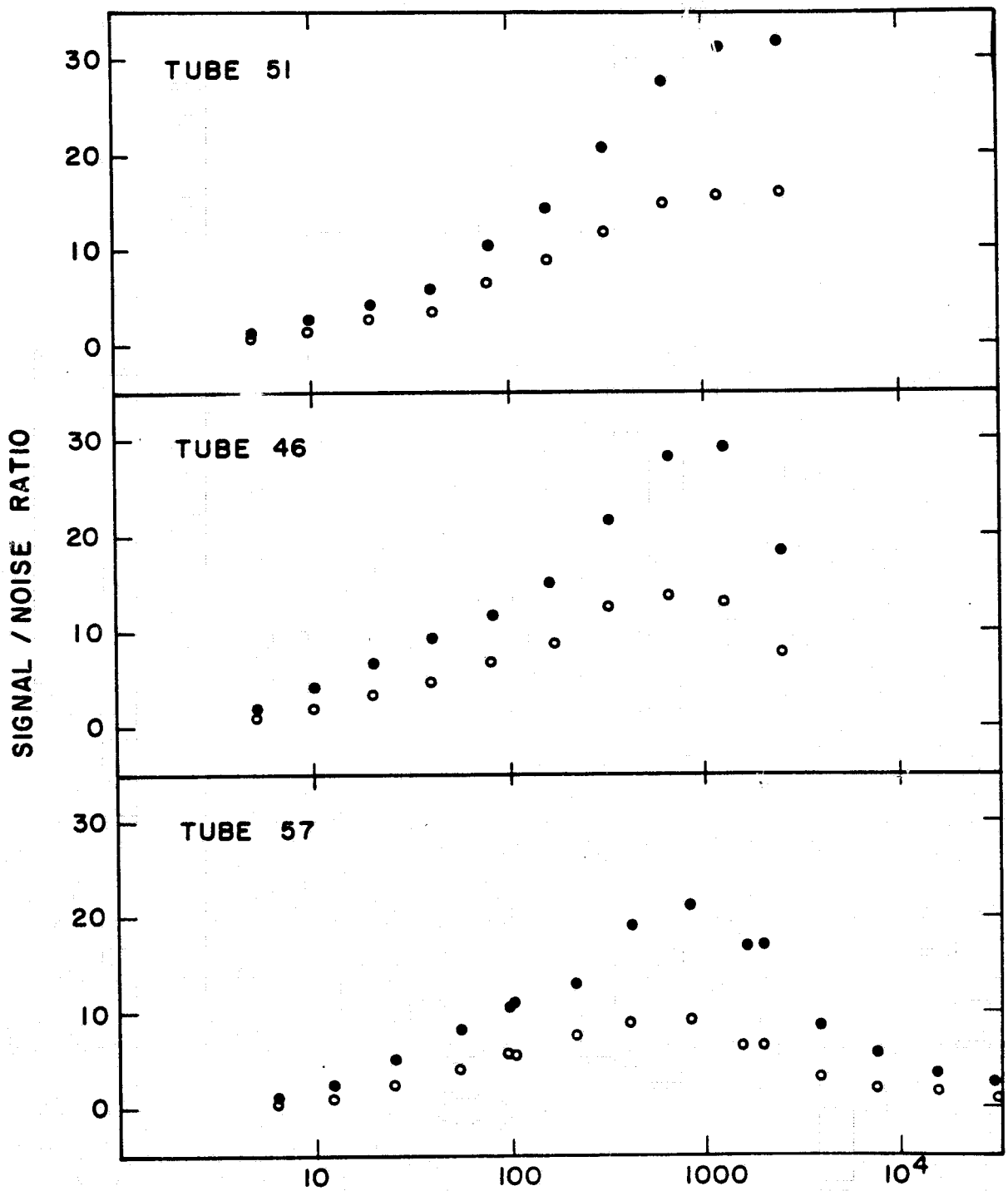

Figure 44.2

Signal-to-noise ratios. Filled circles represent 50μ pixels, open circles 25μ pixels.

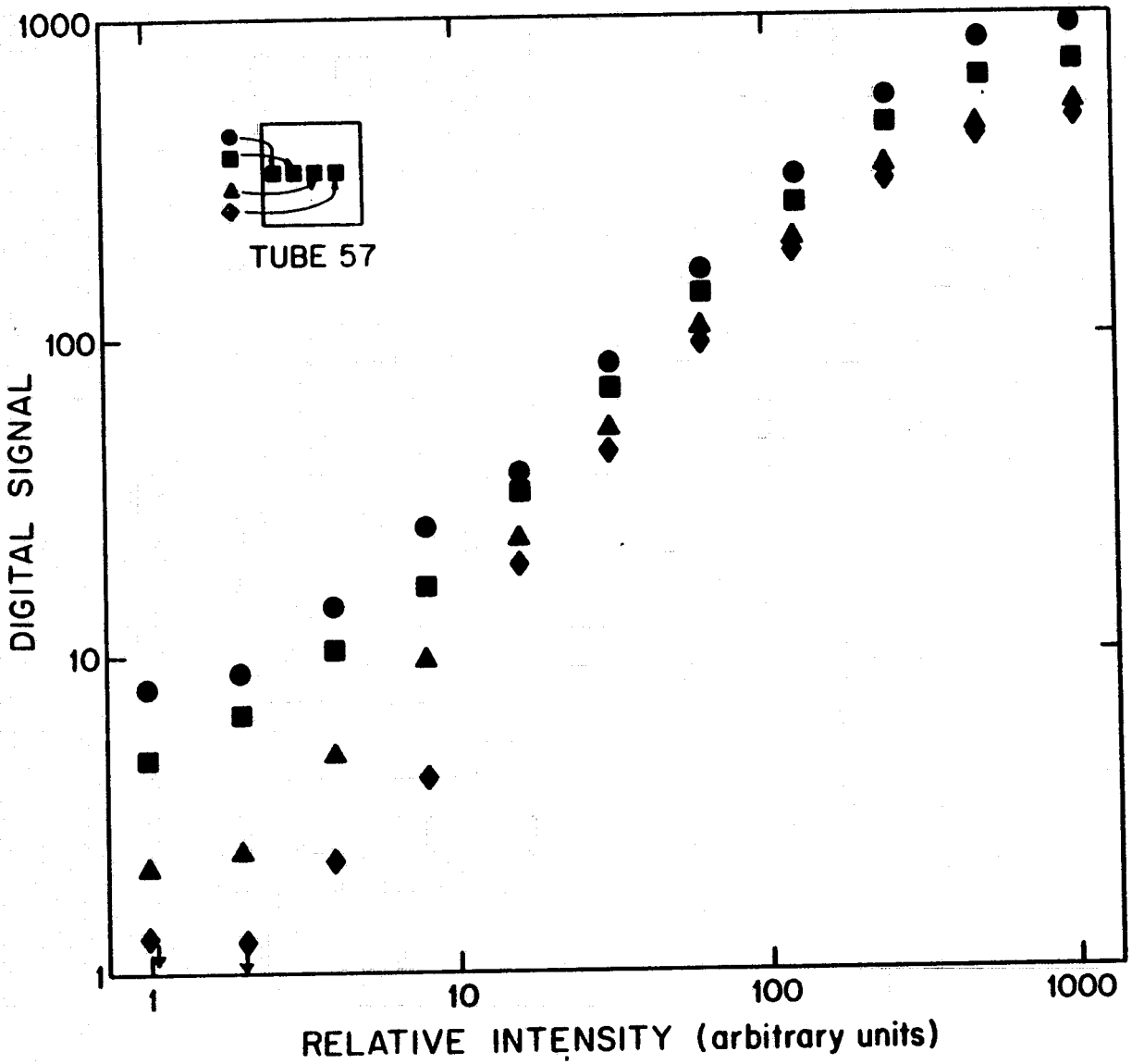

Figure 443

Response curves at four different places on Tube 57. The diagram shows the locations of the patches.

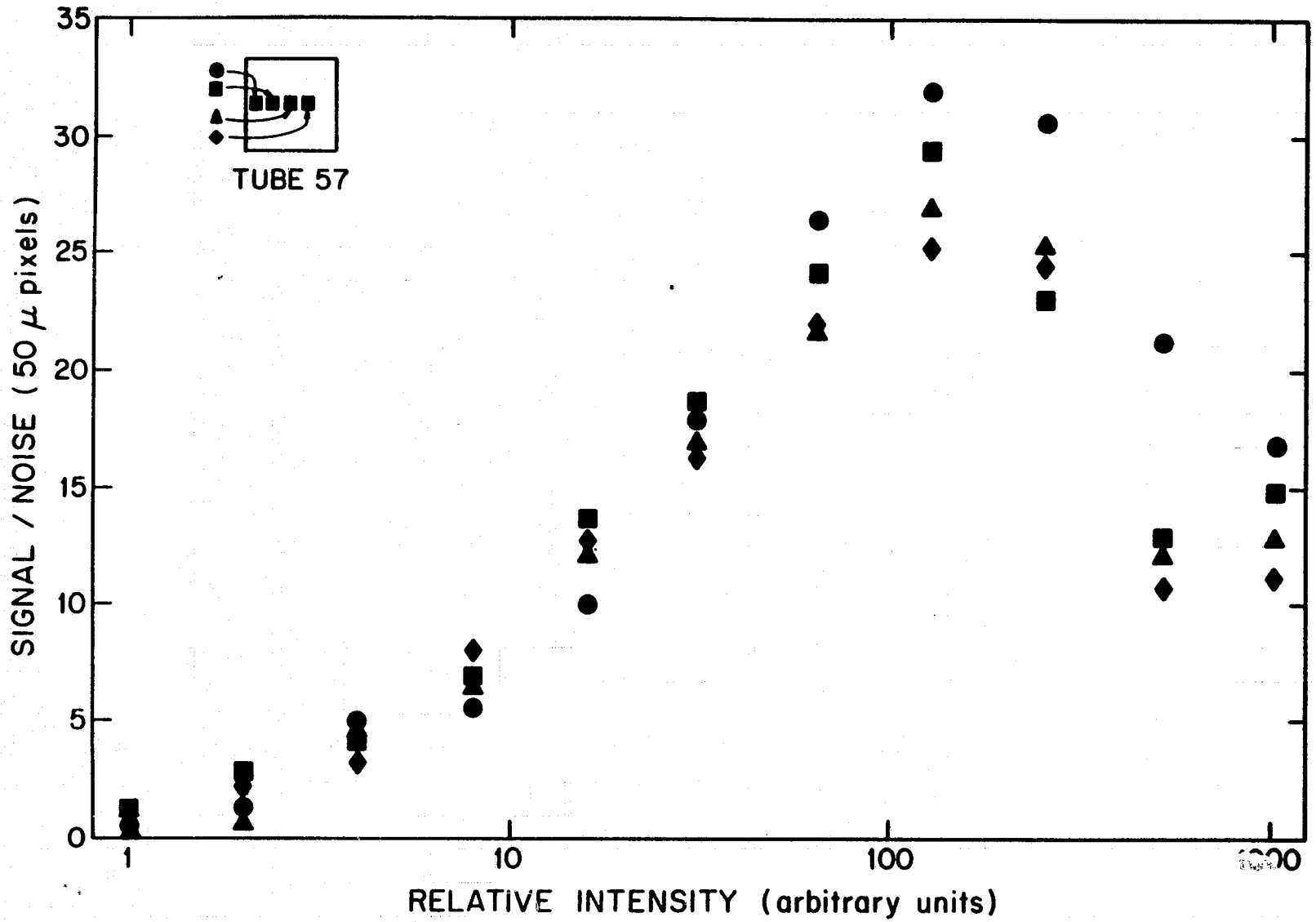

Figure 444

Signal-to-noise ratios for 50 micron pixels at four different places on Tube 57. The diagram shows the locations of the patches.

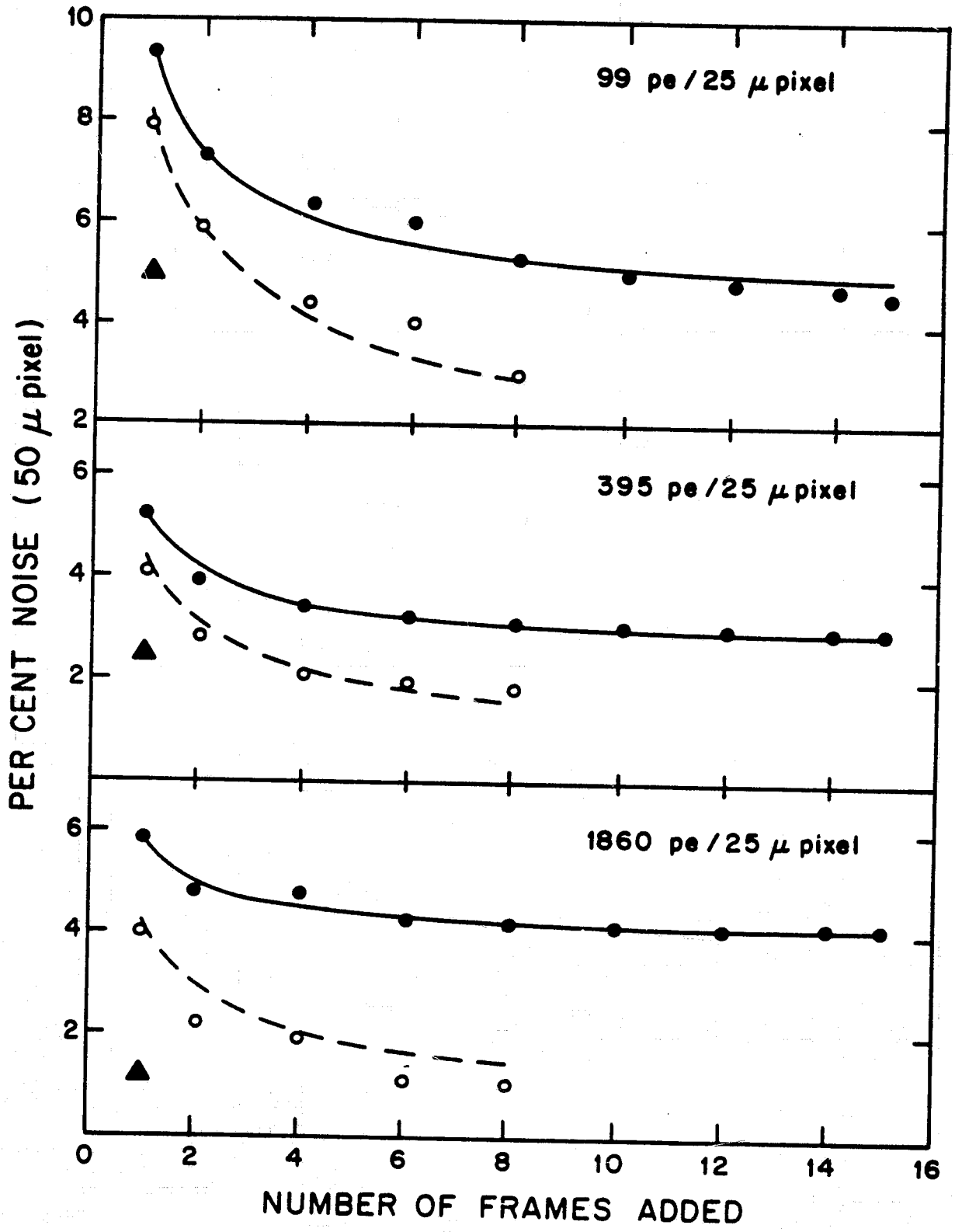

Figure 445

Multiple frame statistics for tube 57. Filled circles are noise in multiple frame summations. Solid curves are fit of $\sigma = (A^2 + B^2/N)^{1/2}$ to those data. Dashed curves are $B/\sqrt{N}$ part of solid curve. Open circles are noise in subtracted frames. Triangles represent the noise in an ideal detector.

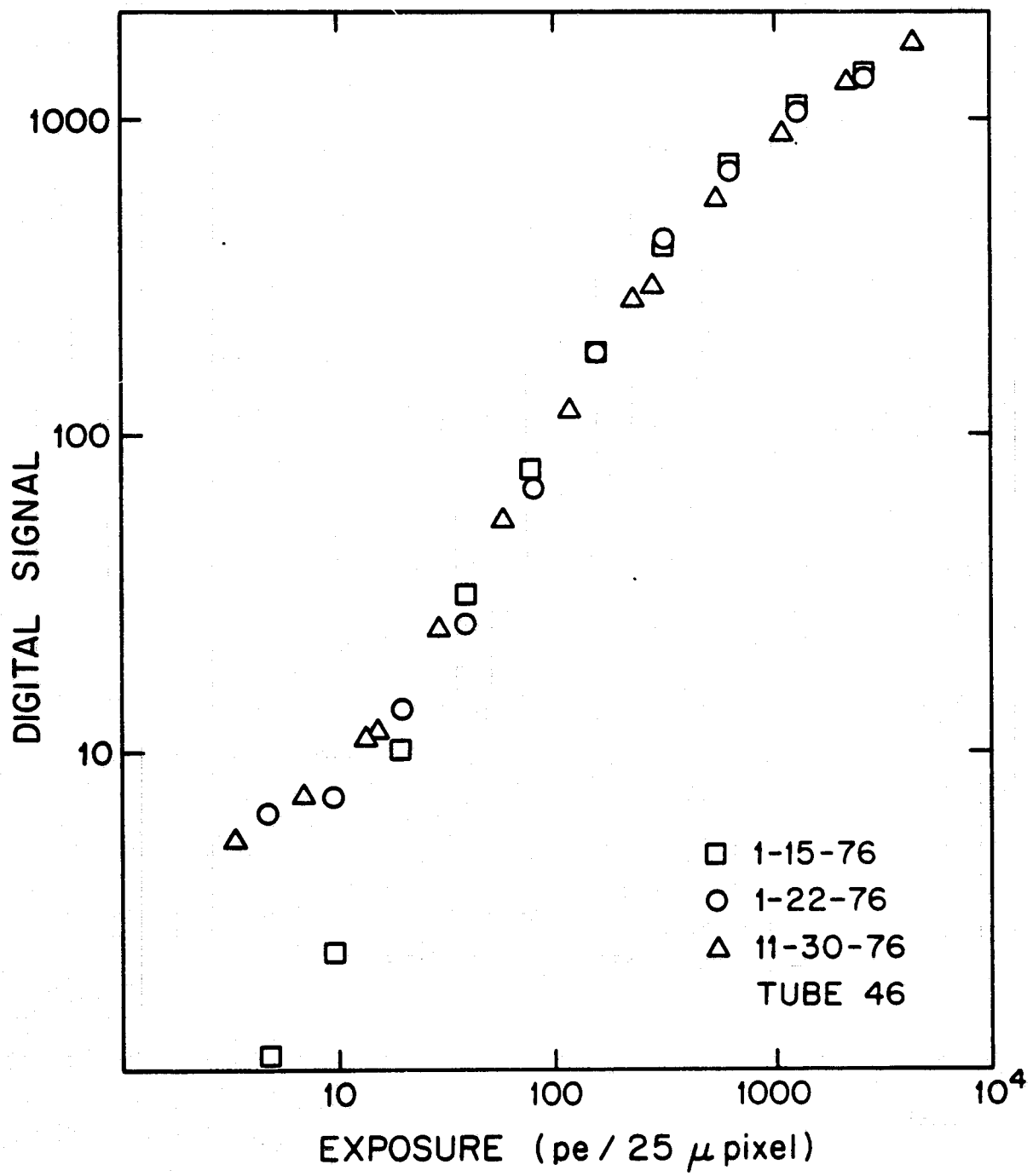

Figure 446

Reproducibility of photoresponse. Squares are 1-15-76 measurements; circles are 1-22-76 measurement. Triangles are 11-30-76 measurements. There is an arbitrary shift in both axes between the triangles and the other two sets of points.

Section 51 Magnetic Material in Tube Assembly.

Kovar is an alloy of nickel whose thermal expansion coefficient closely matches that of the glass used in vacuum tube fabrications. Unfortunately it is magnetic and results in magnetic field distortion. It also provides a mechanical coupling of the magnetic deflection field to the tube structure which can generate microphonic signals especially from the target membrane and mesh.

In the design of the 70 mm SEC tube, the target frame was designed to be alumina, a ceramic replacing the Kovar frame. This removed the magnetic field distortion right at the edge of the scanned area. Other Kovar parts were removed where it did not require development of a new manufacturing process; a conservative approach taken to minimize the problems in building this new tube, and to see how well it performed with those magnetic parts that were left, such as the glass to Kovar seal at the junction of the image section and the gun section. Kovar rings formed the image section electrodes and a Kovar flange was used to mount the MgF_2 window to the image section because the ceramic parts had about the same thermal expansion coefficient too and Westinghouse made a number of their tubes with Kovar to ceramic brazed parts.

As noted in Section 43 the off-axis performance of the tube is below that on-axis. This is attributed primarily to the relatively thick Kovar flanges at the front and back of the image section. We have explored the possibility of replacing the Kovar front flange with molybdenum. Westinghouse had the company that electron beam welds the gold foil to the Kovar do the same with molybdenum. The weld was found to be vacuum tight. From this preliminary test we are optimistic that the critical seal of the MgF_2 window to the tube can be made. The MgF_2 is sealed to gold foil with frit glass, with the flexible gold foil serving to accommodate the difference in thermal expansion coefficient between

the window and the flange. Molybdenum has been used in place of Kovar in the past for glass to metal seals. However, it is not normally used because Molybdenum is much more difficult to work.

Section 52 Microphonics during Readout.

Microphonic noise signals, generated in the SEC tubes, have bothered users of these devices to varying degrees whenever the large format SEC tubes have been used at slow scan rates. Both the SEC target, and to a lesser extent, the field mesh, are capable of high-Q vibrations in various "drum head" modes. Since there is a large potential difference (about 500 volts) between the field mesh and the target, and they are rather large parallel elements (spaced about 6 mm apart), they form an excellent capacitor microphone.

Even in a spacecraft application, where mechanical and acoustical excitation would be rather unlikely, there are other mechanisms for exciting microphonic vibrations of the target and field mesh assembly. A major input source can be the deflection fields for scanning the target during readout. Even non-magnetic parts can be driven by varying magnetic fields. Electrostatic excitation is another input mode. Ball Brothers Research Corp. discovered that a fast rise time of their field mesh potential would induce microphonic causing target-field mesh vibrations.

The frequencies involved in both the 35 mm and the 70 mm format SEC tubes range from a few hundred Hertz up to about two kiloHertz. As one would expect, the 70 mm tube microphonic frequencies are mostly in the lower part of the range, while the 35 mm tube's microphonics are in the upper portion. Unfortunately these frequencies are virtually centered in the slow-scan video signal spectrum.

There are four basic approaches to solving the microphonic problem:

1. Avoiding the excitation.
2. Processing the data.
3. Changing the data spectrum.
4. Redesign the SEC tube.

Of these four approaches, the first: avoiding the excitation of the vibrating modes, has been the usual technique. Controlling deflection and electrode rise

times, turning off of cooling gas streams during readout, and simply delaying a data readout until the vibrations damp down, are all used to try to control the problem.

The second approach, processing the data, has been met with very little enthusiasm among those who will have to efficiently extract scientific data from the television signals. The data extraction problem (including pixel-to-pixel calibrations) is difficult enough without adding another filtering process that may well contribute unanticipated artifacts to the data. It does not seem prudent to rely on this approach to cope with the bulk of the microphonic problem.

The third approach to the microphonic problem: changing the data spectrum, has a definite appeal because it is a "sure-cure" solution. Unfortunately it has side effects. It is not feasible to simply increase or decrease the scan rate sufficiently to separate the video spectrum from the microphonic spectrum, because the change would have to be so great, about 200:1, that the low noise readout properties would be lost.

A more practical way of spectrally separating the data from the microphonics, is to put the data on a carrier by modulating or chopping the readout beam. A beam chopping rate of two beam-on pulses per pixel is sufficient to spectrally separate the data from the microphonic signals. This method has been tried at Princeton (in fact, is still part of the test set, but rarely used) with complete success at eliminating the microphonics, but the preamplifier noise performance was degraded by a factor of about 3:1. It is not clear whether it is theoretically or practically possible to have a chopped beam video system that has the same low noise characteristics as a direct beam system. We recommend this topic for further research.

The fourth approach: redesigning the SEC tube, has some clear-cut limitations. First, the very nature of the SEC target and its vacuum environment tend to make

it an excellent vibrator. Many changes have already been implemented in the past to help minimize microphonics. For example, the target frame is intentionally rectangular as opposed to round or square. Unless someone has an entirely new idea, there does not seem to be much opportunity to significantly help the microphonic situation by means of tube design changes.

Section 53 Target Antireflection Coatings.

The high photometric accuracy required from the f/24 Detector system makes it important to minimize the internal optical reflections within the image section of the tube. The walls are now coated with chrome oxide which results in a flat green surface. The aperture plate that precedes the target is made out of metal and can be easily darkened. The SEC target also needs to be made antireflecting and this is a more complex problem.

The target as shown schematically in Figure 211 is composed of a transparent aluminum oxide substrate with an aluminum signal plate. This makes a mirror-like surface. Aluminum is evaporated in an argon atmosphere to create a coating of aluminum particles called "aluminum black" that traps the light. This layer is critical in that its uniformity and thickness affect the target's performance. In the energy range of the photoelectrons hitting the target, 8kV, the energy loss and transmission are nearly linear functions of the mass traversed by the electrons. Therefore, one wants a very thin low mass layer of material preceding the KCl so that almost all of the photoelectrons generated at the photocathode actually reach the KCl and contribute to the video signal. Any nonuniformity in this layer is undesirable also, resulting in a fine grain fixed pattern of noise or broad shading if the nonuniformity is smoothly changing.

A 35 mm tube, No. 46, has a target that is coated with an antireflecting coating of "aluminum black" over half of its area. This has facilitated the study of the effect of the antireflection coating on the effective quantum efficiency of the tube.

The reflected light from the uncoated portion of the target was found to be 4.2% while the reflected light from the aluminum black side was immeasurably small.

Figure 531 shows the tube's signal current in pico amperes as a function of accelerating voltage for both sections of the target, including an area near the center where the aluminum black was thicker. At low photocathode voltages the lower signal is due to loss of energy by photoelectrons that pass through the aluminum black but reach the KCl layer and also to absorption of photoelectrons before reaching the KCl layer. At higher accelerating voltages the photoelectrons that reach the KCl do so at an energy that results in about the same gain in both the coated and uncoated sides of the target as evidenced by the flattening of the curves. The 20% lower signal on the aluminum black side is attributed, to a first approximation, to a corresponding loss in photoelectrons. Therefore, it is important to make the aluminum black coating just thick enough to kill the optical reflection since it also reduces the tube's overall quantum efficiency.

Westinghouse will be working in the continuing contract for the 70 mm SEC tube development, to develop a uniform aluminum black layer on the target that is the minimum thickness necessary to attenuate the optical reflection of the target. They anticipate some problems in achieving good uniformity near the edges of the target because of the shape of the target support. The aluminum oxide membrane is stretched across the rectangular ceramic frame on the electron gun side. This results in a step at the edge of the target on the photocathode side that is the thickness of the ceramic frame. Some relief of this edge may be necessary to present a more gradual change in depth as seen by the aluminum particles during evaporation.

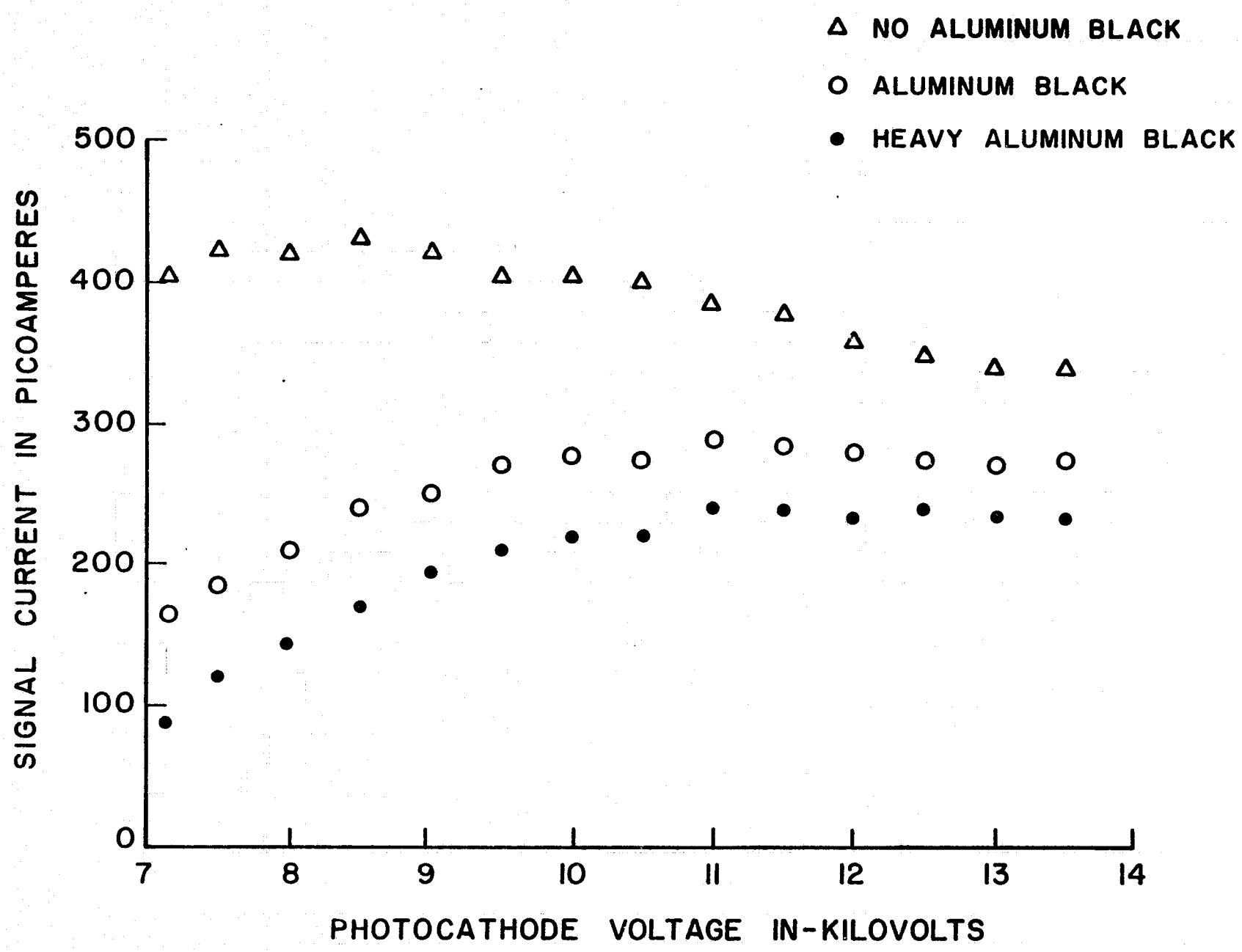
NO ALUMINUM BLACK
ALUMINUM BLACK
HEAVY ALUMINUM BLACK
SIGNAL CURRENT IN PICOAMPERES
500
400
300
200
100
0
7
8
9
10
11
12
13
14
PHOTOCATHODE VOLTAGE IN-KILOVOLTS

Figure 531

Section 54 Target Leakage

For many years, the image storing properties of the SEC target were well beyond the requirements of the ST mission. SEC targets would typically store images for days without measurable change. Unfortunately that is not the case with current SEC targets. They have significant leakage of the stored image pattern after storage periods of from several minutes up to about ten hours. (See the tube census data in section 41.)

For the ST mission the targets should ideally store an image for at least one orbital period of the spacecraft without any measurable charge leakage. Somewhat less than ideal, would be a leakage magnitude that could be corrected in the data reduction for one orbit stores.

This problem is now getting priority attention in the continuing SEC tube development program, and since SEC targets were made in the past with superb storage capabilities, there is every reason to think this problem will be solved in the near future.

Section 55 Image Section Background

One of the major goals in developing a television tube for future space astronomy missions was to reduce the tube's internal background such that very long exposures could be made at near ambient temperature without the resultant signal being dominated by the dark current of the tube. Here it should be pointed out that dark current of the tube is not just the dark current from the photocathode but includes any stray signals generated in the tube that are stored in the target. Early tubes were improved by coating the walls of the image section of the tube with chrome oxide. This green opaque coating served to block light that might be generated due to fluorescence in the glass. It also tended to reduce voltage gradients along the wall of the tube. With bi-alkali photocathodes very long exposures, i.e., very low tube background, were possible. In a six-hour exposure at room temperature the image section background was less than 10% of the dynamic range as measured on one occasion when observing at the 200" telescope at Mt. Palomar. However, in all cases, the image section background of the tube has been found to be appreciably larger than the published values for the photocathode dark current in photoelectrons per square centimeter. While we do not fully understand the mechanisms for this it seems to be tied to gas in the tube and some emission from the walls of the tube which may generate electrons, or photons, that, in turn, excite the photocathode. Electrons generated on the wall of the tube itself are not able to reach the target because of the 80 Gauss magnetic field that is aligned with the axis of the tube. A photoelectron emitted from the wall of the tube usually has an energy in the order of a Volt or two. This is insufficient for the electron to move very far from the wall because of the constraining magnetic field. However, if this electron is accelerated along the wall until it hits something and is reflected or generates a secondary emission electron then the electron having

an energy of several Volts can perhaps get out into the region where it will land on the target. Tubes which have good red response, i.e., a low work function also seem to have much higher dark current as is typical for red response photocathodes. We feel that this is primarily due to cesium reacting with other photocathode materials that find their way to the wall of the image section of the tube, thereby lowering the work function of these surfaces and making them more likely to have both photo emission and field emission. It would, of course, be an advantage to process the tubes in such a way that the photocathode materials do not coat the walls of the tube, however, making a transfer photocathode is not within Westinghouse's present capability and the cost of developing such manufacturing techniques has never been within the financial scope of the development program. In the present 70 mm tube design the image section is made up of ceramic rings about $\frac{1}{2}$" apart with thin Kovar metal annular rings forming the metal electrodes. These metal electrodes now protrude only about 1/16" into the image section. It has been recommended that the inner diameter of the Kovar rings be reduced such that electrons accelerated along the walls of the tube by the voltage between the rings will hit the rings and not continue to cascade down the tube. Extending the rings further into the tube also provides a means of shadowing the ceramic walls of the tube from the antimony evaporation and some of the other photocathode constituents. This shadowing, of course, is not complete but it does break up the coating particularly near the photocathode end of the tube where the electrons generated have the greatest possibility of reaching a higher energy. Extending the Kovar rings into the tube can of course accentuate any deleterious effects on the magnetic field near the region of interest, however, as discussed elsewhere in this report these rings will be replaced by non-magnetic parts in the near future. The other source of background signal is the residual gas in the tube being ionized, and these ions striking the photocathodes. Others have reported a yield of about

25 photoelectrons per ion hitting the photocathode of the tube. For ions to contribute no more than the sky background these ions must be no more than about 25 per square cm per sec in the tube. Westinghouse has experience where the background in other tubes has been reduced by what they call scrubbing the tube. That is, running the tube for an extended period of time with the electron gun operating and scanning the mesh and target of the tube. Indeed, most all tubes up until recently have been routinely operated at fast scan (broadcast) rates in the Westinghouse test set as a part of the preliminary testing of the tube. This would serve to do a certain amount of scrubbing. In the special tubes made on this contract often the tubes have not been operated at all by Westinghouse, or have been operated at slow scan where the actual number of minutes of operation at beam currents comparable to those used for scrubbing have been insignificant. A program to reinstate scrubbing and including, in some cases, scrubbing the tube while still being pumped is being seriously considered.

Section 60 Photocathode/Window Development.

The f/24 Camera mission calls for a tube sensitive from the vacuum ultraviolet into the far red. The photocathode/window combination that meets that requirement is a magnesium fluoride window with a S-20 type photocathode. Magnesium fluoride windows had been used with bi-alkali photocathodes in a number of 35 mm format tubes and the techniques for sealing the MgF_2 windows to the tube was well worked out. The window is bonded around the outer surface to a flat annular ring of gold foil. The outer edge of the gold ring is electron beam welded to a Kovar metal flange which is, in turn, heliarc welded to a mating Kovar flange brazed to the tube's image section.

Some 35 mm format tubes with S-20 photocathodes had been made and were used for ground-based observing. However, attempts to make S-20 photocathodes on MgF_2 windows resulted in a relatively low peak quantum efficiency and lower than normal red response. In addition, there were problems learning how to process photocathodes in the geometry presented by the new 70 mm tube envelopes.

After making several 70 mm tubes with poor photocathodes it was decided that a special effort should be initiated to first work out the problems of making an S-20 photocathode on magnesium fluoride. This was broadened to include oxidized bi-alkali photocathodes which our photocathode consultant, Dr. Alfred Sommer, recommended as having a very high quantum efficiency in the visible and respectable red response. He also predicted that the ultraviolet response of the bi-alkali would be higher than that of the S-20 photocathodes. The response of one 70 mm tube made with an oxidized bi-alkali photocathode is shown in Fig. 608.

Westinghouse proposed a photocathode development program in which 50 photodiodes and 8 of the 35 mm SEC tubes would be built and evaluated. The effort under this existing contract was redirected to start this work with the expectation that the program would be continued under the next contract with NASA for the 70 mm SEC tube development.

The test vehicle for these experiments was the image section of the 35 mm tube. These were inexpensive and could be quickly fabricated from standard parts. Both a glass and magnesium fluoride window were mounted inside the glass envelope to allow comparison of the photoresponse in the two cases.

Experimental Data

Table 601 presents a summary of the photodiodes that were made under this contract. The second column, reference window, indicates the 7056 glass window that was included in each tube to act as a control on the process with the magnesium fluoride. Under the experimental window column the magnesium fluoride in most cases was coated with a semi-transparent layer of chrome or paladium, and the thickness 80, 90% indicates the visible light optical transmission of this layer. It should be noted that the metal layer serves two purposes. In some photocathodes, not necessarily the S-20, the resistivity of the photocathode is high enough that a metal underlayer is necessary to lower the lateral resistivity ofthe surface so that variations in the electrostatic field do not occur, both as a function of light and when turning on and off the photocathode supply. A metal layer was also felt to be worth pursuing in this application as a buffer layer to chemically isolate the photocathode materials from the magnesium fluoride. This was based on experience we had had in developing a bi-alkali photocathode on magnesium fluoride in an earlier program where it was found that a paladium underlayer yielded very acceptable quantum efficiencies in the blue and in the ultraviolet. Under the Glow Discharge is a cleaning process in which a gas, usually oxygen, is ionized by RF field which then acts to clean the window and other parts of the tube. Of the twenty-eight photo diodes made, 22 had S-20 photocathodes, 3 had bi-alkali photocathodes, and 3 were mechanical failures.

Table 602 presents the photoresponse obtained on the magnesium fluoride windows in each photodiode. The third column gives the wavelength in nanometers of maximum response of the photocathodes. The fourth column gives the response

TABLE 601

Experiment No.	Reference Window	Experimental Window	Propanol Vapor Cleaning Sch.	Glow-Discharge	Remarks
001	Clear Glass	Clear MgF_2	Window Assembly	Yes	
002	Clear Glass	Clear MgF_2	Window only	Yes	
003	Clear Glass	Glass + 70%Cr	Window only	Yes	
004	Clear Glass	Glass + 70%Cr	Window only	No	
005	Clear Glass	MgF_2 + 70%Cr	Window only	No	
006	Clear Glass	Glass + 70%Cr	All parts	No	
007	Clear Glass	MgF_2 + 70%Cr	All parts	No	
008	Clear Glass	Clear MgF_2	All parts	Yes	
009	Clear Glass	MgF_2 + 70%Cr	All parts	No	S-25 Schedule for Photocathode Processing
010	Clear Glass	MgF_2 + 80%Cr	All parts	No	
011	Clear Glass	MgF_2 + 80%Cr	All parts	No	
012	Clear Glass	MgF_2 + 90%Cr	All parts	No	
013	Clear Glass	MgF_2 + 90%Cr	All parts	No	
014	Clear Glass	Clear MgF_2	All parts	30 sec	
015	Clear Glass	Clear MgF_2	All parts	2 min.	
016	Clear Glass	Clear MgF_2	All parts	2 min.	
017	No Glass Portion	Clear MgF_2	All parts	2 min.	
018	Clear Glass	MgF_2 + 95%Cr	All parts	No	
019	Clear Glass	MgF_2 + 95%Cr	All parts	No	
020	Clear Glass	MgF_2 + 90%Pd	All parts	No	S-20 Schedule for Processing
021	Clear Glass	MgF_2 + 90%Pd	All parts	No	
022	Clear Glass	MgF_2 + 80%Pd	All parts	No	
023	Clear Glass	MgF_2 + 95%Pd	All parts	No	
024	Clear Glass	MgF_2		2 min.	
025	Clear Glass	MgF_2 + 95%Pd	All parts	No	Bi-alkali
026	Leaker			2 min.	
027	Clear Glass	MgF_2 + 95%Pd	All parts	No	Bi-alkali
028	Clear Glass	MgF_2 + 95%Pd	All parts	No	Bi-alkali

* The percentage of chrome means white transmission

TABLE 602

A. MgF_2

Exper No.	Under layer	λ max nm	PR max mA/w	PR 500 mA/w	PR 600 mA/w	PR 700 mA/w	PR 800 mA/w	PR 400 mA/w	White PR μA/L	Comment
001	None								No contact	
002	None								110	
003	Glass Cr 70%								44	
004	Glass Cr 70%								73	
005	Cr 70%								43	
006	Cr 70%	480	42.6	42.4	27.9	9.6	0.54	21.4	125	
007	Cr 70%	500	24.4	24.4	17.0	5.9	0.39	7.92	76	
008	None	500	32.7	32.7	21.3	8.1	0.59	13.9	100	
009	Cr 70%	520	20.6	19.9	17.7	8.6	2.3	5.9	96	
010	Cr 80%	440	42.6	37.0	23	11.0	1.9	32.7	121	
011	Cr 80%	520	35.7	35.1	28.4	14.0	4.6	13.1	143	
012	Cr 90%	480	47.6	46.0	28.1	11.3	1.84	25.3	142	
013	Cr 90%	560	20.8	19.4	20.0	11.5	2.39	3.43	103	
014	None	470	40.2	37	17.9	5.79	0.35	21.7	90	
015	None	Measurement		not	done				100	
016	None	460	32.1	27	14.3	5.49	0.464	25.7	73	
017	None	Measurement not possible							105	High leakage Current
018	95%Cr	500	31.8	31.8	20.5	7.8	1.28	11.3	95	
019	95%Cr	460	24.6	20.9	8.07	0.604	-	17.1	57	Sb pre-evaporate (80%)
020	89%Pd								0	Sb pre-evaporate (80%)
021	90%Pd	520	23.7	22.7	19.1	9.27	2.33	4.82	94	
022	95%Pd	460	6.32	5.47	2.48	0.295	-	5.3	11	Sb pre-evaporate & baked @ 250°C
023	95%Pd	380	14.3	7.11	3.11	0.921	0.028	14.1	16	
024	None	560	20.6	18.2	18.6	5.59	0.245	2.64	66	Sb pre-evaporate (90%)
025*	95%Pd	400	18.9	7.7	0.64	-	-	18.9	10	Sb pre-evaporate (90%)
026	None			Leaker						
027*	95%Pd	400	19.0	9.8	1.09	0.01	-	19	9	Sb pre-evaporate (85%)
028*	95%Pd	400	29.3	15.0	0.76	-	-	29.3	17	not oxidized Sb pre-evaporate (85%)

in milliamps per watt at that peak wavelength, and the remaining columns give the photoresponse at the wavelengths shown. The white light photoresponse in microamperes per lumen is the response of the photocathode to a standard white light used at Westinghouse which actually has a great deal of red radiation and therefore tends to accentuate the response of those tubes that have more red response than others. In the latter tubes the antimony was pre-evaporated. This was a change from the standard Westinghouse process where the antimony and potassium are usually evaporated simultaneously to establish some photo response at the very beginning of the evaporation to control the process. Pre-evaporation of antimony is the procedure followed by Dr. Alfred Sommer, that allows one to control the thickness of the antimony.

Table 603 is a similar compilation of the photoresponse for the reference photocathode on glass. The reader will note that while the wavelength of peak response is about the same as on MgF_2 that the photoresponse at this wavelength is usually higher in the case of the glass windows. The response at 7000 Å is also higher in most cases for the glass as compared to the magnesium fluoride.

A better perspective of the photoresponse can be gained by reviewing the spectral response graphs shown in Section 107. In almost all cases the response of the S-20 photocahode's peak in the 4500-5000 Å region and then rolls off rather sharply in the blue. This is attributed to the thickness of the photocathode. Blue photons are absorbed near the entrance surface and the probability of the photoelectron reaching the vacuum surface and being emitted is reduced over those generated by photons absorbed nearer the vacuum side of the photocathode. The three bi-alkali photocathodes were trials at oxidizing the photocathode. In each case the process was not optimum. Too much oxygen was injected. In tubes made since then the oxidization process has been brought under control with very encouraging results.

TABLE 603

B. Reference Glass

Exper. No.	Under layer	2 max nm	PR max mA/w	PR 500 mA/w	PR 600 mA/w	PR 700 mA/w	PR 800 mA/w	PR 400 mA/w	White PR µA/L	Comment
001	None								280	
002	None								110	
003	None								0.5	
004	None								55	
005	None								55	
006	None	520	33.9	33.7	29.7	14.9	4.1	18.41	145	
007	None	500	24.6	24.6	17.2	4.8	0.14	13.3	75	
008	None	480	43.2	42.7	23.4	5.8	0.12	25.2	105	
009	None	540	11.8	10.9	9.2	3.24	0.1	5.0	50	
010	None	440	43.6	32.7	19.0	8.5	1.0	38.0	100	
011	None	500	43.1	43.1	33.3	13.5	2.7	25.3	144	
012	None	460	58.3	53.3	28.2	11.1	1.32	39.6	152	
013	None	480	33.9	33.6	27.1	13.0	1.68	16.1	130	
014	None	460	75.2	68.2	38.4	22.1	9.68	48.1	242	
015	None	Measurement not done							235	
016	None	460	51.5	43.4	29.1	14.4	3.95	38.5	148	
017	None	No glass portion.								
018	None	480	68.5	68.5	40.3	17.3	3.45	37.5	204	
019	None	460	14.3	12.3	4.16	0.15	-	9.26	33	
020	None								0	
021	None	520	37.3	35.8	30.7	14.0	3.29	15.5	135	
022	None	440	11.9	10.4	4.48	0.427	-	7.82	21	
023	None	380	12.7	6.21	2.37	0.494	-	11.9	12.5	
024	None	560	42.5	40.3	39.1	19.8	3.4	14.9	175	Baked @ 350°C glow
025*	None	360	22.1	6.9	0.42	0.002	-	19.7	10	Baked @ 350°C
026				Leaker						
027*	None	460	36.1	32	3.78	0.009	-	27.5	27	Processed with Blue light
028*	None	400	66.4	46.2	3.78	0.005	-	66.4	57	

REPRODUCIBILITY OF T
ORIGINAL PAGE IS POO
REPRODUC

There seems to be a clear tradeoff of blue response for red response since the thicker photocathodes absorb more red photons enhancing their red photo-response. One can expect the ultraviolet response to vary as a functionof the photon energy since high energy photons generate comparable energy electrons which can produce secondaries within the material. This in turn improves the probability that a photoelectron is emitted.

While the photodiodes were useful for measuring the response of the photo-cathodes in visible light they were not suitable for making measurements in the ultraviolet because of the cutoff of the glass envelope. A 35 mm tube was built with a magnesium window to evaluate the ultraviolet response of the S-20 photocathode. Those results are shown in Figures 601 and 602. One notes that the quantum efficiency is not particularly high in this tube; about half the response of the better photodiodes. It has 5% quantum efficiency at the 4600 Å peak. It then levels off at a little over 3% quantum efficiency at shorter wavelengths. The response in the ultraviolet remained at approximately 3% with a slight dip around 2200 Å rising to a quantum efficiency of about 7% near 1200 Å. This tube had a 95% transmission chrome layer and a white light response of 30 micro-amps per lumen. Because of the marginal results with magnesium fluoride S-20 photocathodes combination we decided to explore the oxidized bi-alkali photo-cathode on magnesium fluoride which had been recommended by Dr. Sommer. This is a potassium-cesium-antimony photocathode which, as a final step, after the photocathode has been made, a small amount of oxygen is introduced. This gives the photocathode much more red sensitivity than the straight bi-alkali. Only three photodiodes with bi-alkali photodiodes were made under this contract. However, it was clear that one obtained higher peak quantum efficiencies; in this case around 4000 Å, but at the same time gave up red response. This is clear from looking at Table 602. In the continuation of this program to develop

a good photocathode magnesium flucride we found that the bi-alkali photocathodes do have high quantum efficiency in the ultraviolet, ranging between 10 and 15%. The red response continues to be lower than that obtained with the S-20 photocathodes.

UV Transmission of Magnesium Fluoride and Metal Undercoat

As mentioned above, a metal undercoat serves to reduce the lateral resistivity of photocathodes and we had determined in an earlier work that a metal undercoat resulted in higher quantum efficiency bi-alkali photocathodes. Three different metals were evaluated for possible use as undercoats. These were nickel, chrome and paladium. Figures 603 , 604 , 605 show the transmission of these various layers in the vacuum ultraviolet. Their thickness is designated by the percentage transmission in the visible 90% transmission means 90% of white light was transmitted by this metal layer. These figures indicate a slight advantage in using paladium due to its somewhat higher transmission in the ultraviolet than chrome, both of which are superior to nickel. A 90% visible transmission layer of paladium maintains at least an 80% transmission out to the magnesium fluoride cutoff at 1150 Å.

Figures 606 and 607 show the ultraviolet transmission of three MgF_2 windows, 2 mm, 5.5 mm and 6.3 mm thick. The transmission at aery short wavelengths varies from batch to batch. There is some evidence that the transmission can be improved by polishing. Under a separate contract we are having Harshaw, the MgF_2 vendor, investigate manufacturing techniques that may reduce the fluorescence and phosphorescence of the windows when irradiated with the energetic charged particles anticipated in the Space Telescope orbit. This work at Harshaw may also serve to establish better control over the ultraviolet transmission.

Interim Conclusions and Plans

As noted earlier, this work on photocathode development in the first part of a larger program. In continuing the program several more bi-alkali photocathodes will be fabricated in the photodiode test vehicles to allow comparison with the S-20 photocathode characteristics. This will include making two or more 35 mm tubes so that the ultraviolet response of the oxidized bi-alkali photocathode can be determined. Following this, several S-20 photocathodes will be made using the skills developed in the pre-evaporation of the antimony. Upon the completion of this work and other measurements such as dark current, a recommendation will be made to drop one of the photocathodes and concentrate on developing the other in the 70 mm tube.

It should be noted that subsequent work has shown the ability to consistently make good oxidized bi-alkali photocathodes through the red response is still not as good as the S-20 should give. Dark current measurements using a 35 mm tube with an oxidized bi-alkali photocathode are planned but have not been made.

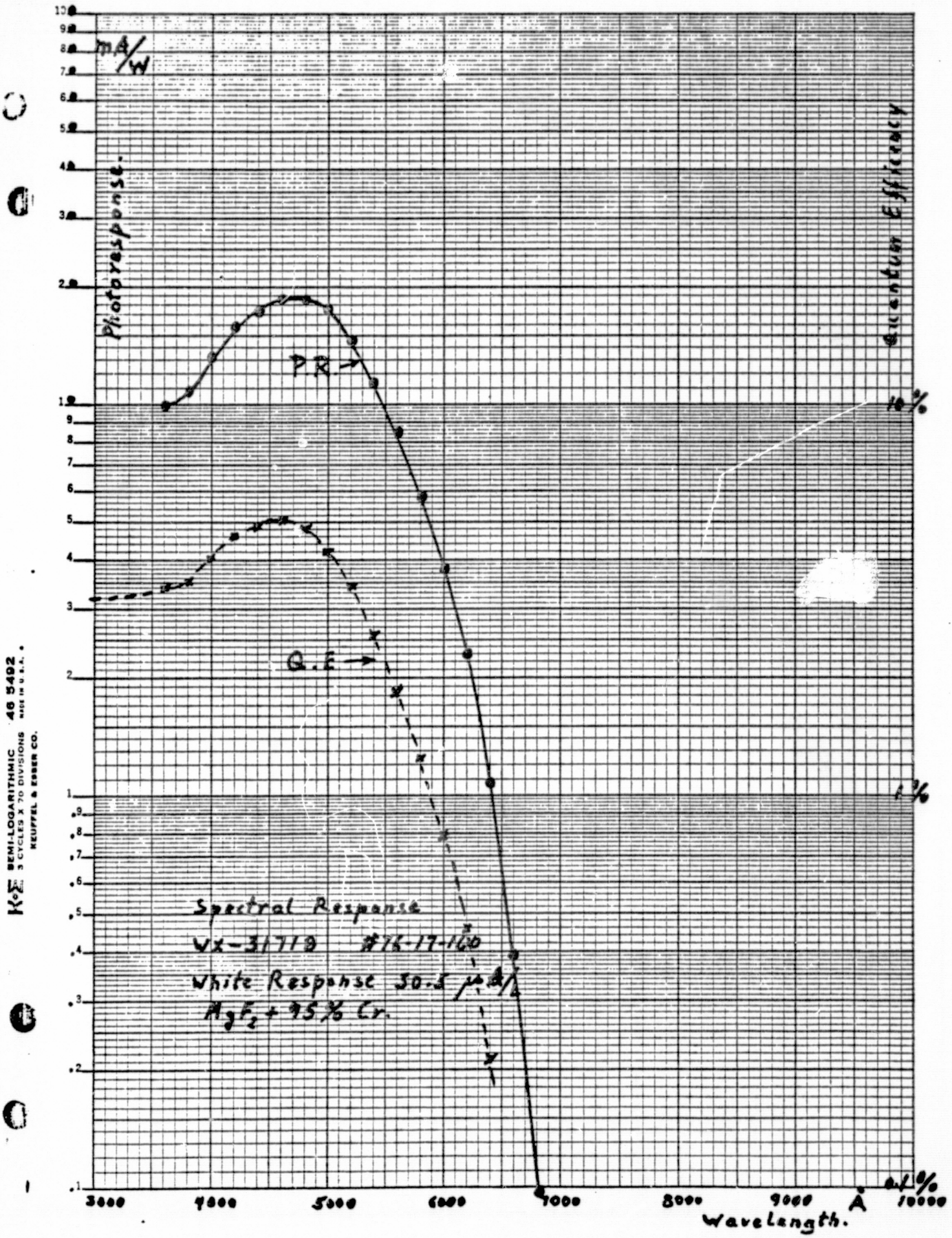
mA/W
Photoresponse.
P.R.
Quantum Efficiency
10%
1%
0.1%
Q.E.
Spectral Response
VX-31710 #76-17-160
White Response 30.5 μA/L
MgF2 + 95% Cr.
3000
4000
5000
6000
7000
8000
9000
Å
10000
Wavelength.
KEUFFEL & ESSER CO.
SEMI-LOGARITHMIC
3 CYCLES X 70 DIVISIONS
46 5492

Figure 601

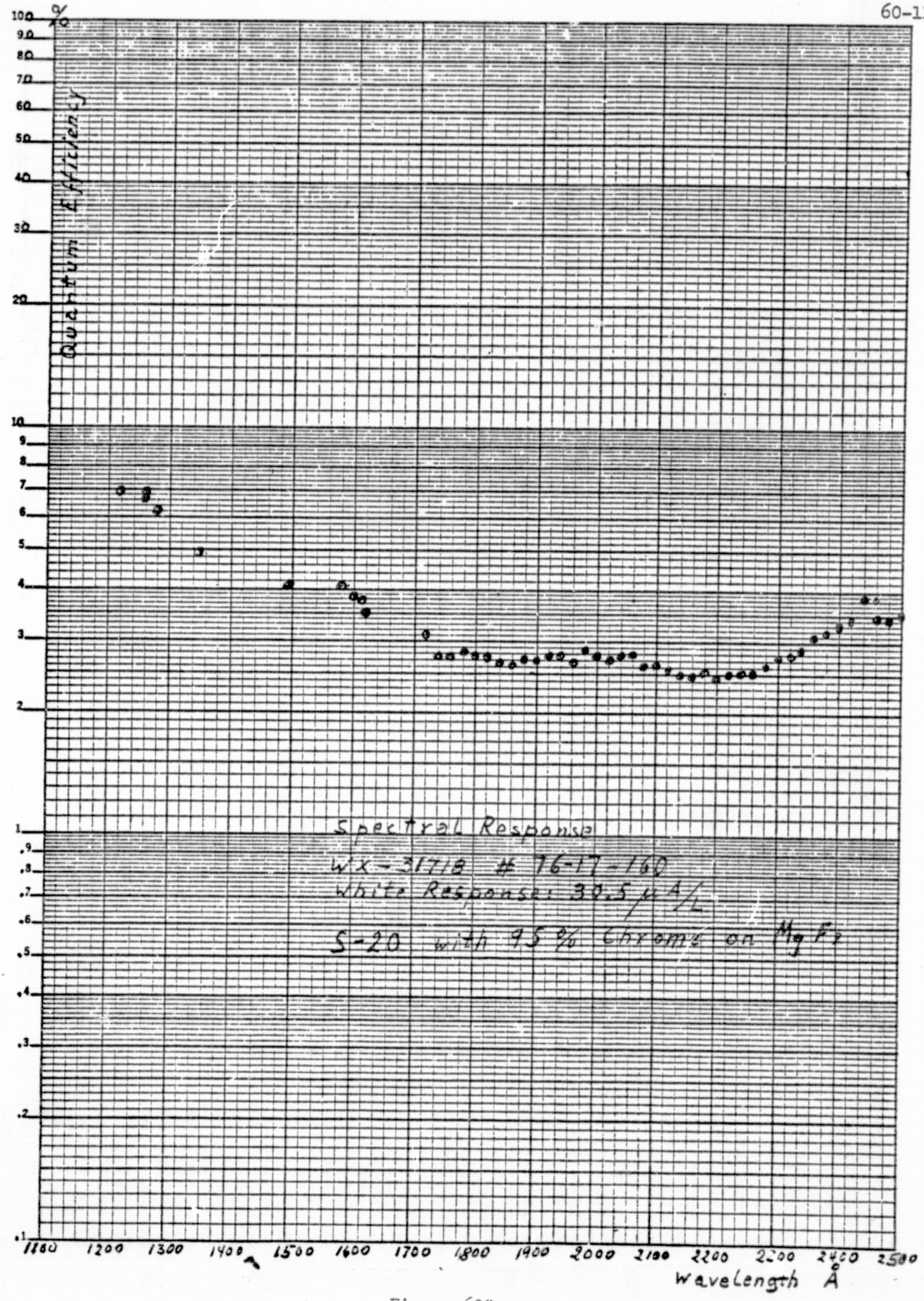
%
Quantum Efficiency
100
90
80
70
60
50
40
30
20
10
9
8
7
6
5
4
3
2
1
.9
.8
.7
.6
.5
.4
.3
.2
.1
1100
1200
1300
1400
1500
1600
1700
1800
1900
2000
2100
2200
2300
2400
2500
Wavelength Å
Spectral Response
W.X. - 31718 # 76-17-160
White Response: 30.5 μA/L
S-20 with 95% Chromic on MgF2
KEUFFEL & ESSER CO.
SEMI-LOGARITHMIC 46 5492
3 CYCLES X 70 DIVISIONS

Figure 602

KEUFFEL & ESSER CO.

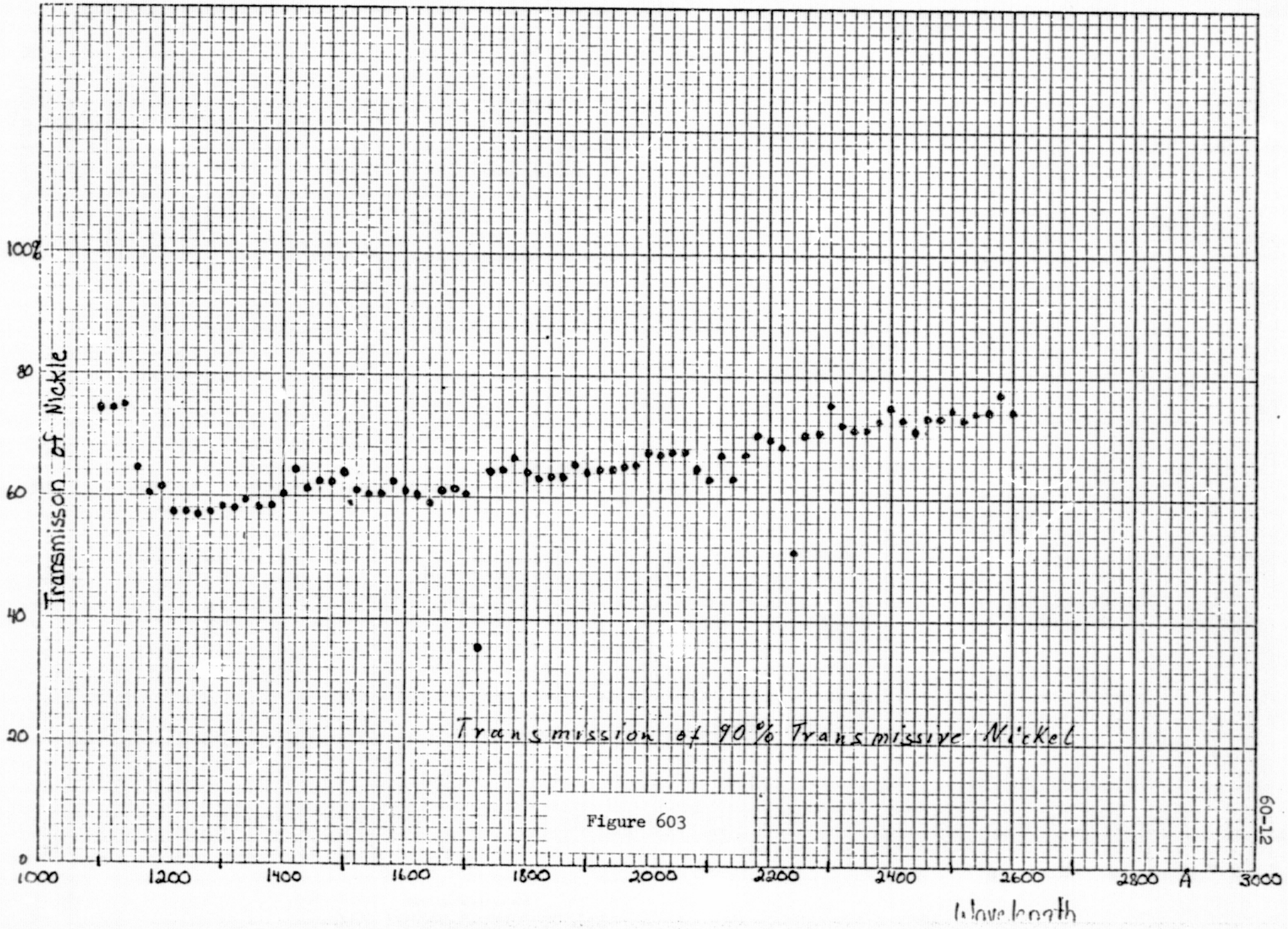

Figure 603

K&E 10 X 10 TO THE INCH 46 0702
7 X 10 INCHES MADE IN U.S.A.
KEUFFEL & ESSER CO.

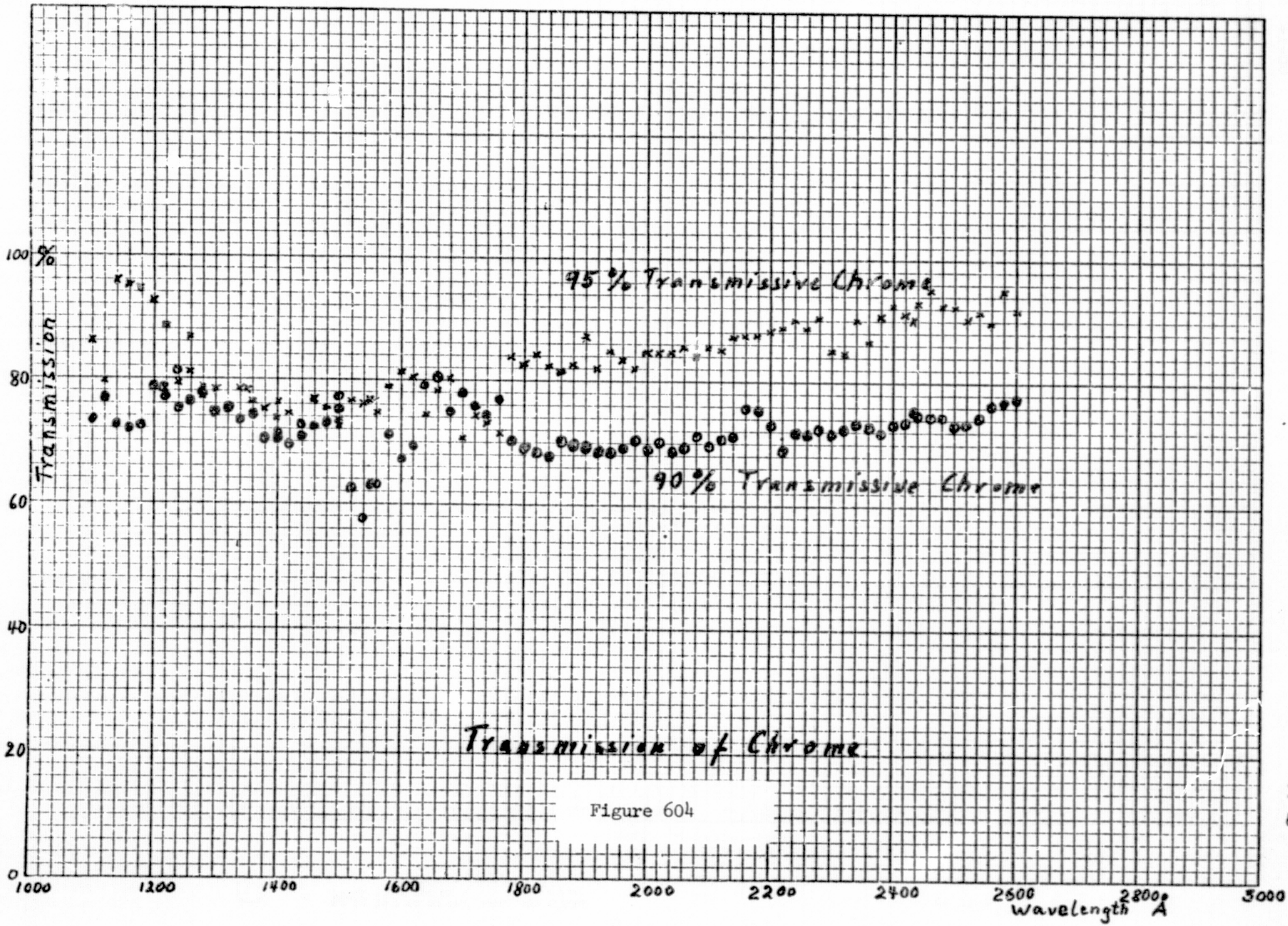

Figure 604

K&E 10 X 10 TO THE INCH 46 0702
7 X 10 INCHES MADE IN U.S.A.
KEUFFEL & ESSER CO.

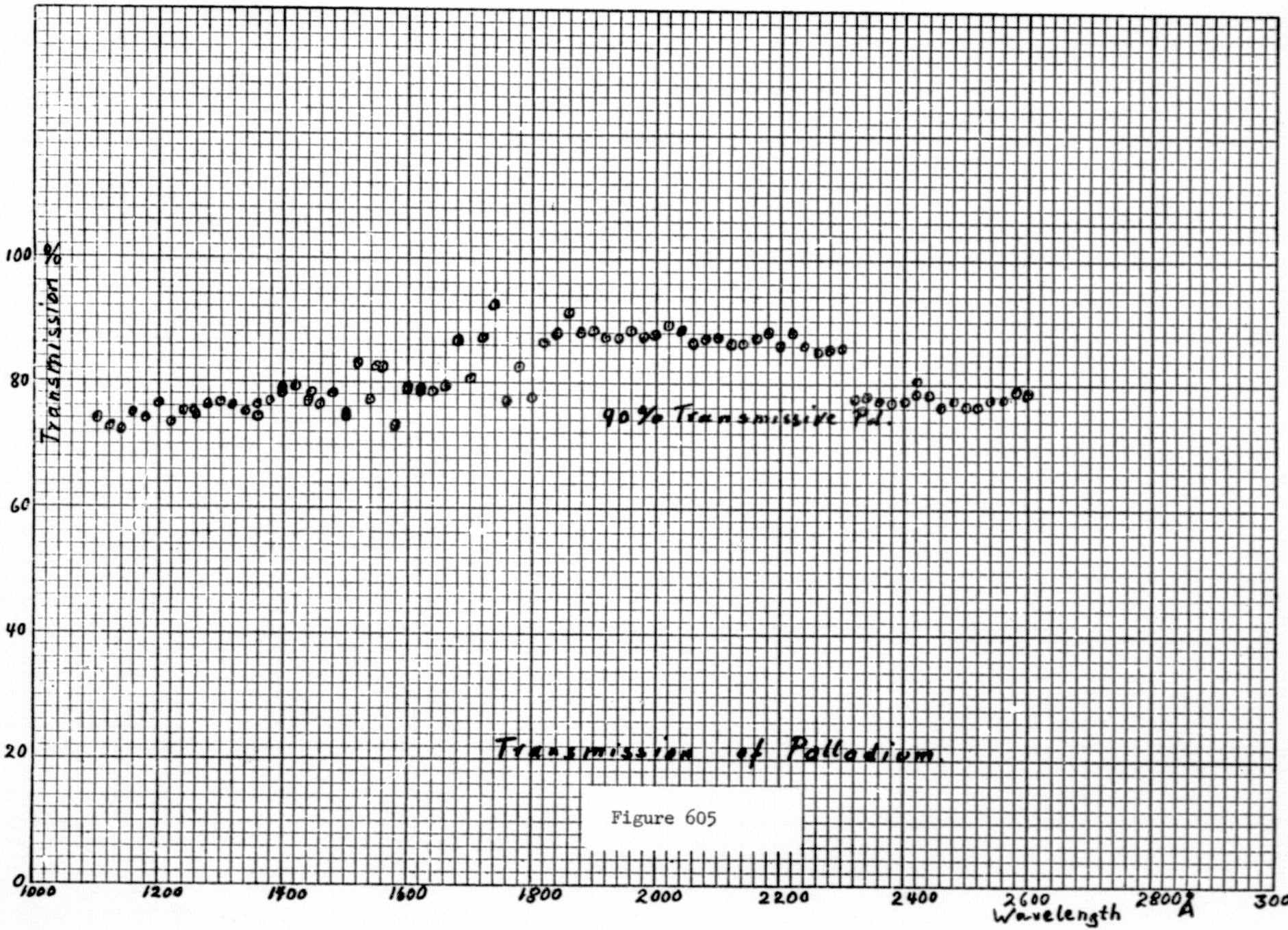

Figure 605

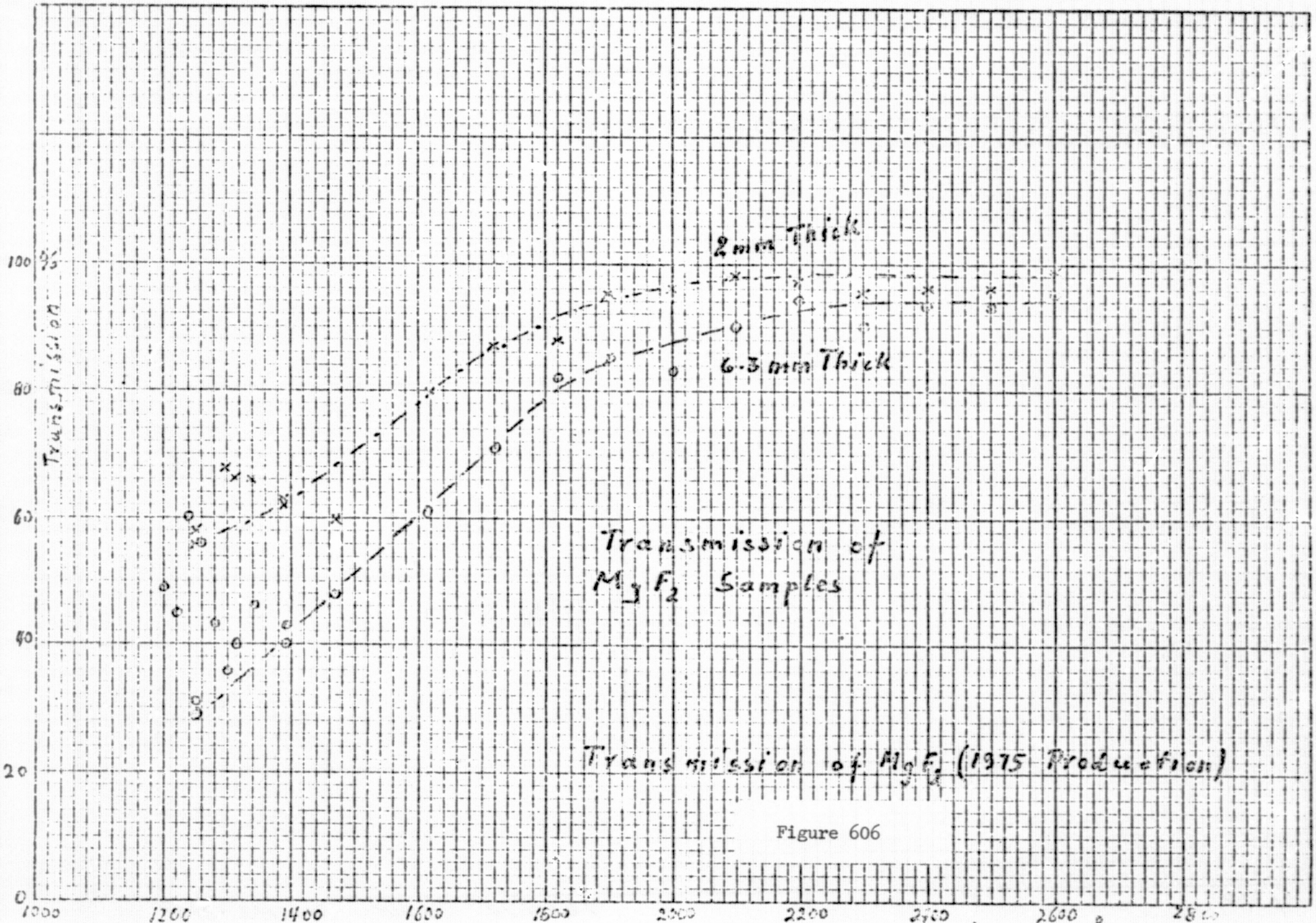
2 mm Thick
6.3 mm Thick
Transmission of
M_3F_2 Samples
Transmission of MgF_2 (1975 Production)
Transmission %
Wavelength Å
0
20
40
60
80
100
1000
1200
1400
1600
1800
2000
2200
2400
2600
2800

Figure 606

KEUFFEL & ESSER CO.

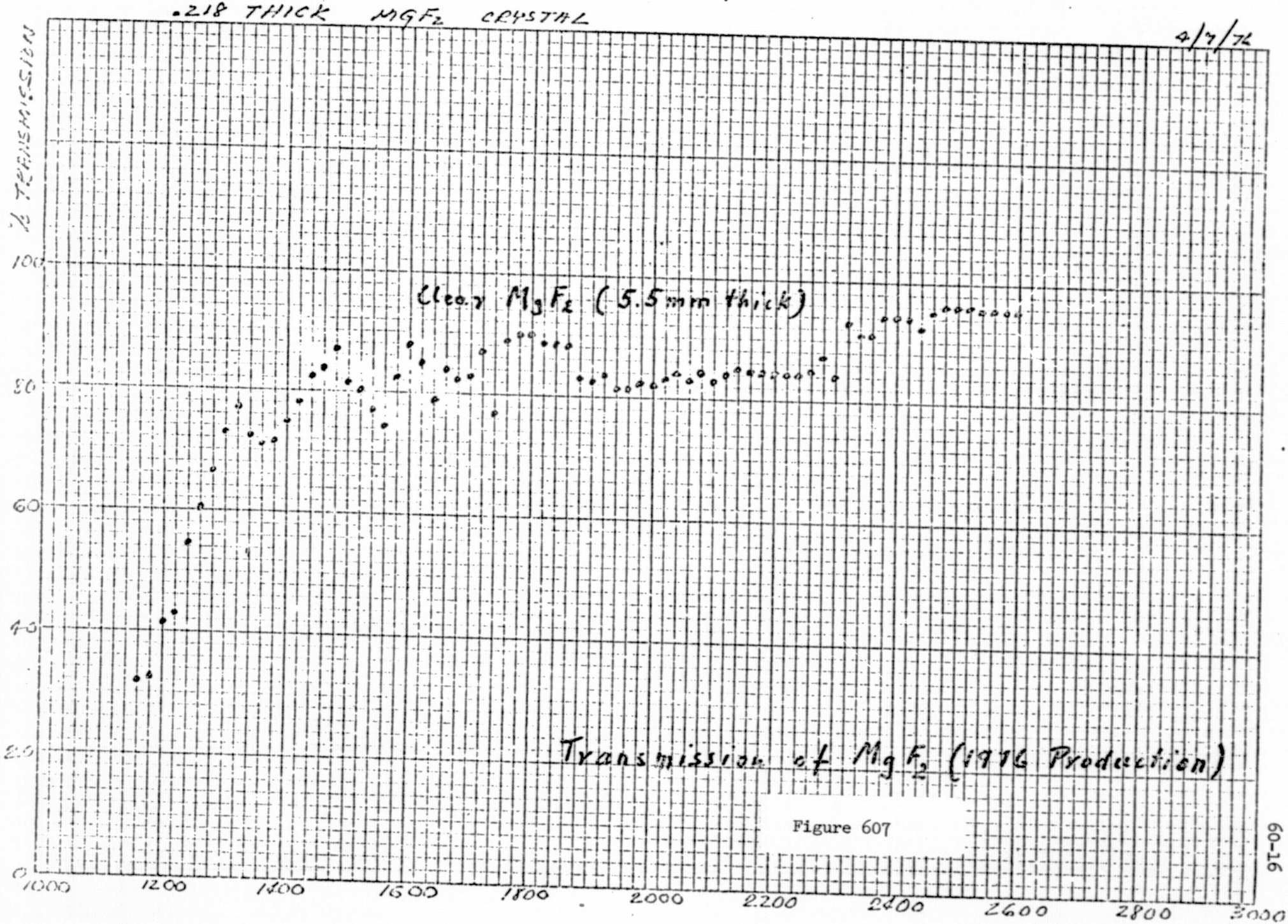

Figure 607

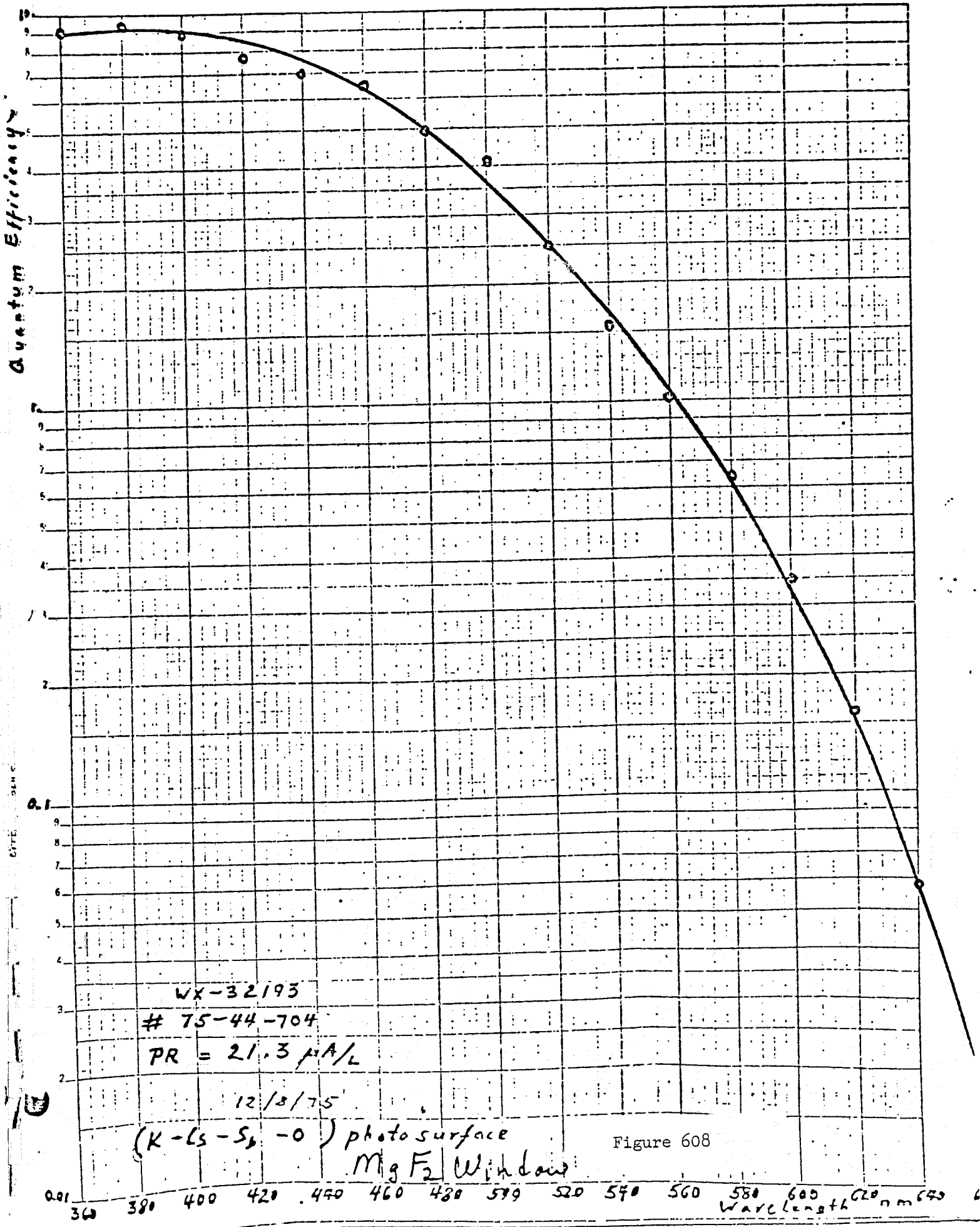
Quantum Efficiency %
Wavelength nm
WX-32193
# 75-44-704
PR = 21.3 μA/L
12/3/75
(K-Cs-Sb -0) photo surface
MgF2 Window

Figure 608

Section 70 Environmental

The first step in designing 70 mm format SEC tube was to establish the ability to manufature an SEC target this large and to determine its capability of withstanding a rocket launch environment. The targets were made, mounted in small evacuated containers, and vibrated to check their mechanical strength. These tests were successful and the tube design was initiated. Appendix 105 contains the results of environmental testing the first 70 mm tubes in September 1974. Three tubes were acoustically tested, and four shock tested. One tube was tested for acceleration with the window of the tube pointed in the direction to hold the window away from the tube as a test of the strength of the gold foil mounting of the magnesium fluoride window. In summary; the acceleration and shock tests were successful. The acoustic test results were mixed in that one tube survived, one tube test resulted in a broken target, and a third tube had a mesh mounting screw come loose. The acoustic tests were felt to be unduly harsh in that the bare tube was suspended in the acoustic chamber by a string. This gave the tube no acoustic damping as would actually be the case when mounted in the TV camera head in the f/24 camera housing.

Under the present contract three 70 mm tubes were subjected to sinusoidal and random vibration tests at GSFC early in 1976. All three tubes survived up to about 10 g random. At higher levels the metal aperture plate mounted about a centimeter in front of the target came loose. It had been spot welded at a few points to one of the Kovar electrodes in the image section. Above 10 g the field mesh also tore and finally the target broke probably as a result of the broken mesh or the metal plate hitting the target. Upon later inspection the mesh frame was found to be rather flexible and may have been the reason for the mesh tearing away from the frame.

It should be noted that the vibration tests were run with the vibration table controlled by an accelerometer mounted on the table rather than the fixture holding the SEC tube. The fixture is shown in Figure 701. The resonance of the fixture at 500 hz in the Z axis and 1500 hz in the X and Y axis is substantial, and resulted in the SEC tube being subjected to much higher accelerations around these frequencies. The vibration table should have been controlled by an accelerometer mounted on the fixture. Following these tests the aperture plate preceding the target was redesigned so that it was brazed rather than spot welded into the tube. In addition, the frame supporting the field mesh was made from stiffer metal stock. Since it had been reported that the tube appeared loose in the front support fixture during part of the test this support was redesigned to provide a V mount with the tube touching it at two points in the bottom half of the fixture. In June of 1976 one tube with a brazed in aperture plate and stiffened mesh frame was vibrated in the redesigned fixture. This time the vibration table was controlled via an accelerometer mounted on the front fixture. In addition the tube itself was instrumented with accelerometers mounted in various locations as shown in the Figure 702. Early in these tests it became apparent that there were problems with the redesigned fixture. The new V block arrangement resulted in the tube being pinched between the two blocks such that the screws holding the two blocks together could not be sufficiently tightened to keep them tight. Also the upper and lower blocks were now separated by a space such that the top block was suspended by the four screws and tension, and the image section of the tube in compression. T his resulted in excessive resonance of the upper half of the front fixture which, in turn, resulted in amplified inputs to the tube. In spite of this the aperture plate which had broken loose in earlier tubes remained in position. The field mesh, however, did not survive.

As a result of this test the fixture is being further redesigned to remove

the upper half of the image section mount and replace it with a strap similar to the mounting fixture for the gun section of the tube. While it is probable that the field mesh would have survived the test in a proper vibration fixture, Westinghouse is planning to further stiffen the mesh support, and will build a tube using a nickel mesh in place of the copper mesh. Separate mesh vibration tests will be conducted at Westinghouse to further evaluate the mesh design by vibrating it separately in an evacuated fixture.

The present qualification specification calls for 21 g random vibration imposed on the f/24 camera. The SEC tube will, of course, be mounted in a magnetic deflection yoke and focus coil assembly which is, in turn, mounted in the f/24 Camera enclosure. The actual vibration input to the SEC tube will depend on the mechanical and accoustical transmission of these structures. High frequency inputs will be greatly attenuated.

At this time one can say that the environmental tests of the bare tube are very encouraging.

RADIATION BACKGROUND

Trapped energetic charged particles and cosmic rays are of particular concern in sensitive electro-optical detectors because of the signal generated by these particles striking and/or passing through the windows and dynodes of the detector. Recent measurement by Viehmann, et al.,[18] of the fluorescence of MgF_2 indicate that in the ST orbit one can expect about 100 photoelectrons cm^{-2} sec^{-1} from an S-20 photocathode.

Measurements of the background in the 35 mm SEC tube with a bialkali photocathode under 42 mev proton bombardment indicated a yield of about 40 photoelectrons per 42 mev proton. Further measurements are planned to determine the background signal of a tube having a red sensitive photocathode for a variety of

energetic particles. Our best estimate at this time is that the exposure should be stopped during a transit of the South Atlantic Anomaly, but outside this region the background signal will not be dominated by trapped energetic particle irradiation.

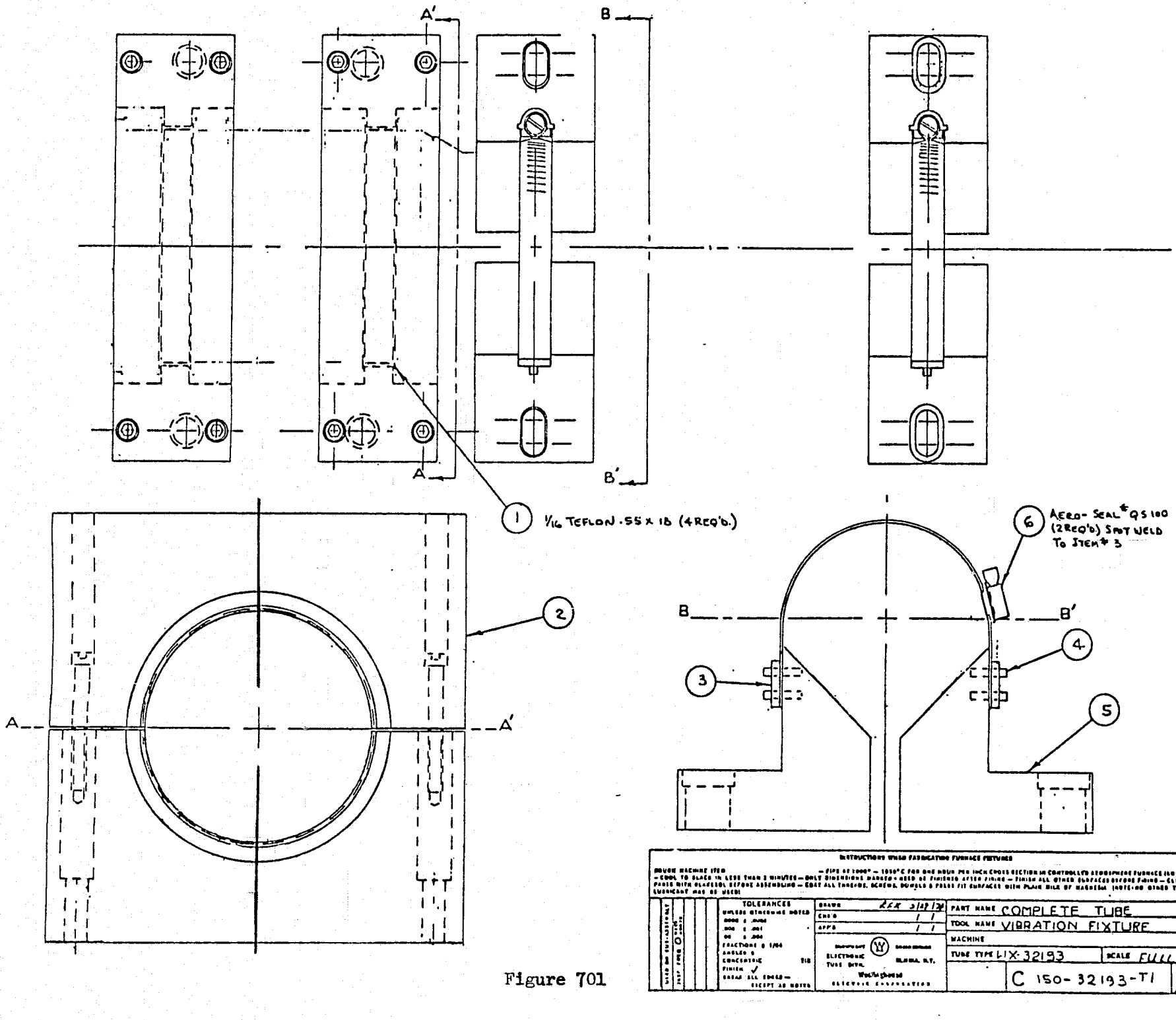

Figure 701

INSTRUCTIONS WHEN FABRICATING FURNACE FIXTURES

BRAZE MACHINE 1720 — FIRE AT 1000° — 1050°C FOR ONE HOUR PER INCH CROSS SECTION IN CONTROLLED ATMOSPHERE FURNACE (H2 OR DA) — COOL TO BLACK IN LESS THAN 3 MINUTES — ONLY DIMENSIONS MARKED * NEED BE FINISHED AFTER FIRING — FINISH ALL OTHER SURFACES BEFORE FIRING — CLEAN ALL PARTS WITH GLASSOL BEFORE ASSEMBLING — COAT ALL THREADS, SCREWS, DOWELS & PRESS FIT SURFACES WITH PLAIN MIX OF MAGNESIA (NOTE: NO OTHER TYPE OF LUBRICANT MAY BE USED)

TOLERANCES UNLESS OTHERWISE NOTED
.XXXX ± .0005
.XXX ± .001
.XX ± .005
FRACTIONS ± 1/64
ANGLES ± 1°
CONCENTRIC .010
FINISH ✓
BREAK ALL EDGES — EXCEPT AS NOTED

DRAWN RKK 3/29/74
CHK'D / /
APP'D / /

ELECTRONIC TUBE DIV. ELMIRA, N.Y.
Westinghouse ELECTRONIC CORPORATION

PART NAME COMPLETE TUBE
TOOL NAME VIBRATION FIXTURE
MACHINE
TUBE TYPE LIX-32193 SCALE FULL
C 150-32193-T1 1/2

70-5

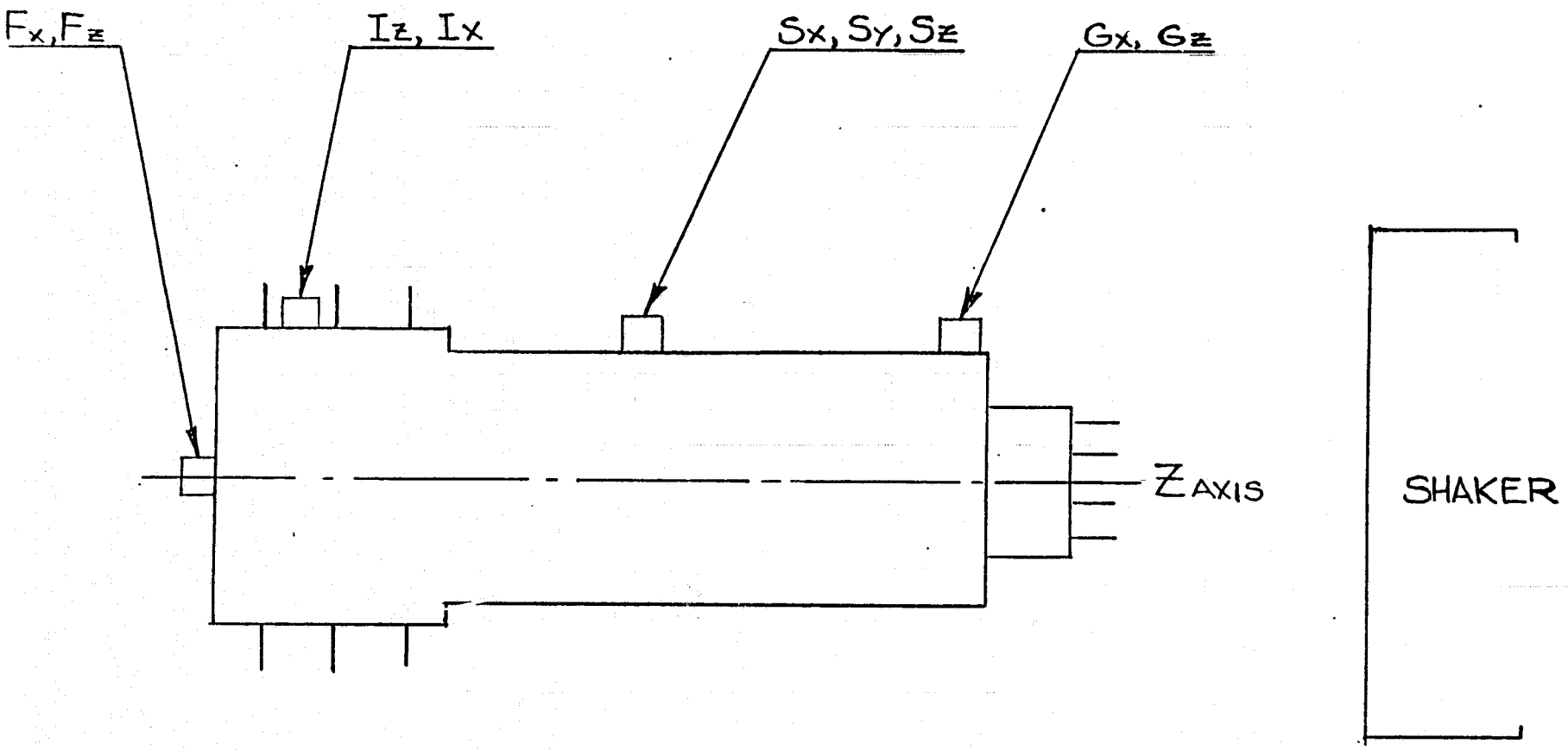

Accelerometer Locations for Test with Tube No. 109

Figure 702

Section 80 Permanent Magnet Focus Assembly (PMA)

In February 1975, Princeton completed a study for NASA of Permanent Magnet Focusing of Astronomical Camera Tubes, Contract No. NAS5-20507. The study was successful in coming up with a design that appeared to meet all the requirements for focusing the SEC tubes. A prototype for the 35 mm SEC tubes was built under this contract to check the design. Figure 801 is a 1/4 cross-sectional drawing of the unit and Table 801 lists the taper of the inner cylinder to generate a uniform magnetic field of 80 gauss. This profile differs slightly from the values in the study final report because of a difference in the actual B/H characteristics of the material use for the inner cylinder. Indeed, considerable difficulty was encountered in obtaining the iron used in fabricating the prototype. Delivery times were long and one batch of material was so far off the mark that it had to be replaced by the vendor after being measured by Armco, the licensee for the iron.

The PMA is assembled and then magnetized as a unit. Following the first attempts to magnetize the unit we found the magnetic field to be weak on one end. Further tests indicated that non-uniformities in the profile tube material caused this problem. Figure 802 shows the computer calculated axial field and the measured field.

TABLE 801

35 MM PMA PROFILE TUBE THICKNESSES

Distance from PMA Center cm	Profile Thickness cm
0	.051
.85	.051
1.70	.053
2.55	.056
3.40	.058
4.25	.061
5.11	.066
5.96	.071
6.81	.076
7.66	.084
8.51	.091
9.36	.099
10.21	.109
11.06	.117
11.91	.130
12.76	.140
13.61	.152
14.47	.165
15.32	.180
16.17	.193
17.02	.208
17.87	.226
18.72	.241
19.57	.259
20.42	.279
21.27	.299
22.12	.320
22.97	.343
23.83	.366
24.68	.394
25.53	.422
26.38	.460
27.23	1.14 (.513)*

*The profile thickness at the magnet boundary is increased from the design value to the thickness of the magnet. This increasing of the contact area reduces the air gap effects.

FIG. 801

QUARTER CROSS-SECTION OF PMA FOR 35 mm SEC

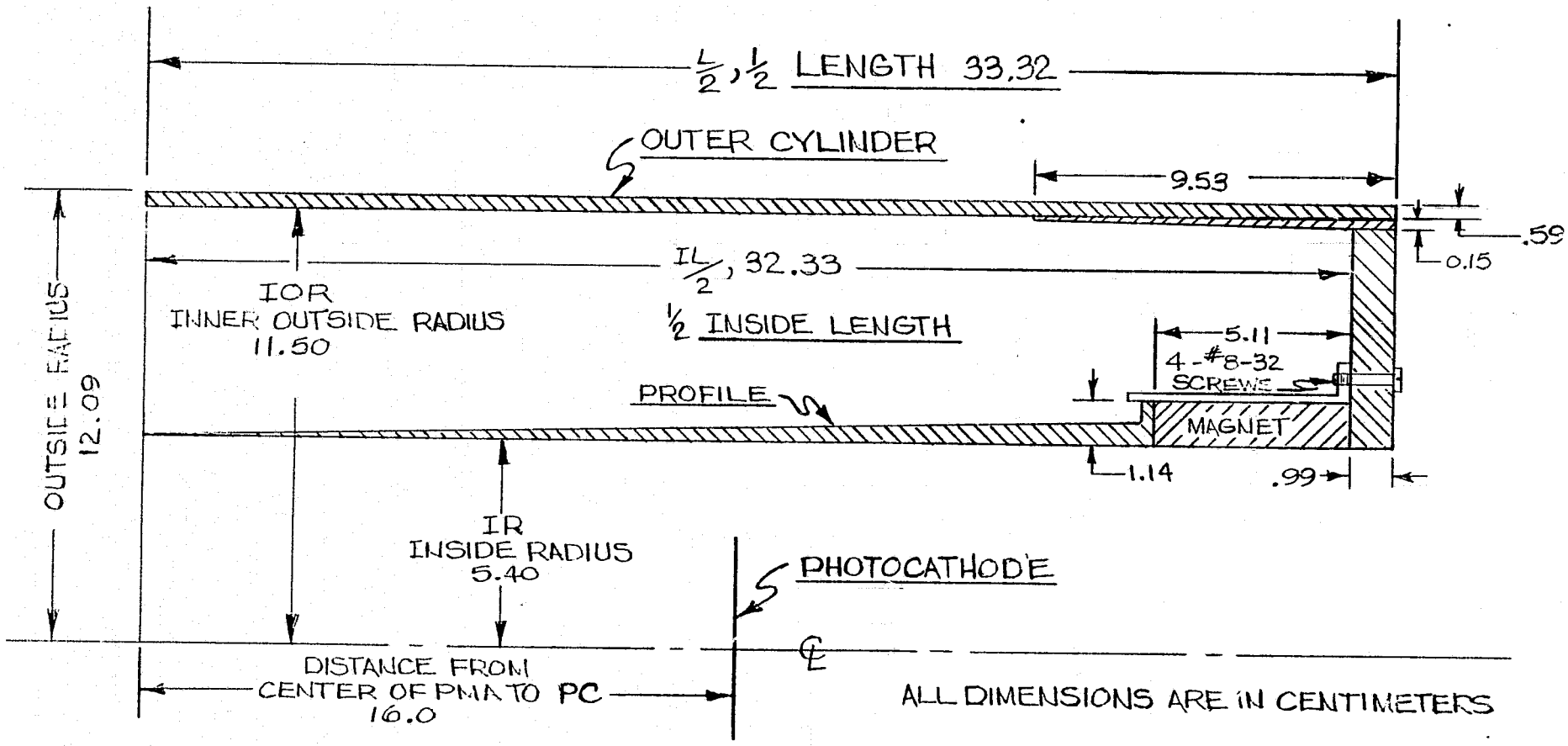

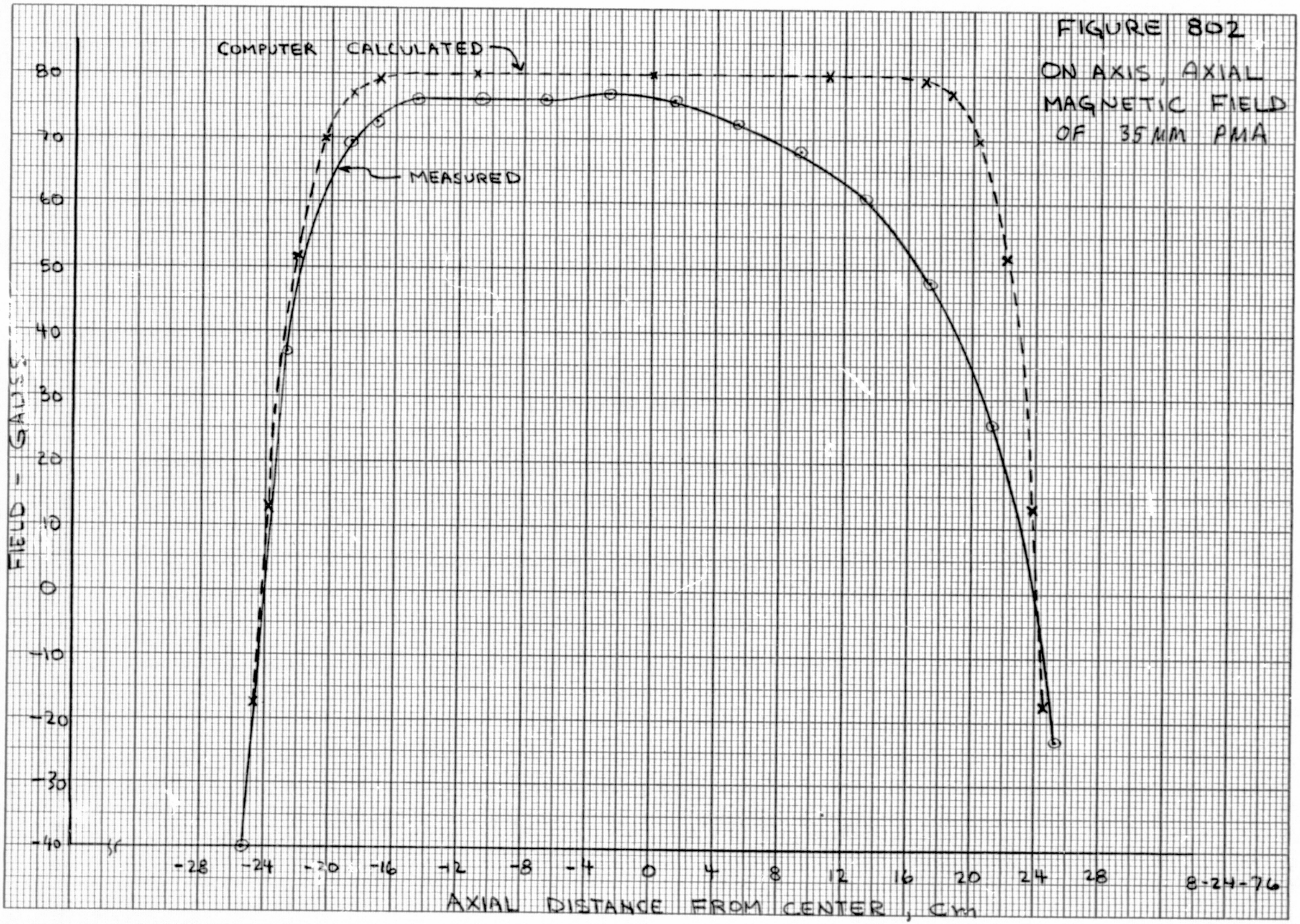
FIGURE 802
ON AXIS, AXIAL MAGNETIC FIELD OF 35 MM PMA
COMPUTER CALCULATED
MEASURED
FIELD - GAUSS
80
70
60
50
40
30
20
10
0
-10
-20
-30
-40
-28
-24
-20
-16
-12
-8
-4
0
4
8
12
16
20
24
28
AXIAL DISTANCE FROM CENTER, CM
8-24-76

Section 90 Astronomical Observing

In 1968 the first use of the SEC tubes for ground-based astronomical observations was reported by Green and Hansen,[6] and Lowrance and Zucchino.[7] Both of these sets of observations served primarily to show the usefulness of the SEC tubes for guiding on faint objects and their potential for scientific data acquisition. Subsequently, several observatories acquired SEC television cameras for acquisition and guiding with large telescopes.[8]

The first notable astronomical observation made with the SEC tubes from a ground-based observatory was the spectrum of the Quasar PHL-957, (M_V = 16.6) obtained in a 6 hour exposure on the Coudé spectrograph of the Hale 200-inch telescope in October 1970; Lowrance, Morton, Zucchino, Oke, and Schmidt.[9] Following this successful work the Princeton SEC system was employed by Dr. Morton, P. Crane and collaborators for a number of observations at Palomar, Kitt Peak and McDonald Observatories, with Morton concentrating on spectral observations and Crane on photometry of galaxies and other extended objects.[10,11]

Other astronomers currently using SEC tubes for astronomical observations are Alec Rogers at Mt. Stromlo Observatory, and Hong Yee Chiu at the Goddard Institute for Space Studies. Chiu has built a television system using the 35 mm format magnetically focused SEC tube, (WX-31718). His observations have been primarily on Kitt Peak's McMath Solar Telescope spectrograph to obtain very high dispersion (50 mÅ) spectra of Arcturus and other bright stars. Chiu's instrument includes a cylindrical lens system for optimizing the spectrograph dispersion for stellar observations.[12,13]

Rogers is also using the 35 mm format magnetically focused SEC tube. Their camera system includes a PDP 11/10 computer. The system is currently being used by Da Costa, Freeman and Stapinsky for cross-correlation of radial velocities of field and cluster metal poor giant stars. It is being used by

Hurst and Rogers for main sequence photometry in ω Cen and NGC 6397.

Recently the Princeton 35 mm SEC television camera was used by D. Morton and T. Williams for direct imagery of galaxies and star clusters with the Palomar 60-inch telescope. Figures 901-904 show a few of the exposures obtained by Schwarzschild and Williams on an observing run at the 1.5 m telescope of the Cerro Tololo Interamerican Observatory in June of this year. The f/7.5 Ritchey-Chretien focus was used, yielding a scale of 0".5 per 25 micron pixel, or 7'.7 for the full frame of 10^6 picture elements.

Figure 901 shows a 12 second exposure of the X-ray globular cluster NGC 7099. The exposure was taken through a B filter with seeing of 2" to 3". Neta Bahcall will analyze this and other exposures, searching for anomalies in the stellar distributions near the center of the clusters which may be related to the X-ray sources.

Figure 902 is a sky-limiting exposure of the globular cluster NGC 6362. The exposure was 30 minutes in V with 1" seeing. The series of two color exposures obtained for this cluster will be analyzed to extend its Hertzsprung-Russell diagram to the main sequence.

Figure 903 is a sky limiting exposure of the elliptical galaxy NGC 4697. The exposure is 27 minutes in V with 1" seeing. The nonuniformity of the background, the horizontal bars, and the circular arc are tube artifacts which will be removed by further processing. The series of elliptical galaxy exposures will be analyzed by Martin Schwarzschild to determine if the inner isophotes of the galaxies are aligned with the outer isophotes.

Figure 904 shows the chain of galaxies NGC 6845. This is a 25 minute sky limiting exposure in B, taken with 2" seeing. We have obtained a series of U, B, V, and R exposures on this object that demonstrate the use of the tube in the various wavelength regions.

The first scientific use of the SEC tube in space was in the Smithsonian Celescope Experiment on the first OAO satellite.[14] Indeed, this program got the KCl target out of the laboratory and into an operable tube. This space astronomy application was followed by the SEC color television camera for Apollo, a Naval Research Laboratory OSO satellite solar coronograph with SEC camera readout and several Skylab-ATM applications for pointing and monitoring experiments. The major advantage of the SEC tube over other television camera tubes for most of these applications was the ability to store the image for minutes without the need for cooling the tube. In the OSO-7 experiment the readout was 5 minutes.[15] In the Celescope experiment the readout rate was comparable and the SEC tubes were required to store the image for many minutes prior to readout in some cases.

More recently the magnetically focused, 35 mm format SEC tube, WX-31718, flew as the data sensor for ultraviolet echelle spectrograph in the Utrecht Space Research Laboratory's Balloon Ultraviolet Stellar Spectrometer (BUSS), a joint venture with the NASA Johnson Spacecraft Center.[5] They obtained 24 spectra of 16 stars in 9 hours of observing time. The dispersion of the spectrograph is between 2.1 nm/mm and 1.2 nm/mm at wavelengths of 340 nm and 200 nm, respectively, and the spectral resolution is 3×10^4. A CsTe photocathode was used to eliminate long wavelength response from scattered light.

The International Ultraviolet Explorer Satellite (IUE) scheduled for launch in 1977 employs an electrostatically focused SEC tube (WX-32224) fiber optically coupled to a proximity focused image intensifier. This combination was chosen to meet the constraints of the synchronous orbit payload, where minimum weight and power are important design constraints. The image intensifier has a MgF_2 window for ultraviolet response from 115 to 320 nm using a solar blind CsTe photocathode. The net gain of the intensifier is 6 photoelectrons per photoelectron from the CsTe photocathode. The picture element size at the SEC target is 26 x 26 microns.

The spectral resolution of interest allows the averaging of 3 x 3 groups of pixels with an anticipated peak signal to noise ratio appraoching 100 to 1. Actual test results are anticipated later this year.[14]

The National Center for Atmospheric Research's High Altitude Observatory is building a Coronograph/Polarimeter for the Solar Maximum Mission satellite to be launched in 1979. This instrument employs the magnetically focused SEC tube, WX-31718, as the data sensor. In this mission the spectral response required is from 400 to 656.2 nm, and the tube will have an S-20 photocathode. The picture elements are 33 x 33 micron corresponding to a spatial frequency of 15.4 cycles/mm where the sensor MTF is approximately 70%. The absolute photometric accuracy is expected to be about 10%.

REPRODUCIBILITY OF THE
ORIGINAL PAGE IS POOR

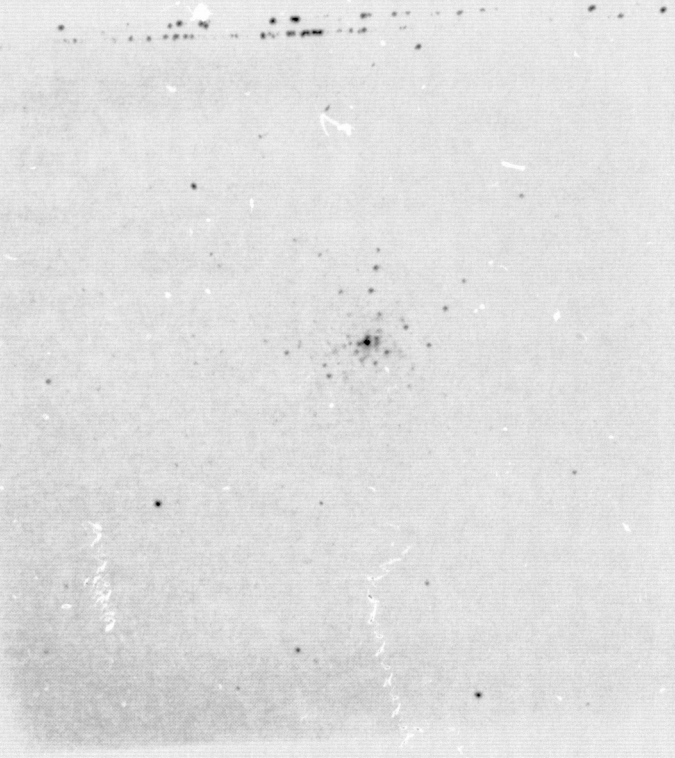

NGC 7099
Figure 901

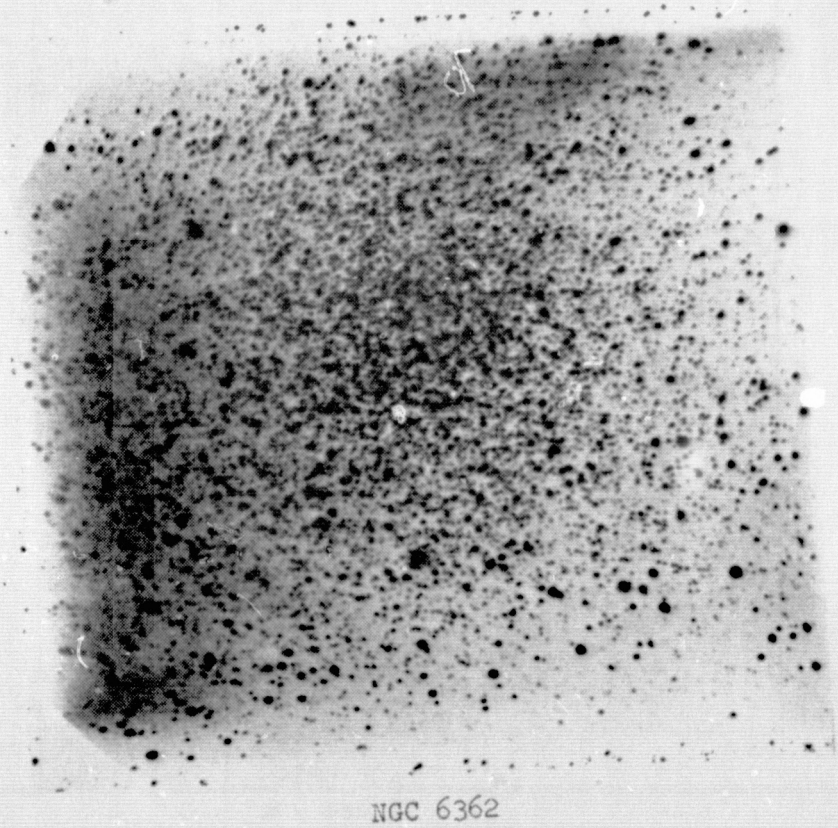

NGC 6362
Figure 902

REPRODUCIBILITY OF THE
ORIGINAL PAGE IS POOR

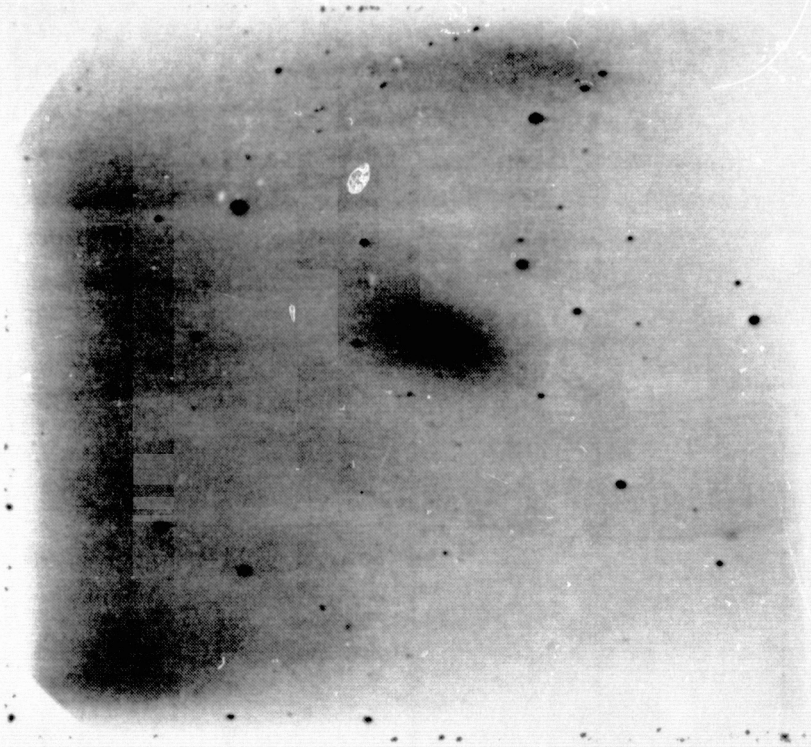

NGC 4697
Figure 903

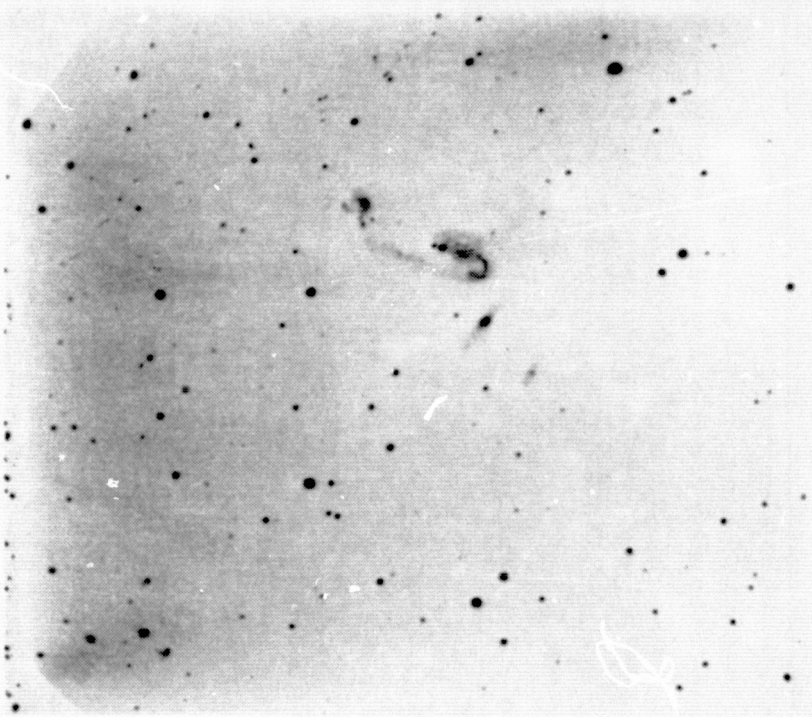

NGC 6845
Figure 904

Section 101 Westinghouse Data on Gross Tube Starts, etc.

Tube No.	Faceplate	Photosurface	P.R.	Remarks
1. 75-48-080	Glass	S-20	0.3 μA/L	Target damage by alkalis
2. 75-52-191	Glass	S-20	---	Leaker, broken target
3. 75-48-090	MgF_2	$(K-C_s-S_b)-O$	10.5 μA/L	Target damage by alkalis
4. 75-48-050	MgF_2	$(K-C_s-S_b)-O$	8.5	Broken target
5. 75-44-704	MgF_2	$(K-C_s-S_b)-O$	49.2 μA/L	Target damage
6. 75-44-404	Glass	$(K-C_s-S_b)$	---	Leaker, broken target
7. 75-44-703	Glass	$(K-C_s-S_b)$	---	Leaker, broken target
8. 75-44-325	Glass	S-20	100 μA/L	Broken target
9. 75-26-030	Glass	S-20	---	Photocathode only partly working
10. 75-22-722	Glass	S-20	18 μA/L	Delivered
11. 75-18-200	Glass	S-20	94 μA/L	Delivered
12. 75-13-855	Glass	S-20	1.5 μA/L	Broken Target

Tubes WX-32193, manufactured during the period of January '76 to June '76.

Contract No. NAS5-20833 Subcontract 1

Report No.				
9. 75-52-191 (salvaged parts)	Glass	S-20	45 μA/L	Target did store but alkali damage.
12. 76-13-829	Glass (half chrome)	C_s-S_b	2.5 μA/L	Antimony bead shorted. Target damage, stored 2-3 min. Delivered.
13. 76-17-170	Glass 95% Pd	C_s-S_b	10 μA/L	Target damage. Stored less than 1 hr.
Summary Report				
76-17-944	Glass 93% Cr.	$K-C_s-S_b$	40 μA/L	Target alkali damage. Stored less than 15 min. at V_T = 4 Volts.

Section 102 Statement of Work, Schedule

The Contractor shall provide the personnel, facilities, equipment and material to accomplish the following:

1. Fabricate 15 of the 70 mm SEC tubes with photocathodes sensitive to visible light, i.e., $400 < \lambda > 650$ nm.

2. Environmentally test representative tubes from this batch of 15. Environmental tests for design qualification shall include vibration, shock, acoustical and thermal testing as described in GSFC document 73-15036, "Environmental Test Specification for a Standard Tape Recorder", subsections 5.2.1, 6.2.81, and 10.2.1, respectively. Environmental tests shall be coordinated with the GSFC Test and Evaluation Division.

3. Perform tube evaluation of the usable tubes, measuring MTF, distortion gain, sensitivity. Also determine the optimum operating conditions and tolerances. All tube tests shall be preceded and followed by active tests to evaluate optical/electronic quality.

4. Improve the electron optics of the 70 mm tube and its focus and deflection coils to achieve improved MTF over the format and minimize distortion.

5. Determine optimum low noise anti-reflection material for targets.

6. Conduct astronomical observations.

7. A documented failure analysis shall be made in each case of tube failure.

8. Several visible cathode tubes shall be made available to the Government for distribution to independent evaluators before contract expiration.

9. Fabricate a permenent magnet focus assembly - and measure its characteristics. The permanent magnet focus assembly should be fabricated on the basis of the existing PMA study (with Princeton University) and its results after consultation with the GSFC Technical Officer.

10. Determine the photometric effects of the antireflection and antisecondary emission target coating.

11. Investigate and provide an optimized process for S-20 type photocathodes on MgF_2. Approximately 20 diodes consisting of the upper section of the 35 mm SEC tube will be used as test vehicles for determining optimum preparation procedure, compatible under layment, and evaporation schedule.

12. Modify the KCl target to increase the storage capacity, the goal being a 2-fold increase without loss in integrating capability and insignificant readout lag in slow scan.

13. Provide improved controlled processing of the photocathodes by parametric monitoring techniques resulting in a defined photocathode growth procedure.

SCHEDULE

The following items are considered to be deliverable under this contract:

Item	Quantity	Description	Schedule
1	15 each	70 mm SEC tubes	15 months after the date of contract award
2	1 each	Permanent Magnet Focus Assembly	15 months after the date of contract award
3	4 each	Environmental Test Report	15 months after the date of contract award
4		Financial Management Reports	See Article XVI
5		Quarterly Progress Reports	See Article XVI
6		Final Project Report	16 months after the date of contract award
7	As Required	Visible Cathode Tube	16 months after the date of contract award
8	4 each	35 mm SEC tubes with S-20/MgF_2 photocathodes and subject to a series of parametric tests to characterize as a minimum: (a) dynamic range (b) modulation transfer function (c) photometric transfer function (d) noise characteristics	July 31, 1976
9	As Required	Tests results and failure analyses for each 35 mm SEC tube and photometric results for all 35 mm test diodes.	August 31, 1976 or as generated.

REFERENCED PUBLICATIONS

1. Goetz, G.W., In "Ad. Electronics and Electron Physics", Vol. 22A, pp. 219-227, Academic Press, New York (1966).

2. Boerio, A.H., Beyer, R.R., and Goetz, G.W., In "Ad. Electronics and Electron Physics", Vol. 22A, pp. 229-239, Academic Press, New York (1966).

3. Weimer, P.K., In "Ad. Electronics and Electron Physics", Vol. 13, pp. 387-437, Academic Press, New York, 1960.

4. Long, D.C., "Study of Magnetic Perturbations on SEC Vidicon Tubes". Final report on NASA Contract NAS Contract NAS5-23254, August 24, 1973.

5. Kamperman, T.M., "SEC Vidicon System for a Balloon Ultraviolet Stellar Spectrometer", Image Processing Techniques in Astronomy, p. 127. Reidel, Dordrecht (1975).

6. Green, M., and Hansen, J.R., "The Application of SEC Camera Tubes and Electrostatic Image Intensifiers to Astronomy", Adv. in Electronics and Electron Physics, Vol. 28B, p. 807, Academic Press, London (1969).

7. Lowrance, J.L., and Zucchino, P., "Integrating Television Sensors for Space Astronomy", Adv. in Electronics and Electron Physics, Vol. 28B, p. 851. Academic Press, London, 1972.

8. Dennison, E., "An Integrating Television System for Visual Enhancement of Faint Stars". Advances in Electronics and Electron Physics", Vol. 33B, p. 795. Academic Press, London, 1972.

9. Lowrance, J.L., Morton, D., Zucchino, P., Oke, J.B. and Schmidt, M., "The Spectrum of Quasi-Stellar Object PHL-957, Ap.J., Vol. 171, January 1972.

10. Crane, P., "Surface Photometry of Galaxies I: The SBO NGC 2950", Ap.J., 197, 317, 1975.

11. Morton, D.C. and Elmergreen, B.G., "Velocity Dispersions of Galaxies V: The Nuclei of M31 and M32", Ap.J., 205, 63, 1976.

12. Chiu, H.Y., "A Slow Scan SEC Vidicon System", Applied Optics (in press), February 1977.

13. Chiu, H.Y., et al., "High Resolution Stellar Vidicon Spectrophotometry. I. Variable Mass Loss from Arcturus and the Hypothesis of Giant Convective Elements", Ap.J., (in press), November 1976.

14. Davis, R.J., "New Astronomy Space Experiments with Television Scanning", Space Applications of Camera Tubes, International Colloquium sponsored by Centre National D'Etudes Spatiales, Paris, November 1971.

15. Brueckner, G.E., "A Digitized SEC-Vidicon System for a Satellite Coronograph", Space Applications of Camera Tubes, International Colloquium sponsored by Centre National D'Etudes Spatiales, Paris, November 1971.

16. Zucchino, P., "Photometric Statistical Performance of the SEC Target", Advances in Electronics and Electron Physics, Vol. 40A. Sixth Symposium on Photoelectronic Image Devices, pp. 239-252, 1976.

17. Long, D.C. and Lowrance, J., "Study of Permanent Magnet Focusing for Astronomical Camera Tubes", Final Report on NAS 5-20507 February 28, 1975.

18. Viehmann, W., Eubanks, A.G., Pieper, G.F., and Bredekamp, J.H. "Fluorescence and Phophorescence of Photomultiplier Window Materials Under Electron Irradiation. GSFC X-Document X-755-74-210, July 1974; revised April 1975.

Section 104 Bibliography of Astronomical Papers based on SEC Camera Observations

In "Ad. Electronics and Electron Physics", Goetz, G.W., Vol. 22A, pp. 219-227, Academic Press, New York (1966).

In "Ad. Electronics and Electron Physics", Boerio, A.H., Beyer, R.R. and Goetz, G.W. Vol. 22A, pp. 229-239, Academic Press, New York (1966).

"The Application of SEC Camera Tubes and Electrostatic Image Intensifiers to Astronomy", Green, M. and Hansen, J.R. Adv. in Electronics and Electron Physics, Vol. 28B, p. 807, Academic Press, London (1969).

"The Spectrum of the Quasi-Stellar Object PHL 957". Lowrance, J.L., Morton, D.C., Zucchino, P., Oke, J.B. and Schmidt, M. Astrophysical Journal, V. 171, p. 233 (1972).

"Absorption-Line Profiles in the Quasi-Stellar Object PHL 957". Morton, D.C. and Morton, W.A. Astrophysical Journal, V. 174, p. 237 (1972).

"Velocity Dispersions in Galaxies I. The E7 Galaxy NGC 7332". Morton, D.C. and Chevalier, R.A. Astrophysical Journal, V. 174, p. 489 (1972).

"Absorption Lines in the Spectrum of the Quasar Ton 1530". Morton, D.C. and Morton, W.A. Astrophysical Journal, V. 178, p. 607 (1972).

"Velocity Dispersions in Galaxies II. The Ellipticals NGC 1889, 3115, 4473 and 4494". Morton, D. . and Chevalier, R.A. Astrophysical Journal, V. 179, p. 55 (1973).

"Velocity Dispersions in Galaxies III. The Nucleus of M31". Morton, D.C. and Thuan, T.X. Astrophysical Journal, V. 180, p. 705 (1973).

"Velocities Dispersions in Galaxies IV. The Nucleus of NGC 1068". Richstone, D.O. and Morton, D.C. Astrophysical Journal. V. 201, No. 2, Pt. 1, pp. 289-295, Oct. (1975).

"The Absorption Line Spectrum of the Quasi-Stellar Object PHL 957". Wingert, D.W. Astrophysical Journal, V. 198, No. 2, Pt. 1, pp. 267-279 (1975).

"Photometry of Galaxies with Integrating Television". Crane, P. Bull. Am. Astron., Soc. 3, 399 (1971).

The SEC Vidicon as a Photometer in Proceedings of the Conference on Astronomical Observations with Television Type Sensors. Crane, P. Edited by Glaspey, J.W. and Walker, G.A.H. (The Institute of Astronomy and Space Science UBC, Canada, pp. 391, 1973.

"Surface Photometry of SBO Galaxies". Crane, P. Bull. Am. Astron. Soc. 5, 349, 1973.

"SEC Vidicon Slitless (OII) Images of NGC 2440". Crane, P., Bernat, A., Ferland, G. and Robbins, R.R. Bull. Am. Astron. Soc. 5, 423, 1973.

"T.V. Photometry of the Crab Nebula", Davidson, K., Crane, P. and Chincarini, G. Astronomical Journal, V. 79, 791, 1974.

"Surface Photometry of Galaxies I: The SBO NGC2950". Crane, P., Astrophysical Journal, V. 197, 317, 1975.

"SEC Vidicon System for a Balloon Ultraviolet Stellar Spectrometer", Kamperman, T.M. Image Processing Techniques in Astronomy, p. 127. Reidel, Dordrecht (1975).

"Fluorescence and Phosphorescence of Photomultiplier Window Materials Under Electron Irradiation". Viehmann, W., Eubanks, A.G., Pieper, G.F. and Bredekamp, J.H. GSFC X-Document X-755-74-210, July 1975.

"Television Surface Photometry of the Edge-on Spiral Galaxies NGC-3987 and NGC-5907". Davis, Marc. Astronomical Journal, V. 80, p. 188, 1975.

"Some Experiments With An SEC Image Tube for High Precision Multi-Colour Photometry of Galactic Clusters", Blecha, A. and Bartoldi, P. Image Processing Techniques in Astronomy. Ed. by de Jager, C. and Nievwenhuijzen, H. D. Reidel, Boston, p. 141, 1975.

"The H and K Lines of CaII in the Nucleus and Bulge of M31". Morton, D.C. and Andereck, C.D. Astrophysical Journal, V. 205, 356, 1976.

"Spectroscopic Photoelectric Imaging Fabry-Perot Interferometer: Its Development and Preliminary Observational Results". Smith, Wm. Hayden., Born, Joachim., Cochran, Wm. D. and Gelfand, Jack. Applied Optics, V. 15, pp. 717-724, March 1976.

"High DQE Image Detectors", Coleman, C.I. International Conference on Image Analysis and Evaluation. Toronto, July 1976.

"A Photometric Study of Clusters of Galaxies". Hoffman, A.W. and Crane, P. Astrophysical Journal (in press), 1976.

"Velocity Dispersion of Galaxies V. The Nuclei of M31 and M32". Morton, D.C. and Elmergreen, B.G. Astrophysical Journal, V. 205, 63, 1976.

Section 105 Environmental Test of WX-32193 SEC Tubes; Sept. '74 Appendix.

One of the major tasks under this contract was to environmentally test the 70 mm format SEC tubes. Westinghouse designed a fixture for holding the tube during shock, vibration, and acceleration. Figures 2 and 3 are views of the tube mounted in this fixture which holds the image section of the tube in a rigid collar that is lined with a relatively hard rubber sleeve which in turn bears on one of the ceramic rings of the image section. The electron gun end of the tube mounts in a V block that is lined with the hard rubber material and secured by a flexible metal strap across the top of the tube. The gun support is designed to float relative to the front support to accommodate any misalignment of the gun axis relative to the image section.

Preliminary vibration tests were made at Westinghouse using their own vibration facilities at Horseheads, N.Y., (MB-C50 vibration exciter and UD slip plate). These tests provided that the fixture design was adequate and that the tube would survive low frequency vibration levels up to 15g, but that the Westinghouse vibration facility was inadequate to run the proposed environmental tests specified by Goddard, GSFC B-15036, Environmental Test Specification for a Standard Tape Recorder. It was agreed that the testing would be carried out using Goddard's facilities with Princeton and Westinghouse participation.

Environmental Tests at Goddard

On September 19 and 20, four WX-32193 SEC camera tubes were evaluated for shock and acoustics. The purpose of these tests was to determine if this camera tube could survive the environment produced by launch of the LST. The shock and accoustic noise test specification is included in Appendix A. The following is exerpted from the report.

Initially three tubes were subjected to acoustics test. This test consisted of suspending the tubes by parachute shock cord in a chamber producing a spectrum of acoustic noise from 8 Hz to 8000 Hz with an overall level of 152 dB. Following are details of the test and the results.

Tube #	Duration	Results
(1) 73-48-201	2 min	Loose screw
(2) 73-30-650	30 sec.	OK
	30 sec.	OK
	30 sec.	OK
	30 sec.	OK
(3) 73-30-653	30 sec.	Target broken

Failure analysis: The loose screw on 73-48-201 was from the field mesh assembly.

The broken target in 73-30-653 initially was thought to be caused by peeling of the target substrate from the ceramic target support. Opening of the tube revealed that the support was of hand-molded glass and no peeling was evident. The breakage may have been caused by a particle, but no loose particles were found.

The tube which survived, 73-30-650, was also a tube having a hand-molded glass target support. No heaters failed to survive the test.

Four tubes were subjected in the Y and Z axis to the esign Qualification Shock Test. This test is performed by mounting the tube in a combination shock, vibration and acceleration fixture mounted to an electrodynamic vibration exciter. Two high shocks are then fed into the vibrator by use of a series of wave form generators which produce the following spectrum of shock. Starting at 200 Hz with 57 g's to 400 Hz with 225 g's; from 200 Hz to 1250 Hz at 225's; from 1250 Hz at 225 g's to 1600 Hz at 300 g's; from 1600 Hz to 4000 Hz at 300 g's. During the initial set-up tube No. 73-48-201 was subjected to approximately 1000 g's in the Z-axis at the 1600 to 4000 Hz level because the control accelerometer was mounted on the vibration table. Recalibration using a fixture mounted accelerometer produced the following results:

Tube #	Test	Results
73-48-201	25% power Z axis	OK
"	100% power Z axis	OK
"	100% power Z axis	OK

At this point the shaker table failed and the foregoing acoustics tests were performed. After completion of these, shock testing was resumed.

73-48-201	25% power Y axis	OK
"	100% power Y axis	OK
"	100% power Y axis	OK
73-30-650	25% power Z axis	OK
"	100% power Z axis	OK
"	100% power Z axis	OK
73-52-714	25% power Z axis	OK
"	100% power Z axis	OK
"	100% power Z axis	OK
73-30-650	25% power Y axis	OK
"	100% power Y axis	OK
"	100% power Y axis	OK
73-52-714	25% power Y axis	OK
"	100% power Y axis	OK
"	100% power Y axis	OK

Failure analysis: No heaters failed in any tubes tested. 73-48-201 had developed a broken target earlier at Westinghouse during 2g's sinusoidal vibration between 200 Hz and 2000 Hz so was used only as a set-up tube; however, its heater was OK after each test. 73-30-653 was not tested because its target was broken earlier at the acoustics test. Of the two remaining tubes, 73-60-650 had a resistive target connection prior to testing and could not be evaluated except for visual damage to the target or breakage of the heater. 73-52-714 showed a number of one to two TV line white spots on the target that were not visible in earlier photographs. It is not possible to determine if these are holes in the substrate or loss of KCl. From past experience in other tubes, the cause is probably holes caused by particles of the chromic oxide paint coming loose in the front end of the tube.

Conclusions: Although it would have been ideal to have no failures in these tests, the problem areas pointed to are not considered serious. Loose screw problems are commonly solved by using torque screwdrivers. The broken target may have been caused by flexure of the glass target support or by loose particles in the tube. Since the glass target support is no longer used, if flexure is the problem, then this should be solved by using the more rigid ceramic support. The appearnce of white target spots in the one good tube, if caused by the chrome oxide paint, could be alleviated by the use of ultra-cleaning of the tube parts. This technique was not used in the engineering feasibility models evaluated in these tests but will be in the future.

Acceleration Test

One tube was accelerated by Associated Testing Laboratories, Inc., without damage. The acceleration was 33 g's for 1 minute in the Z axis with the face-plate opposite the pivot of the centrifuge.

APPENDIX A

ENVIRONMENTAL TEST SPECIFICATIONS

SHOCK TEST LEVELS

A transient whose positive and negative acceleration shock response spectra satisfy the requirements of Figure 1 for design qualification tests and Figure 2 for flight acceptance tests, within the allowable tolerances of +50%, -10%, shall be applied to the component.

The transient shall be applied twice along each of the three axes for design qualification tests and once along each axis for flight acceptance tests.

The spectrum analysis verifying compliance with the specification requirements shall be made at a maximum of one-third octave increments for a damping value of $c/c_c = .05$, (Q = 10).

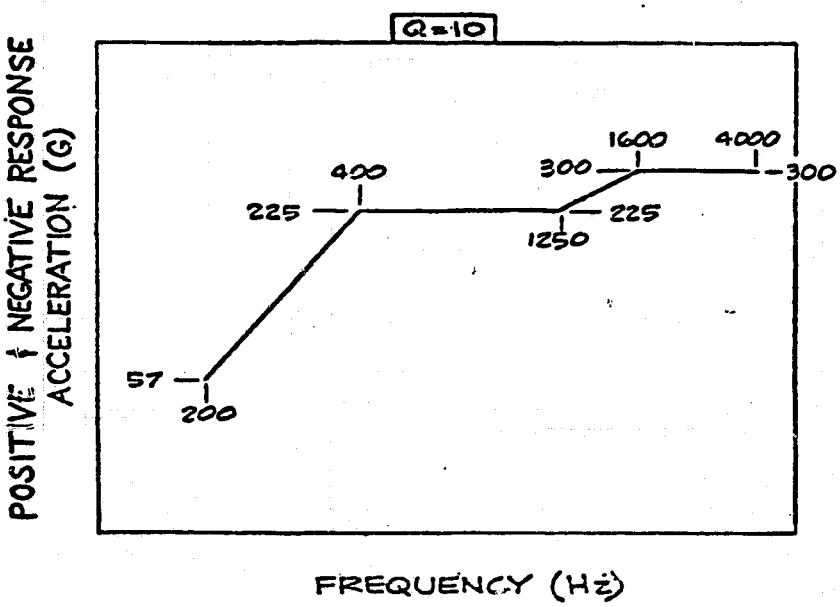

Figure 1 - Design Qualification Mechanical Shock Requirements

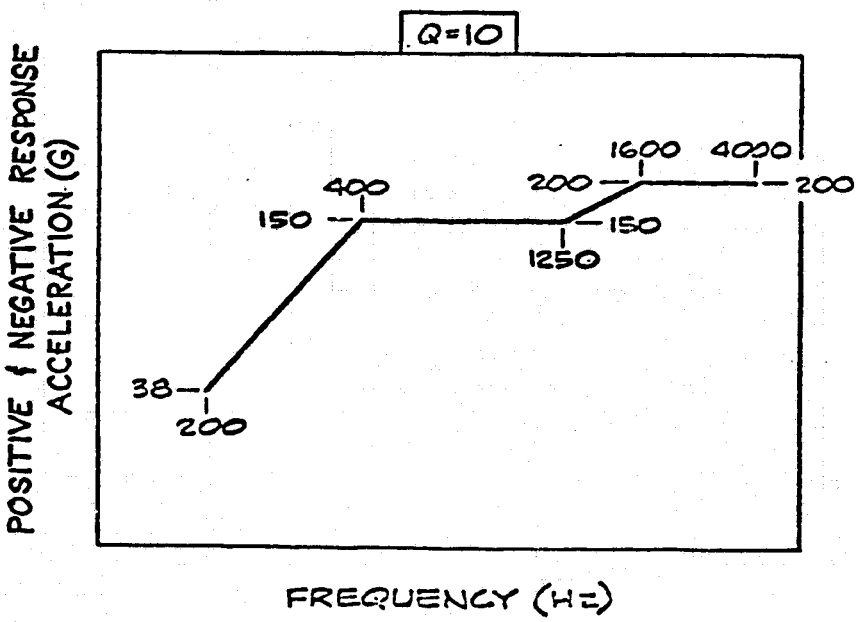

Figure 2 - Flight Acceptance Mechanical Shock Requirements

ACOUSTIC NOISE REQUIREMENTS

During the launch the component will be subjected to high-level noise environment. Vibratory response to this acoustic environment will be adequately simulated by the random vibration test requirements. Nevertheless, design qualification and flight acceptance levels are presented in Table VI for design considerations only.

ACOUSTIC NOISE REQUIREMENTS (For Design Consideration Only)

Octave Band Center Frequency (Hz)	Octave Band Noise Level (dB: re 20 N/m^2)	
	Design Qual.	Flight Accept.
8	141	137
16	142	138
32	142	138
63	140	136
125	138	134
250	143	139
500	147	143
1000	141	137
2000	138	134
4000	132	128
8000	132	128
Overall	152	148

Duration: 2 min.

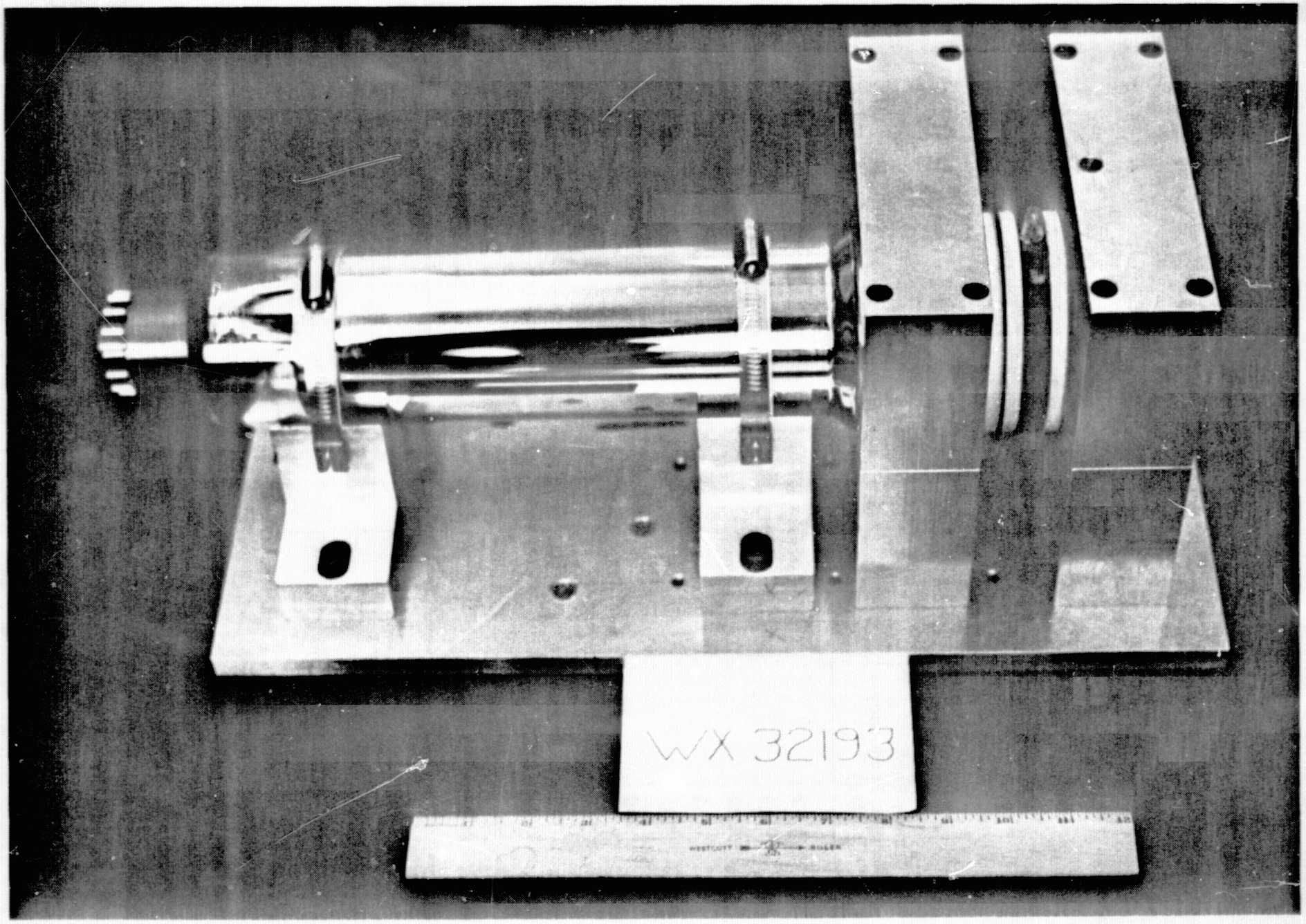

Figure 2 - Side view of SEC tube vibration test fixture.

REPRODUCIBILITY OF THE
ORIGINAL PAGE IS POOR

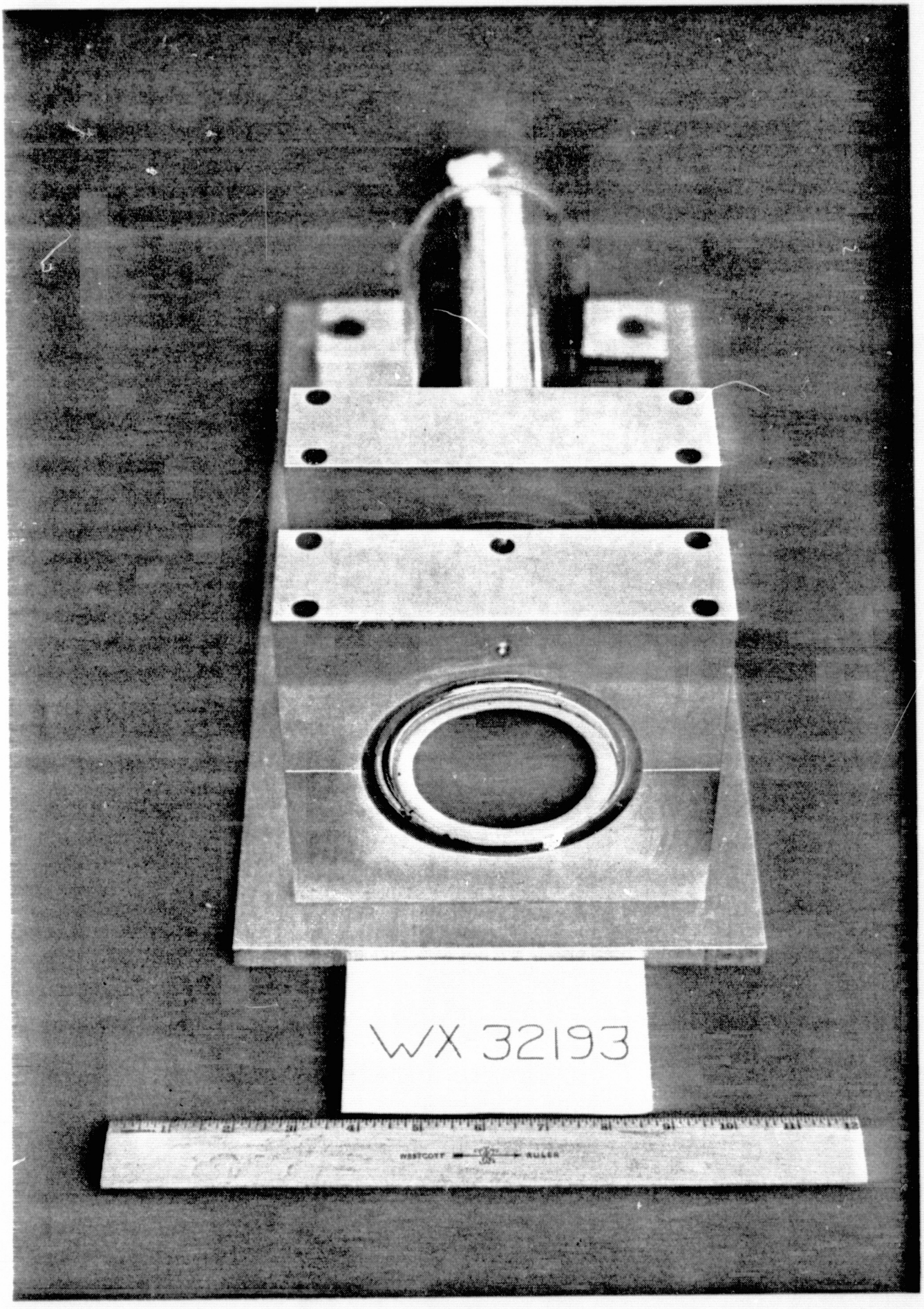

Figure 3 - Front view of SEC tube vibration test fixture.

Section 106 Computer Program for Photometric Noise Analysis.

```
C*****************************************************************************
C
C         SCRATCH - PHOTOMETRIC ANALYSIS OF SEC TV PERFORMANCE
C         THIS VERSION WRITTEN BY TED WILLIAMS - PRINCETON UNIVERSITY OBSERVATORY
C
C*****************************************************************************



      REAL*8 SUM,SUMSQ,AVE,STDEV
      REAL*4 FCOMM(10),PCOMM(10,16),GHEAD(25),PHEAD(25),CARD(9)
      INTEGER*4 TOPL(16),BOTL(16),LPIX(16),RPIX(16),HATCH(16),RGTP
      INTEGER*2 INPUT(1024),OUTPUT(100,100)
      COMMON /STAT/ SUM,SUMSQ,AVE,STDEV,NUMB
      EQUIVALENCE (INPUT(1),PHEAD(1)),(INPUT( 67),GHEAD(1))
      DATA FILE,PATCH,TAPE,STOP/'FILE','PATC','TAPE','STOP'/
      DATA MAXP/16/
      CALL BUFFER (8,1,2048,INPUT)
      JFILE=1
    1 READ(5,100) BRANCH,NUM,FCOMM
  100 FORMAT(A4,1X,I5,10A4)
      IF(BRANCH.EQ.FILE) GO TO 7
      IF(BRANCH.EQ.PATCH) GO TO 2
      IF(BRANCH.EQ.TAPE) GO TO 6
      IF(BRANCH.EQ.STOP) STOP
      WRITE(6,101) BRANCH
  101 FORMAT(1HO,'*****     SKIPPING ILLEGAL CONTROL CARD: ',A4,'     **
     ****')
      GO TO 1



    2 ISKIP=0
      IF(NUM.LE.MAXP) GO TO 3
      ISKIP=NUM-MAXP
      WRITE(6,102) NUM,MAXP
  102 FORMAT('0*****     ',I5,' PATCHES SPECIFIED, BUT ONLY ',I2,' ACCEP
     *TED - REST SKIPPED     *****')
      NUM=MAXP
    3 DO 4 LOOP=1,NUM
      READ(5,103) TOPL(LOOP),BOTL(LOOP),LPIX(LOOP),RPIX(LOOP),HATCH(LOOP
     *),(PCOMM(I,LOOP),I=1,10)
  103 FORMAT(5I5,10A4)
    4 CONTINUE
      NUMP=NUM
    5 IF(ISKIP.EQ.0) GO TO 1
      READ(5,103) J
      ISKIP=ISKIP-1
      GO TO 5
    6 ITAPE=NUM
      GO TO 1
    7 CALL SKPFIL(8,NUM-JFILE)
      JFILE=NUM
```

REPRODUCIBILITY OF THE
ORIGINAL PAGE IS POOR

```
      DO 10 LOOP=1,NUMP
      CALL GETREC(8,&11,&12,
      CALL ASCII(INPUT(1),264)
      WRITE(6,104) ITAPE,JFILE,LOOP,GHEAD,PHEAD,FCOMM,(PCOMM(I,LOOP),I=1
     *,10),TOPL(LOOP),BOTL(LOOP),LPIX(LOOP),RPIX(LOOP)
  104 FORMAT(1H1,'TAPE ',I4,5X,'FILE ',I3,5X,'PATCH ',I2/10X,'COMMON HEA
     *DER: ',25A4/10X,'PARTICULAR HEADER: ',25A4/10X,'FILE COMMENT: ',10
     *A4/10X,'PATCH COMMENT: ',10A4/10X,'TOP LINE: ',I4,5X,'BOTTOM LINE:
     * ',I4,5X,'LEFT PIXEL: ',I4,5X,'RIGHT PIXEL: ',I4/1H0,5X,' 25 MICRO
     *N PIXELS')
      SUM=0.0D0
      SUMSQ=0.0D0
      CALL SKPREC(8,TOPL(LOOP)-1,&11)
      LS=TOPL(LOOP)
      LE=BOTL(LOOP)
      LFTP=LPIX(LOOP)
      RGTP=RPIX(LOOP)
      L=0
      DO 8 LINE=LS,LE
      CALL GETREC(8,&11,&12)
      L=L+1
      K=0
      DO 8 IPIX=LFTP,RGTP
      K=K+1
      SUM=SUM+INPUT(IPIX)
      SUMSQ=SUMSQ+INPUT(IPIX)*INPUT(IPIX)
    8 OUTPUT(K,L)=INPUT(IPIX)
      NLINE=LE-LS+1
      NPIX=RGTP-LFTP+1
      NUMB=NLINE*NPIX
      CALL STATS
      CALL CLEAN(NLINE,NPIX,OUTPUT)
      CARD(1)=AVE
      CALL DIFF(OUTPUT,100,NLINE,NPIX,CARD(2))
      CALL BATCH  (HATCH(LOOP),NLINE,NPIX,CARD,OUTPUT)
      IBAT=HATCH(LOOP)+1
      WRITE(7,105) ITAPE,JFILE,LOOP,(CARD(I),I=1,IBAT)
  105 FORMAT(I4,I3,I2,8X,9F7.2)
      CALL  BCKREC(8,BOTL(LOOP)+1,&11)
   10 CONTINUE
      GO TO 1
   11 WRITE(6,106)
  106 FORMAT('0*****     UNEXPECTED EOF ENCOUNTERED - EXECUTION TERMINAT
     *ING     *****')
      STOP
   12 WRITE(6,107)
  107 FORMAT('0*****     PARITY ERROR - EXECUTION TERMINATING     *****'
     *)
      STOP
      END
```

```
      SUBROUTINE CLEAN (NLINE,NPIX,INPUT)
      REAL*8 AVE,STDEV,SUM,SUMSQ
      INTEGER*2 INPUT(100,100),HILIM,LOLIM
      LOGICAL*1 FIRST
      COMMON /STAT/ SUM,SUMSQ,AVE,STDEV,NUM
      DATA PCUT/5.0/
      FIRST=.TRUE.
      NUME=0
      HILIM=HFIX(SNGL(AVE+PCUT*STDEV+1))
      LOLIM=HFIX(SNGL(AVE-PCUT*STDEV))
      WRITE(6,100) PCUT
  100 FORMAT(10X,'AUTOMATIC PIXEL ELIMINATION AT ',F5.2,' STANDARD DEVIA
     *TIONS')
      DO 2 I=1,NLINE
      DO 2 J=1,NPIX
      IF(INPUT(J,I).GT.HILIM) GO TO 1
      IF(INPUT(J,I).LT.LOLIM) GO TO 1
      GO TO 2
    1 K=J+10
      IF(K.GT.NPIX) K=J-10

      SUM=SUM+INPUT(K,I)-INPUT(J,I)
      SUMSQ=SUMSQ+INPUT(K,I)*INPUT(K,I)-INPUT(J,I)*INPUT(J,I)
      RAT=DABS((INPUT(J,I)-AVE)/STDEV)
      IF(FIRST) WRITE(6,101)
  101 FORMAT(15X,'LINE',5X,'PIXEL',7X,'OLD',5X,'SIGMA',7X,'NEW')
      FIRST=.FALSE.
      WRITE(6,102) I,J,INPUT(J,I),RAT,INPUT(K,I)
  102 FORMAT(9X,3(6X,I4),4X,F6.2,6X,I4)
      INPUT(J,I)=INPUT(K,I)
      NUME=NUME+1
    2 CONTINUE
      IF(NUME.LE.0) GO TO 4
      WRITE(6,103) NUME
  103 FORMAT(10X,I3,' PIXELS ELIMINATED')
      CALL STATS
      RETURN
    4 WRITE(6,104)
  104 FORMAT(10X,'NO PIXELS ELIMINATED')
      RETURN
      END
```

```
      SUBROUTINE BATCH (IB,NLINE,NPIX,CARD,INPUT)
      REAL*8 SUM,SUMSQ,AVE,STDEV
      REAL*4 CARD(9)
      INTEGER*4 ISUM(50)
      INTEGER*2 INPUT(100,100),OUTPUT(50,50)
      COMMON /STAT/ SUM,SUMSQ,AVE,STDEV,NUM
      IF(IB.LT.2) RETURN
      DO 5 IBIN=2,IB
      BSQ=IBIN*IBIN
      SUM=0.0D0
      SUMSQ=0.0D0
      NL=NLINE/IBIN
      NP=NPIX/IBIN
      LOCL=0
      DO 3 IL=1,NL
      DO 1 I=1,NP
    1 ISUM(I)=0
      DO 2 I=1,IBIN
      LOCL=LOCL+1
      LOCP=0
      DO 2 IP=1,NP
      DO 2 J=1,IBIN
      LOCP=LOCP+1
    2 ISUM(IP)=ISUM(IP)+INPUT(LOCP,LOCL)
      DO 3 IP=1,NP
      OUTPUT(IP,IL)=HFIX(ISUM(IP)/BSQ+0.5)
      SUM=SUM+OUTPUT(IP,IL)
    3 SUMSQ=SUMSQ+OUTPUT(IP,IL)*OUTPUT(IP,IL)
      ISIZE=25*IBIN
      WRITE(6,100) ISIZE
  100 FORMAT(1H0,5X,I3,' MICRON PIXELS')
      NUM=NL*NP
      CALL STATS
      CALL DIFF(OUTPUT,50,NL,NP,CARD(IBIN+1))
    5 CONTINUE
      RETURN
      END
```

```
      SUBROUTINE DIFF(ARRAY,ISIZE,NLINE,NPIX,ASTDEV)
      REAL*8 SUM,SUMSQ,AVE,STDEV
      INTEGER*2 ARRAY(ISIZE,ISIZE)
      COMMON /STAT/ SUM,SUMSQ,AVE,STDEV,NUM
      SUM=0.0D0
      SUMSQ=0.0D0
      NPM2=NPIX-2
      NLM2=NLINE-2
      DO 3 IL=3,NLM2
      ILM2=IL-2
      ILP2=IL+2
      DO 3 IP=3,NPM2
      IPM2=IP-2
      IPP2=IP+2
      IPM1=IP-1
      IPP1=IP+1
      ISUM=0
      DO 1 I=ILM2,ILP2
    1 ISUM=ISUM+ARRAY(IPP2,I)+ARRAY(IPM2,I)
      DO 2 I=IPM1,IPP1
    2 ISUM=ISUM+ARRAY(I,ILP2)+ARRAY(I,ILM2)
      X=ARRAY(IP,IL)-ISUM/16.0
      SUM=SUM+X
      SUMSQ=SUMSQ+X*X
    3 CONTINUE
      NUM=(NPIX-4)*(NLINE-4)
      WRITE(6,100)
  100 FORMAT(10X,'DIFFERENTIAL NOISE MEASUREMENT')
      CALL STATS
      ASTDEV=STDEV/1.0308
      WRITE(6,101) ASTDEV
  101 FORMAT(10X,'REDUCED STANDARD DEVIATION: ',F7.2)
      RETURN
      END
      SUBROUTINE STATS
      REAL*8 SUM,SUMSQ,AVE,STDEV
      COMMON  /STAT/ SUM,SUMSQ,AVE,STDEV,NUM
      AVE=SUM/NUM
      STDEV=DSQRT((SUMSQ-(NUM*AVE*AVE))/(NUM-1))
      WRITE(6,100) NUM,AVE,STDEV
  100 FORMAT(10X,'NUMBER: ',I5,5X,'MEAN: ',F7.2,5X,'STANDARD DEVIATION:
     *',F7.2)
      RETURN
      END
```

```
ASCII    CSECT                                                          0010
*  R1  POINTER TO ARGUMENT LIST                                         0020
*  R2  ADDRESS OF ARRAY                                                 0030
*  R3  ADDRESS OF LENGTH                                                0040
*  R4  OR-ING POINTER                                                   0050
*  R5                                                                   0060
*  R6  INCREMENT                                                        0070
*  R7  ADDRESS OF ARRAY+LENGTH (LAST BYTE IN HEADER + 1)                0080
         SAVE    (14,12),,*                                            0090
         LR      12,15                                                 0100
         USING   ASCII,12                                              0110
         ST      13,SAVEAREA+4                                         0120
         LA      13,SAVEAREA                                           0130
         L       2,0(0,1)      ADDRESS OF ARRAY                        0140
         L       3,4(0,1)      ADDRESS OF LENGTH                       0150
         LA      6,1           LOOP INCREMENT                          0160
         L       4,0(0,1)      ADDRESS OF ARRAY                        0170
         L       7,0(,3)       LENGTH                                  0180
         AR      7,2           ADD ADDRESS OF ARRAY                    0190
LOPPAR   NI      0(4),X'7F'    CLEAR PARITY BIT                        0200
         BXLE    4,6,LOPPAR                                            0210
*                                                                      0220
         L       3,0(,3)       LENGTH                                  0230
         XLATE   0(,2),0(,3)                                           0240
         L       13,4(13)                                              0250
         RETURN  (14,12),RC=0                                          0260
SAVEAREA DC      F'72',17F'0'                                          0270
         END
```

SECTION 107 PHOTODIODE SPECTRAL RESPONSE CURVES

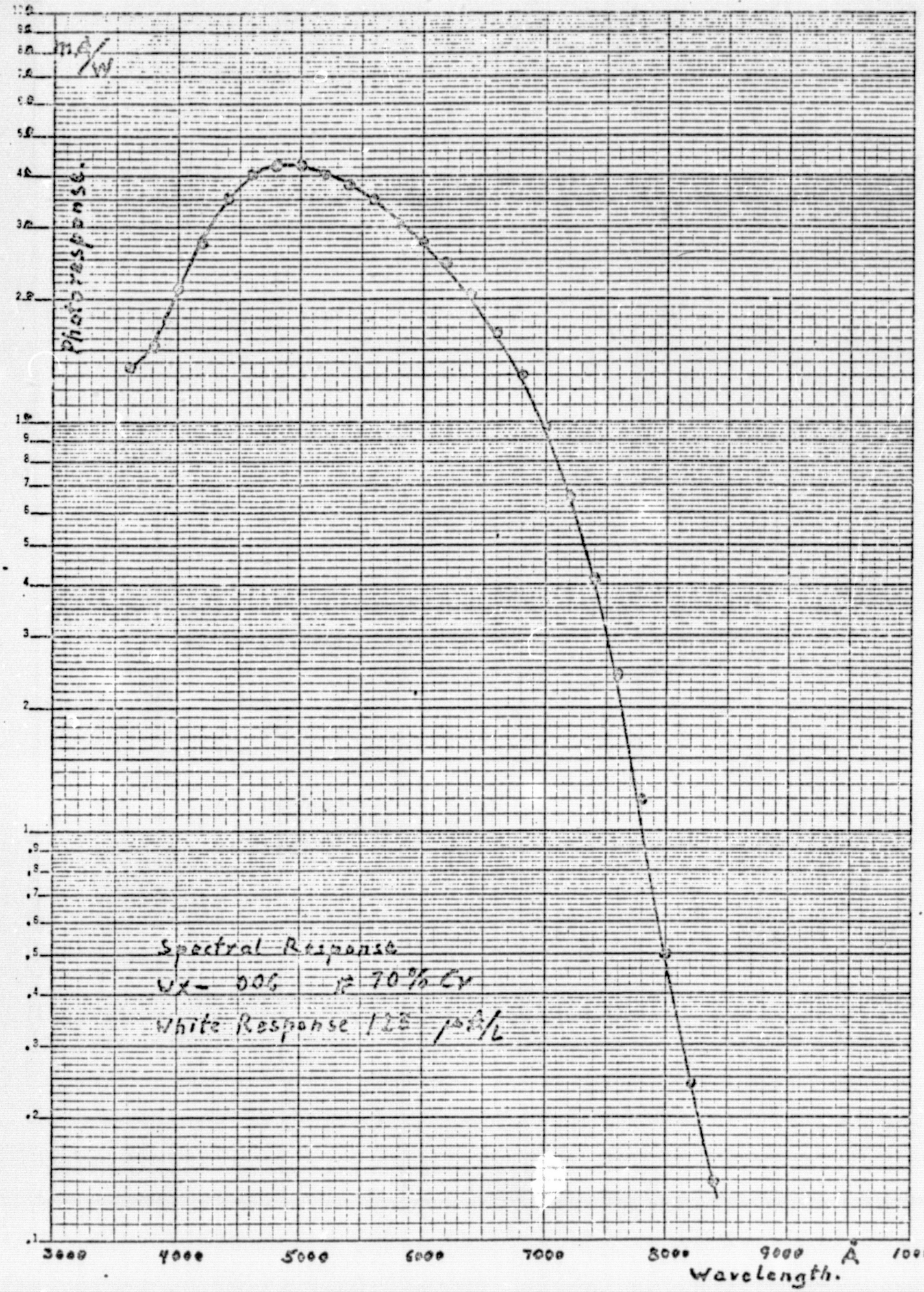
mA/W
Photoresponse
Spectral Response
Wx- 006 ≥ 70% Cr
White Response 125 μA/L
3600
4000
5000
6000
7000
8000
9000
Å
10000
Wavelength.

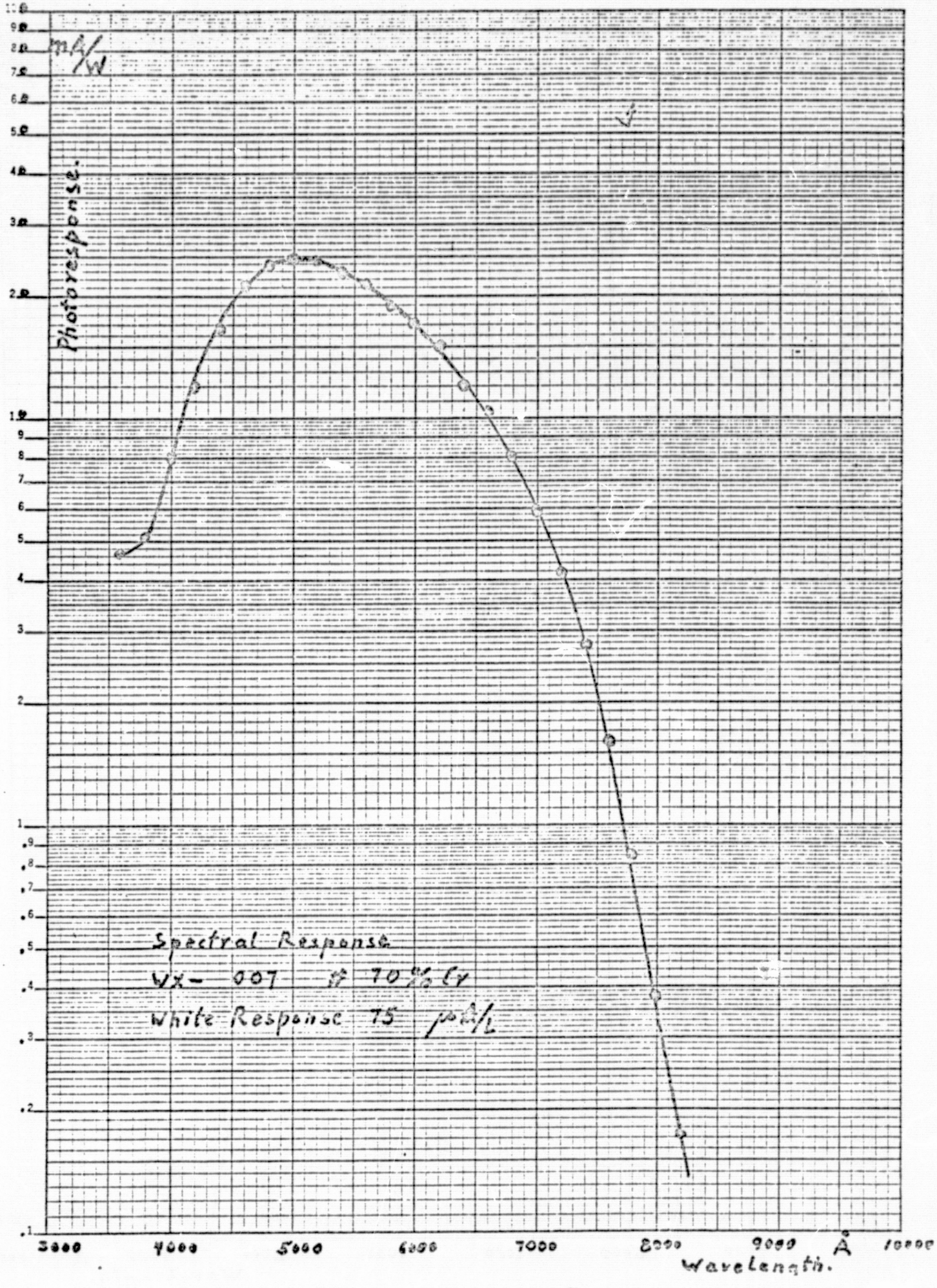

SEMI-LOGARITHMIC 46 5492
3 CYCLES X 70 DIVISIONS
KEUFFEL & ESSER CO.

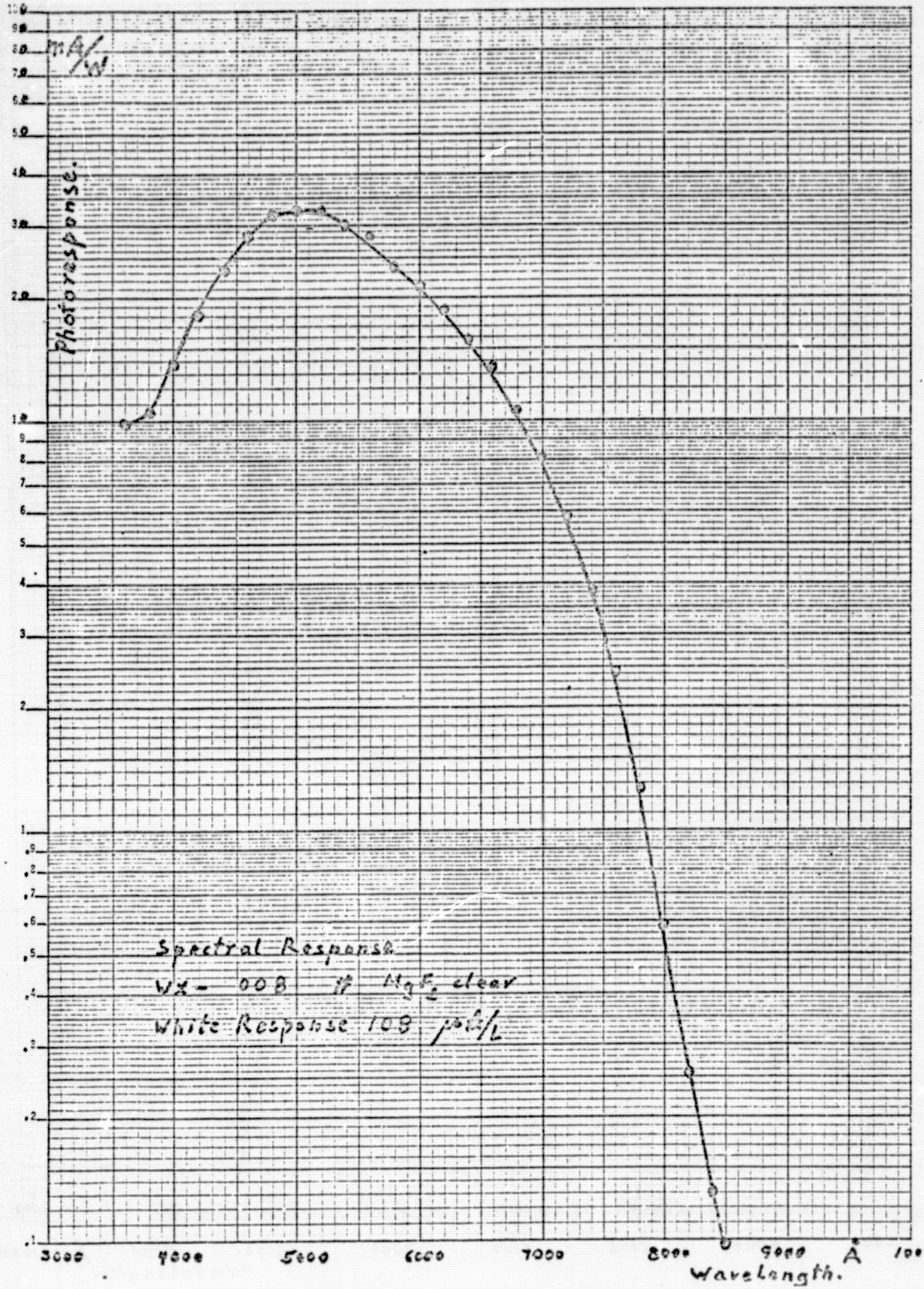

KEUFFEL & ESSER CO. MADE IN U.S.A. 46 5492 SEMI-LOGARITHMIC 3 CYCLES X 70 DIVISIONS

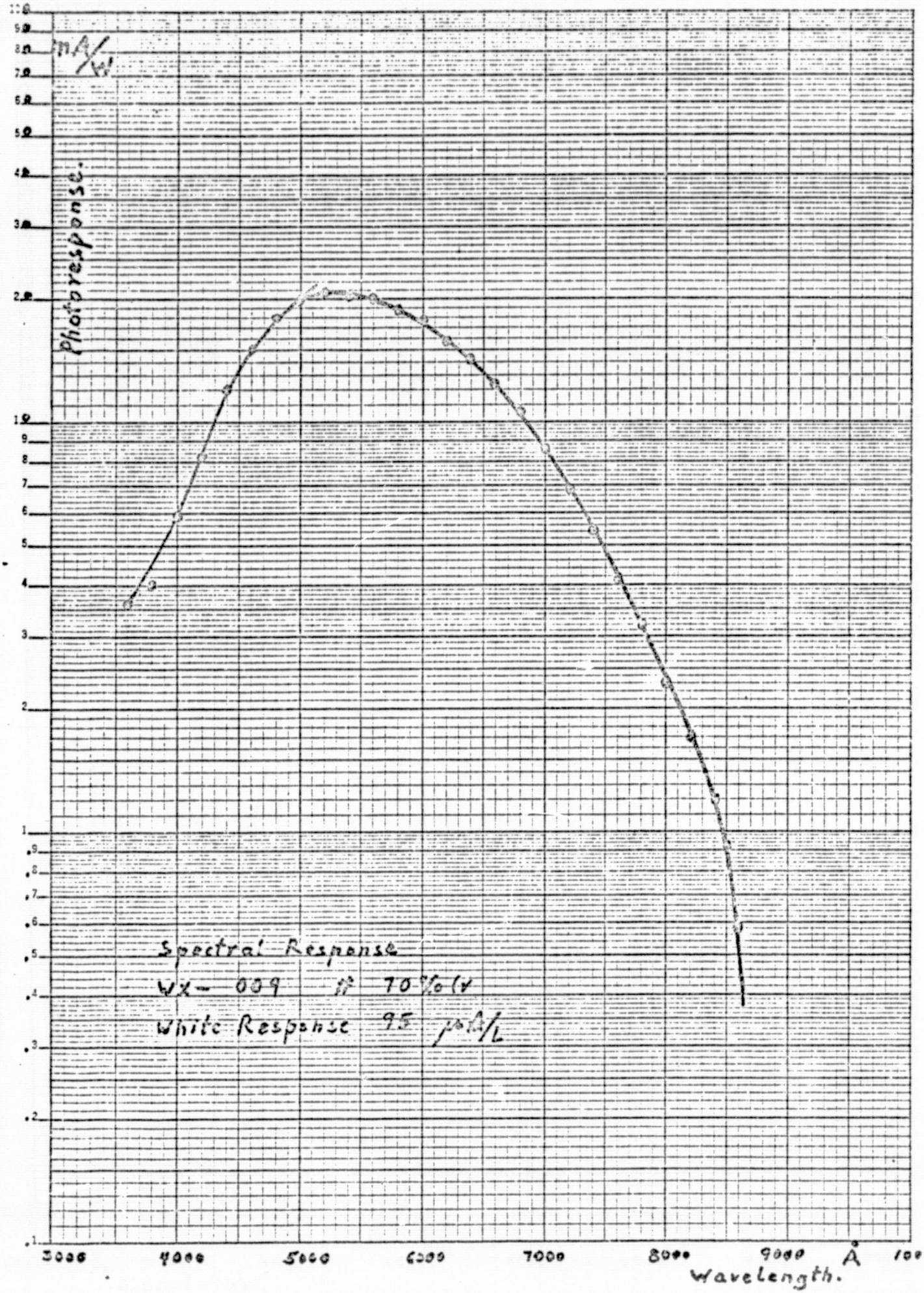
mA/W
Photoresponse.
Spectral Response
Wx - 009 # 70%(r
White Response 95 μA/L
3000
4000
5000
6000
7000
8000
9000
Å
10000
Wavelength.

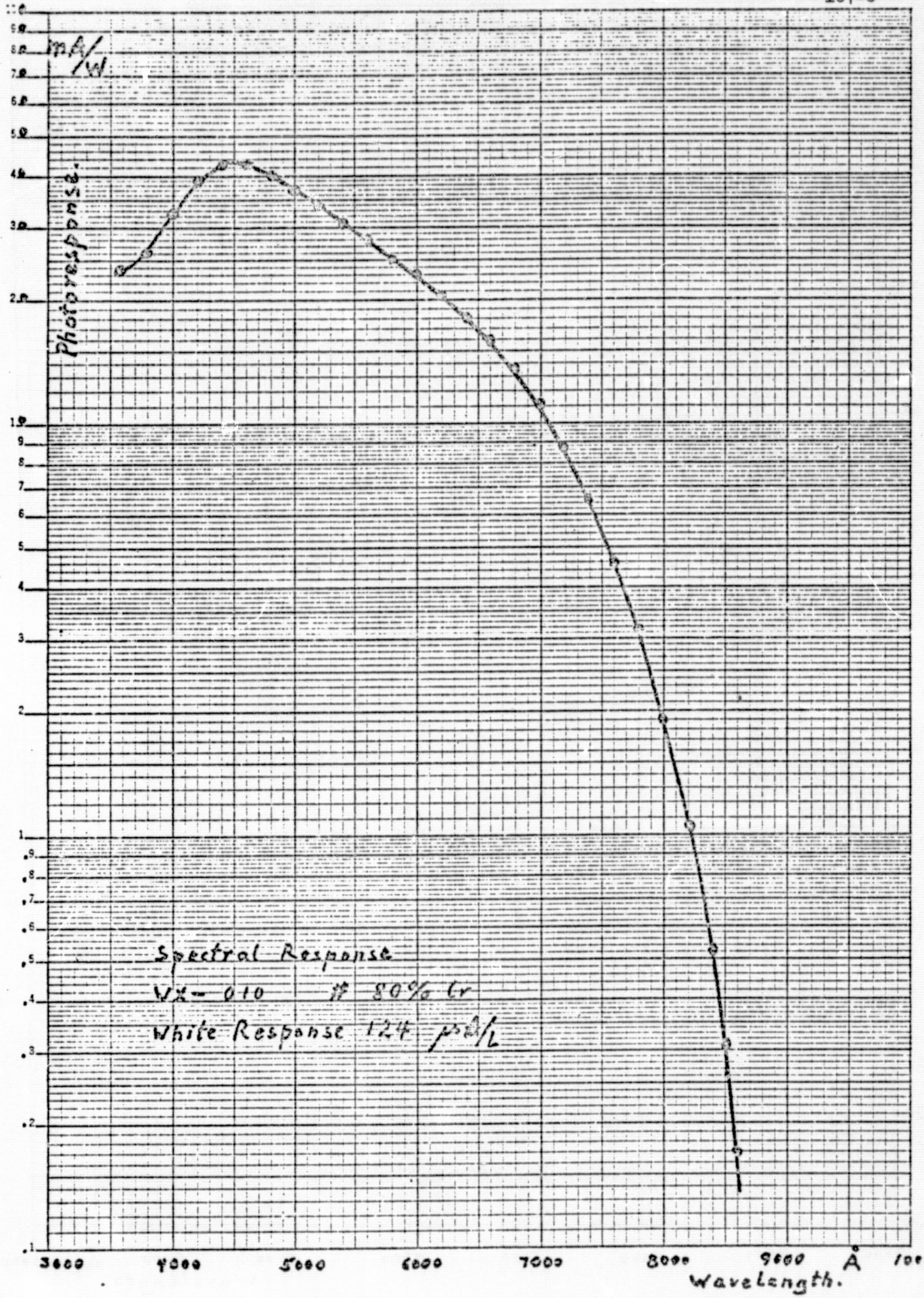

KEUFFEL & ESSER CO. 46 5492 SEMI-LOGARITHMIC 3 CYCLES X 70 DIVISIONS MADE IN U.S.A.

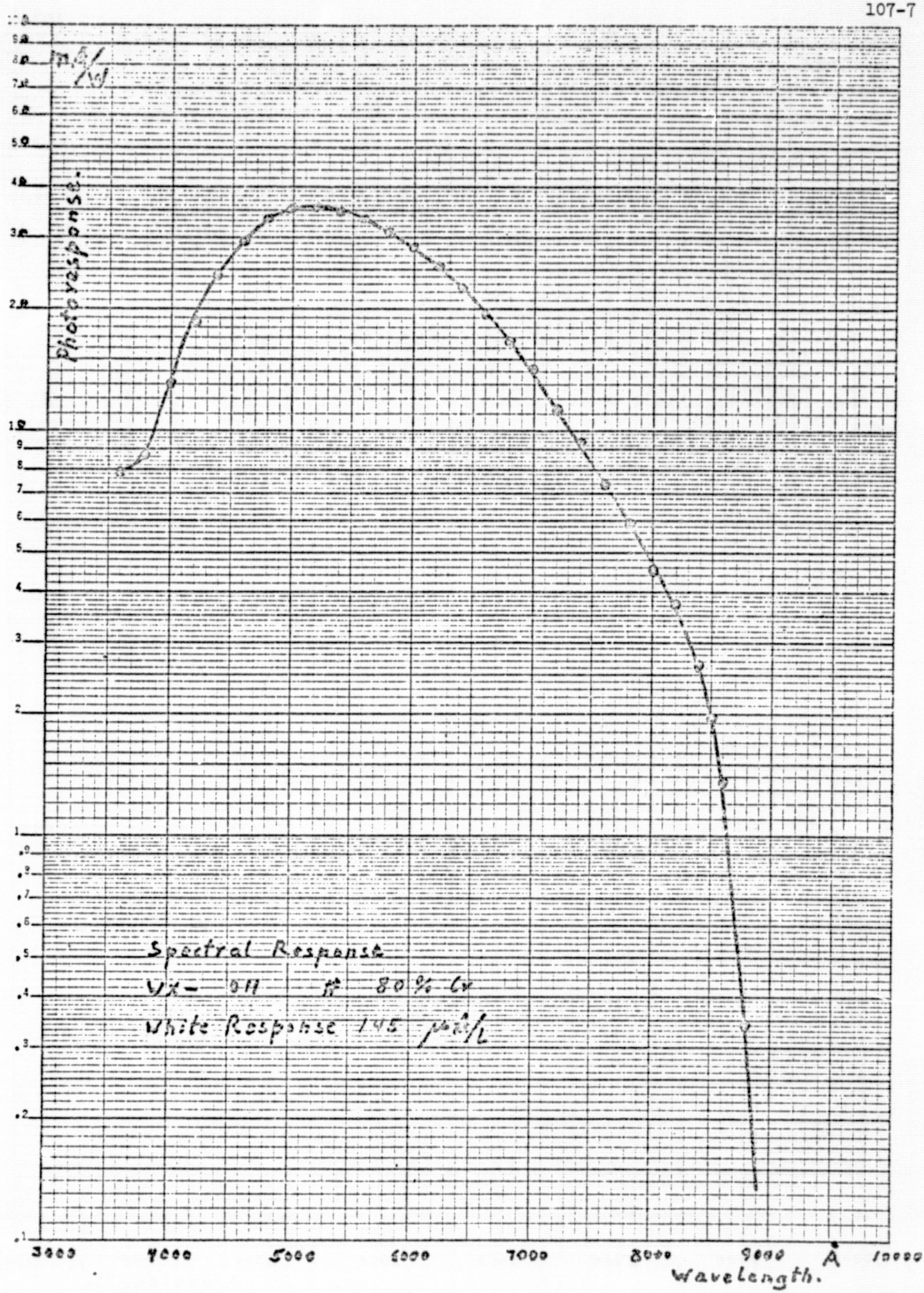

KEUFFEL & ESSER CO. SEMI-LOGARITHMIC 3 CYCLES X 70 DIVISIONS 46 5492 MADE IN U.S.A.

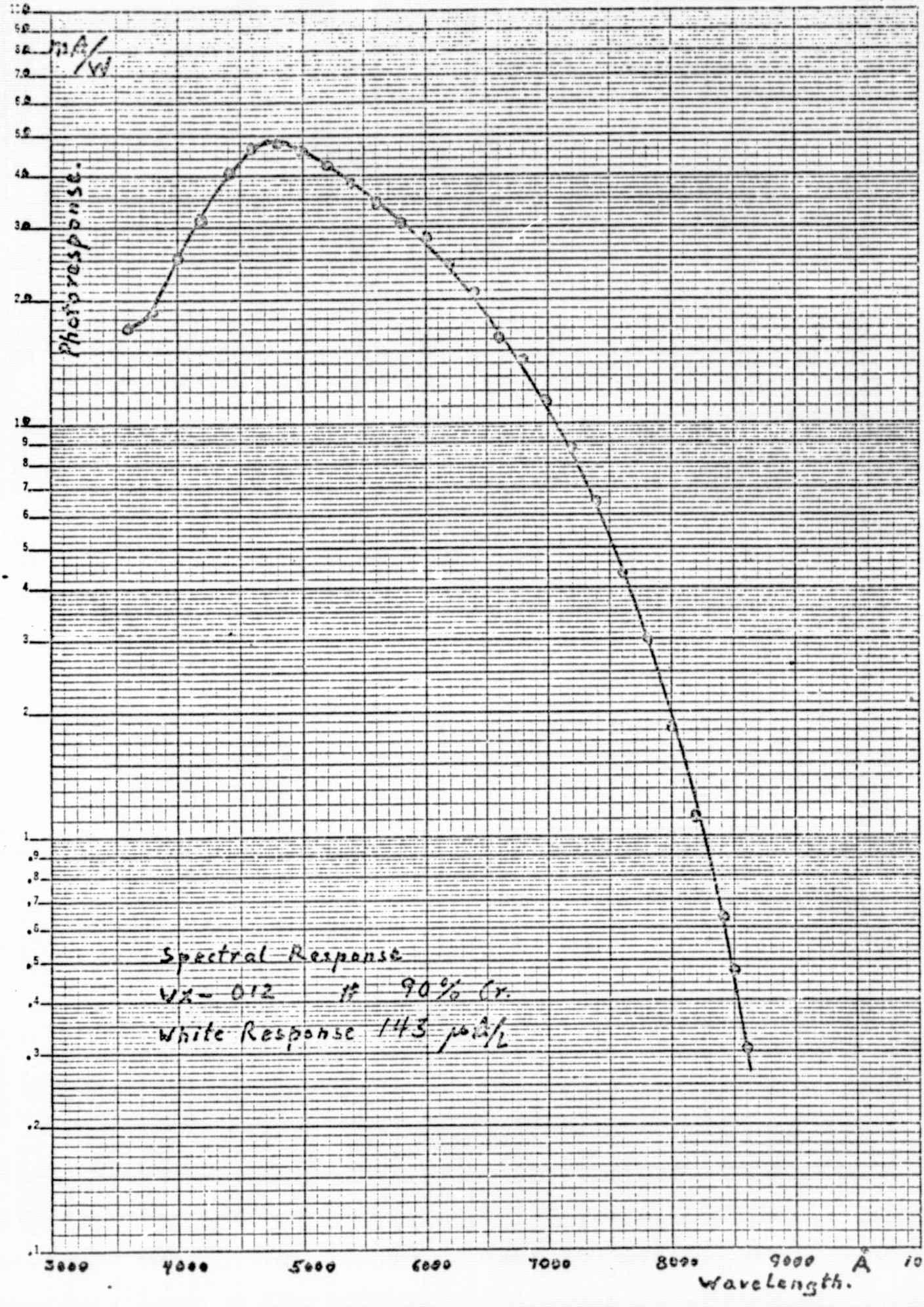

KEUFFEL & ESSER CO. SEMI-LOGARITHMIC 46 5492

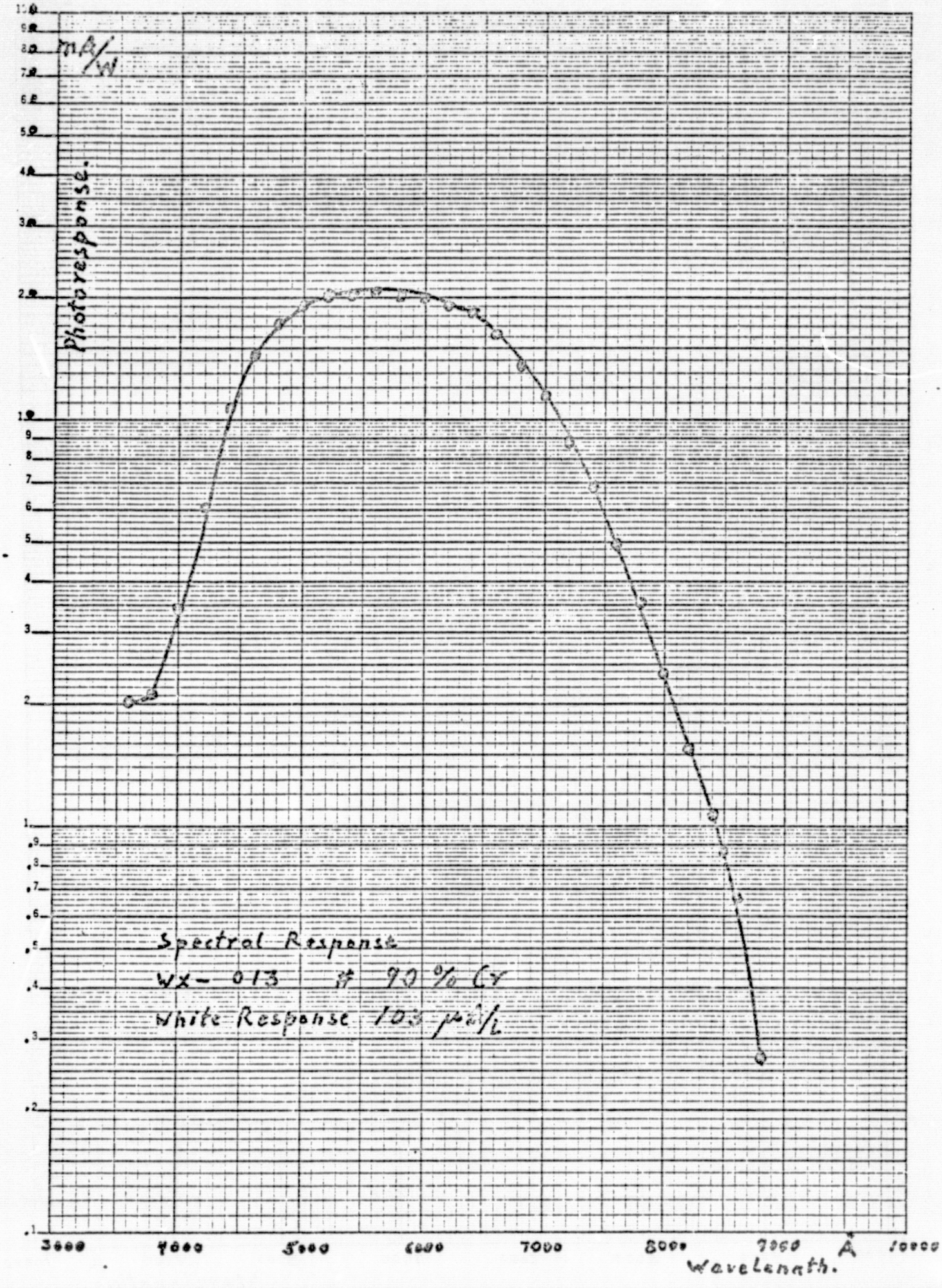
mA/W
Photoresponse.
Spectral Response
WX-013 # 90% Cr
White Response 103 μa/L
3000
4000
5000
6000
7000
8000
7950 Å
10000
Wavelength.

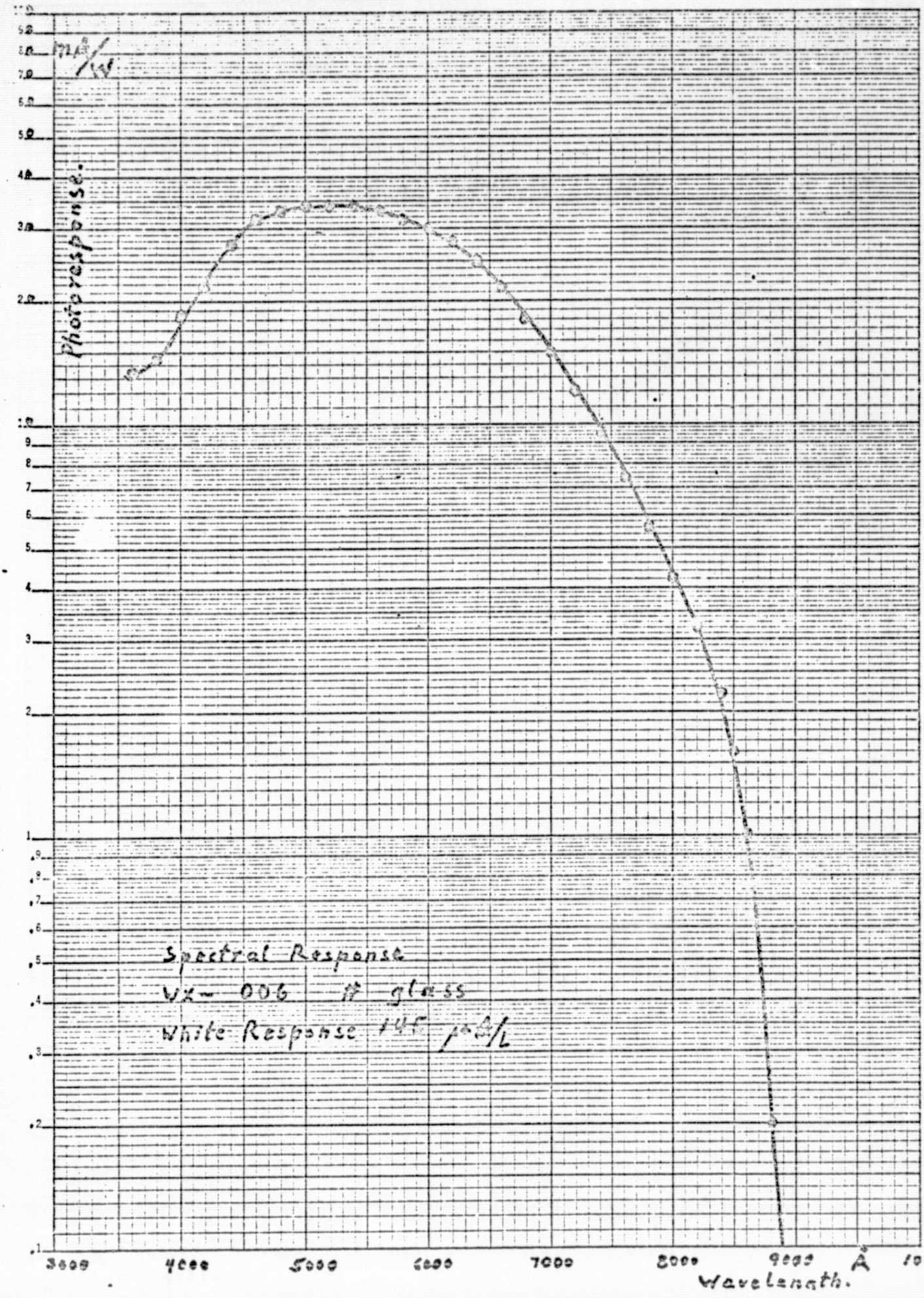

KEUFFEL & ESSER CO. 46 5492 SEMI-LOGARITHMIC

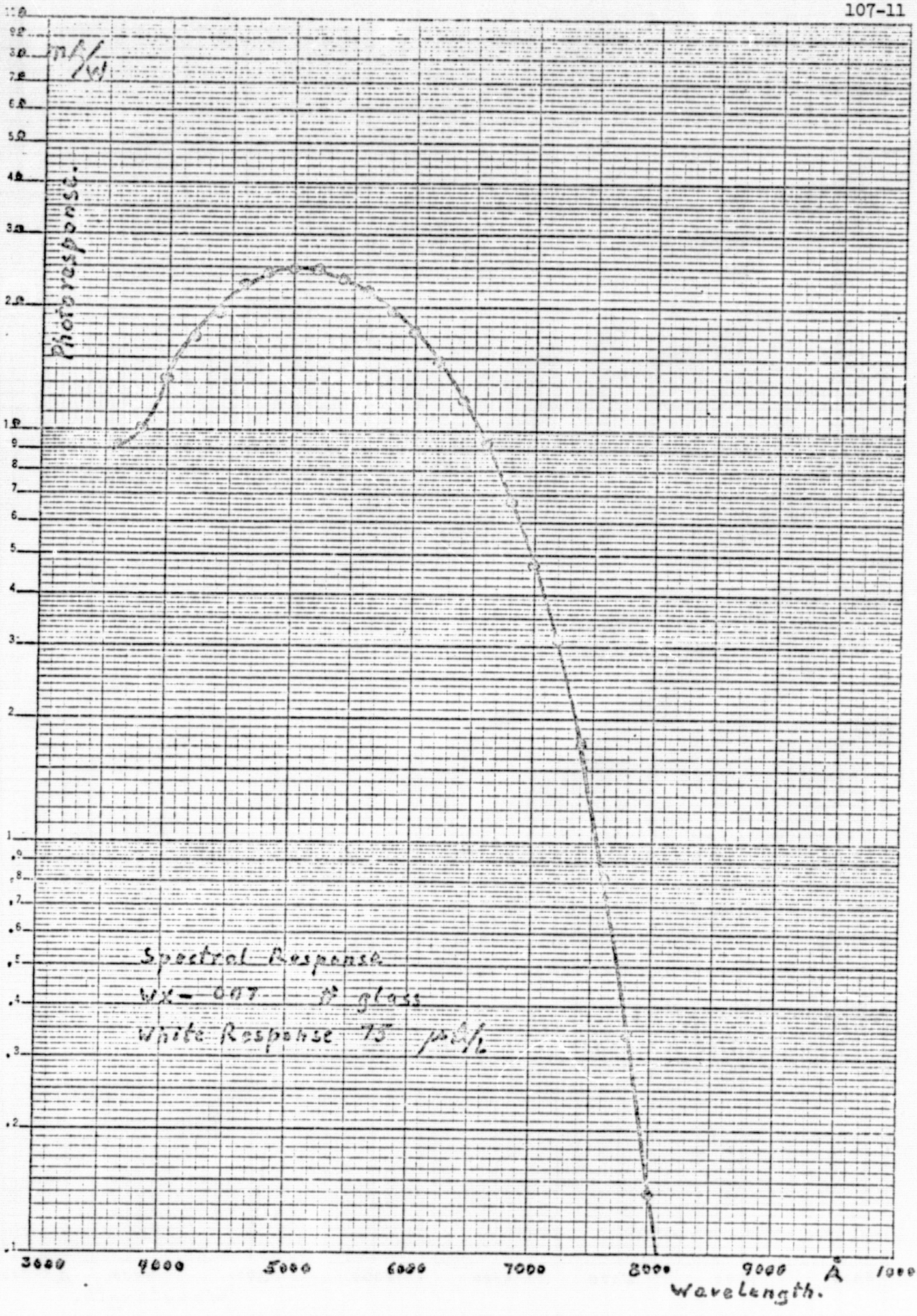

K&E SEMI LOGARITHMIC
46 5452
KEUFFEL & ESSER CO.

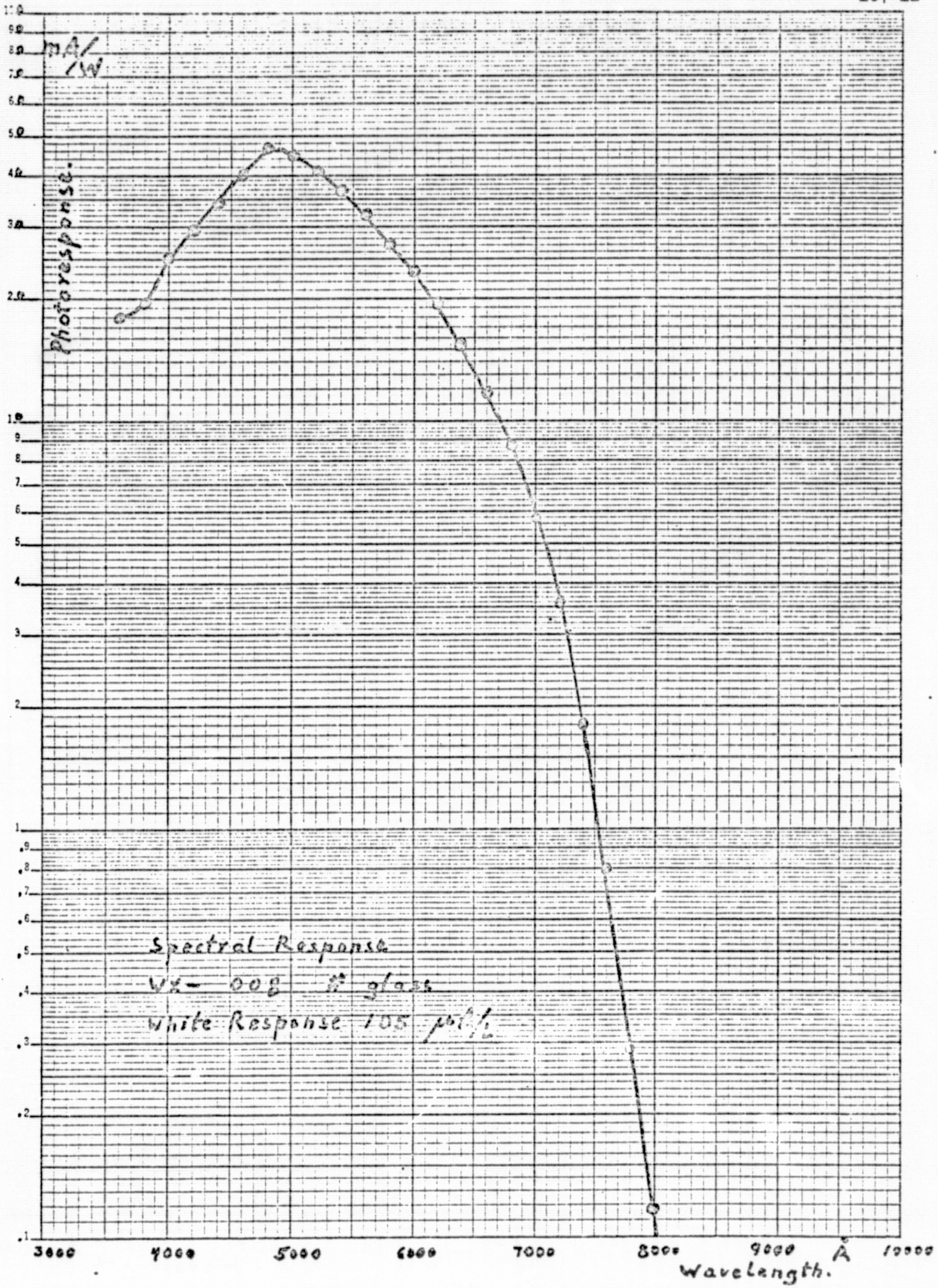
mA/W
Photoresponse.
10.0
9.0
8.0
7.0
6.0
5.0
4.0
3.0
2.0
1.0
9
8
7
6
5
4
3
2
1
.9
.8
.7
.6
.5
.4
.3
.2
.1
3000
4000
5000
6000
7000
8000
9000
Å
10000
Wavelength.
Spectral Response
VX- 008 # glass
White Response 105 μA/L
SEMI LOGARITHMIC
46 5492
KEUFFEL & ESSER CO.

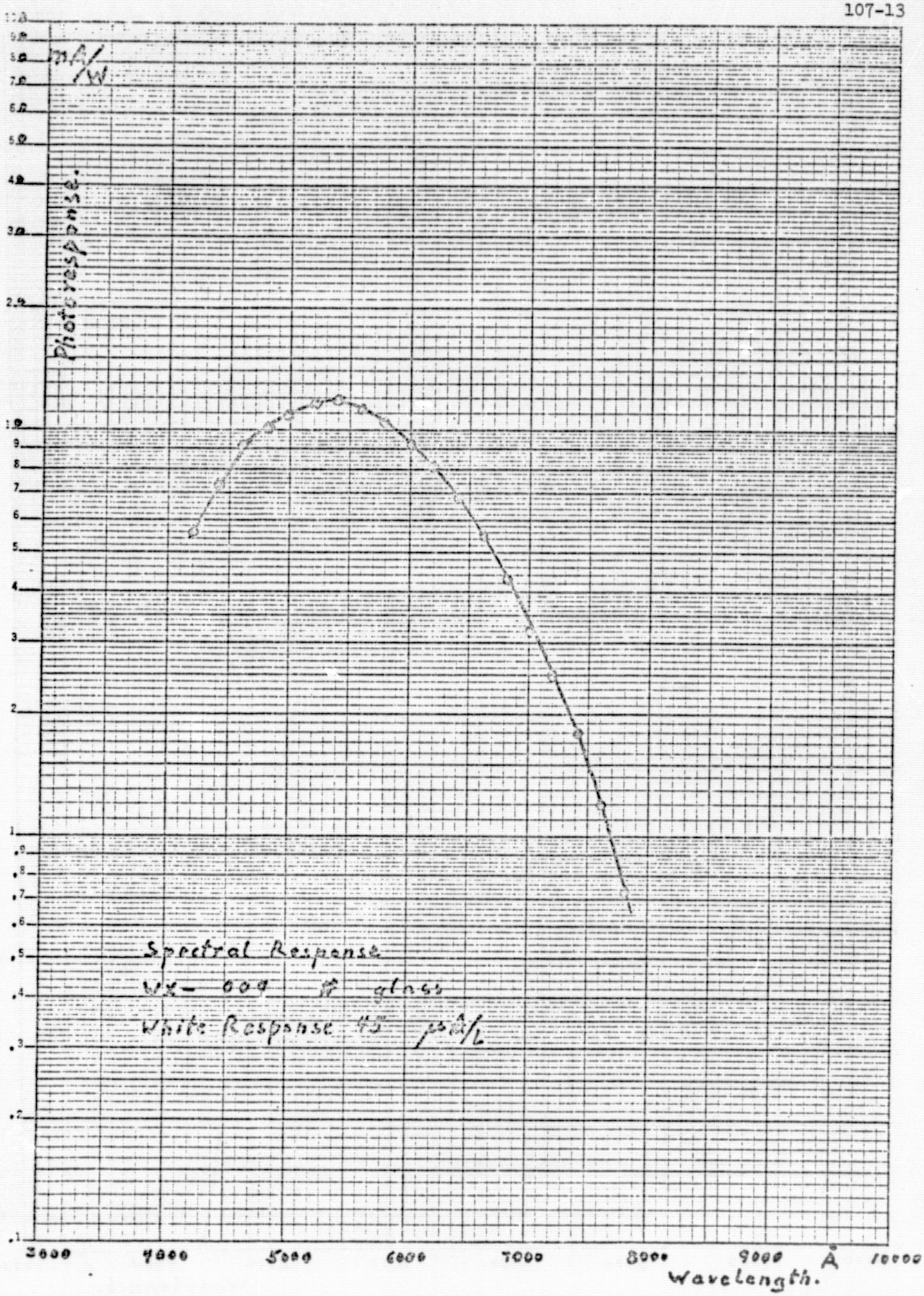

KEUFFEL & ESSER CO.
46 5492
SEMI-LOGARITHMIC

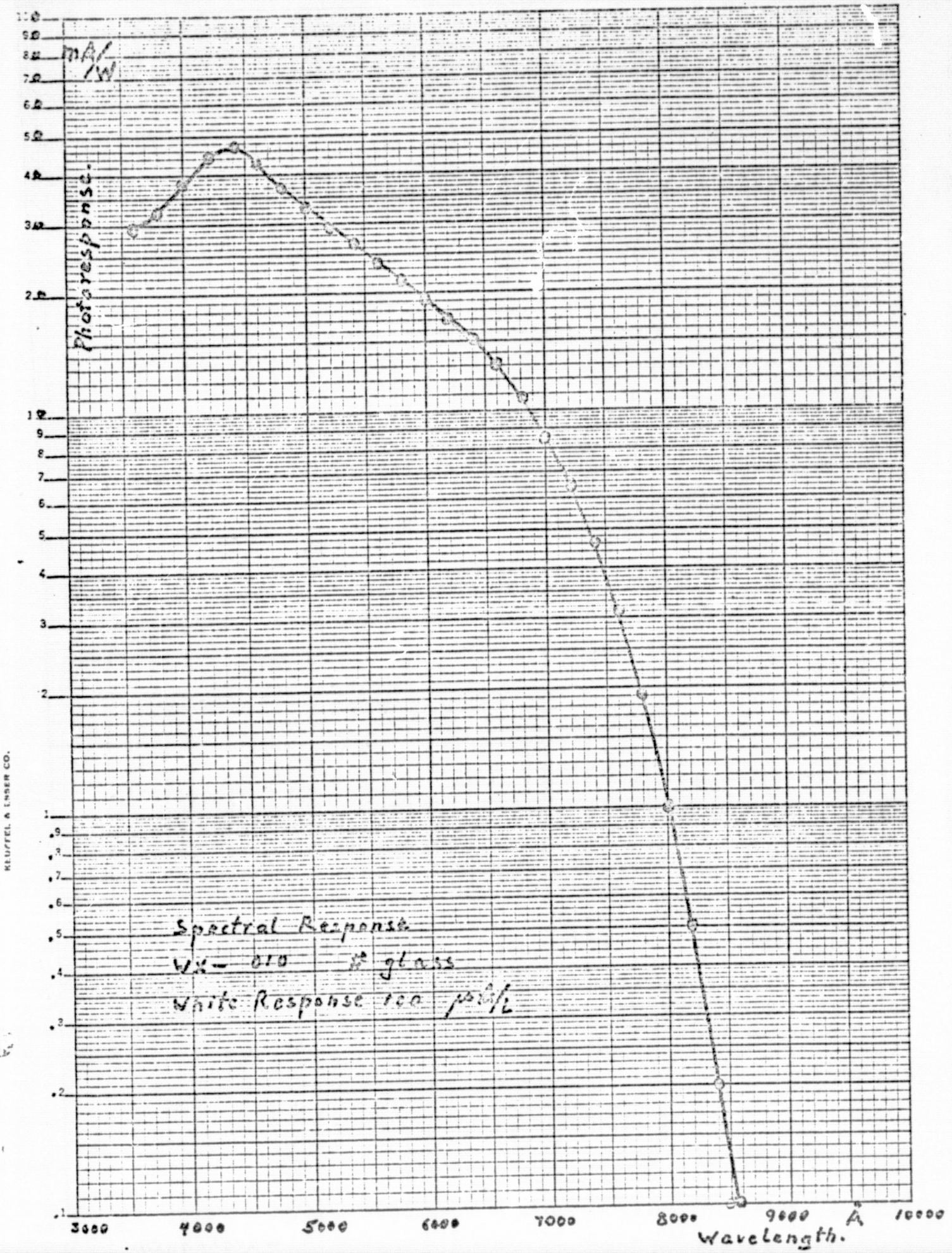

KEUFFEL & ESSER CO.

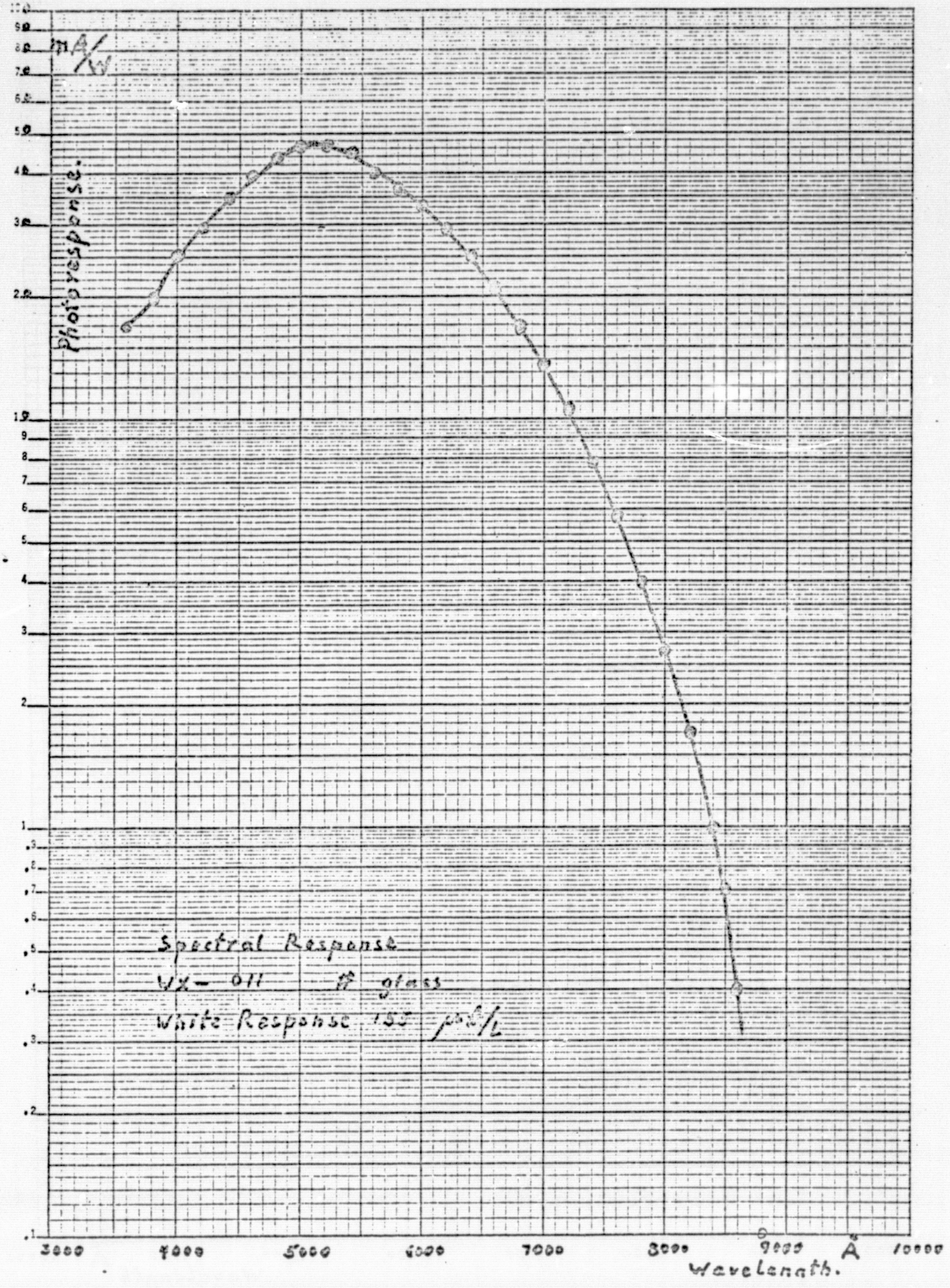
mA/W
Photoresponse.
Spectral Response
Wx - 011 # glass
White Response 150 μa/L
3000
4000
5000
6000
7000
8000
9000 Å
10000
Wavelength.

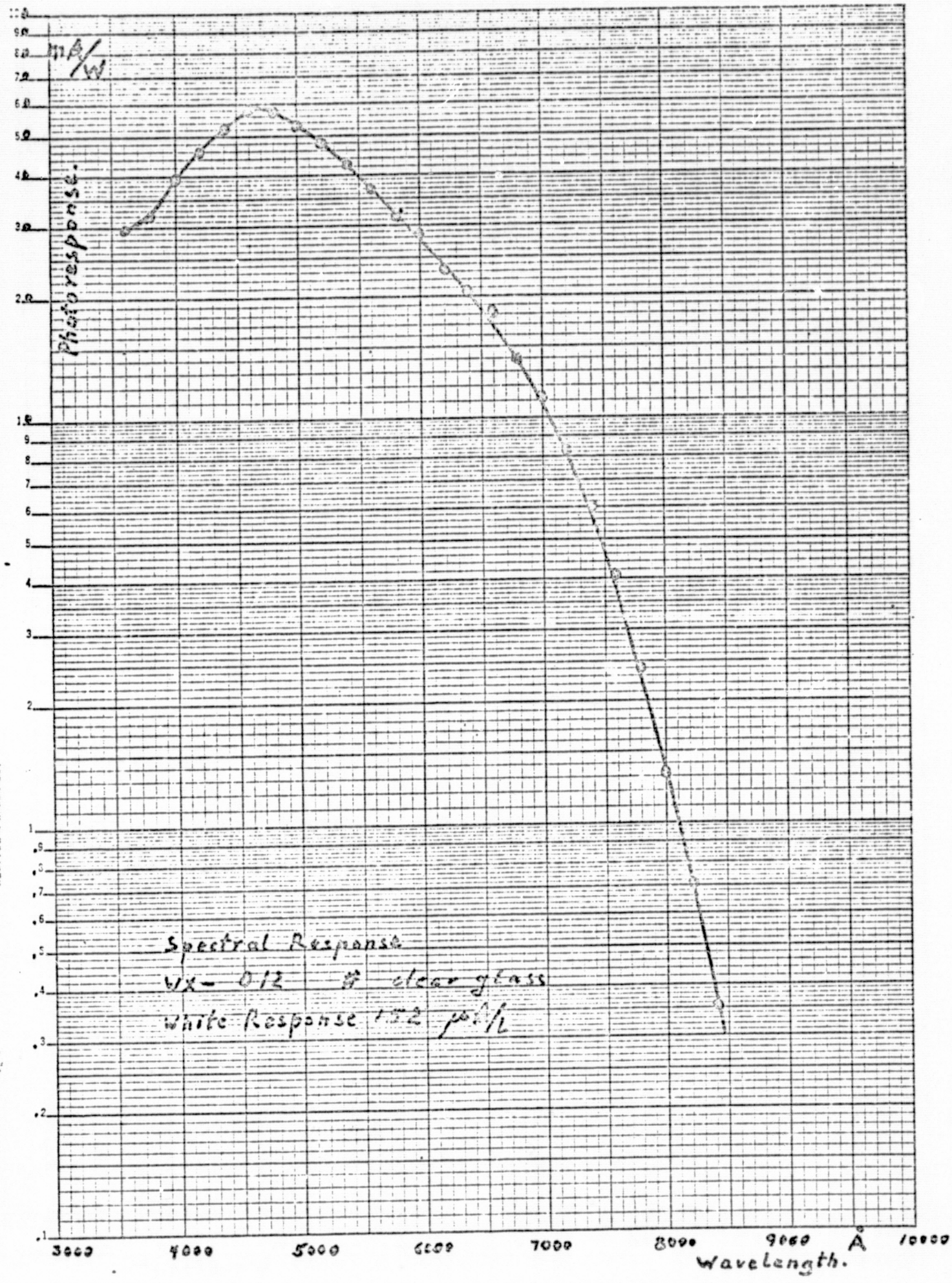

KEUFFEL & ESSER CO. MADE IN U.S.A. 46 5492 SEMI LOGARITHM.C

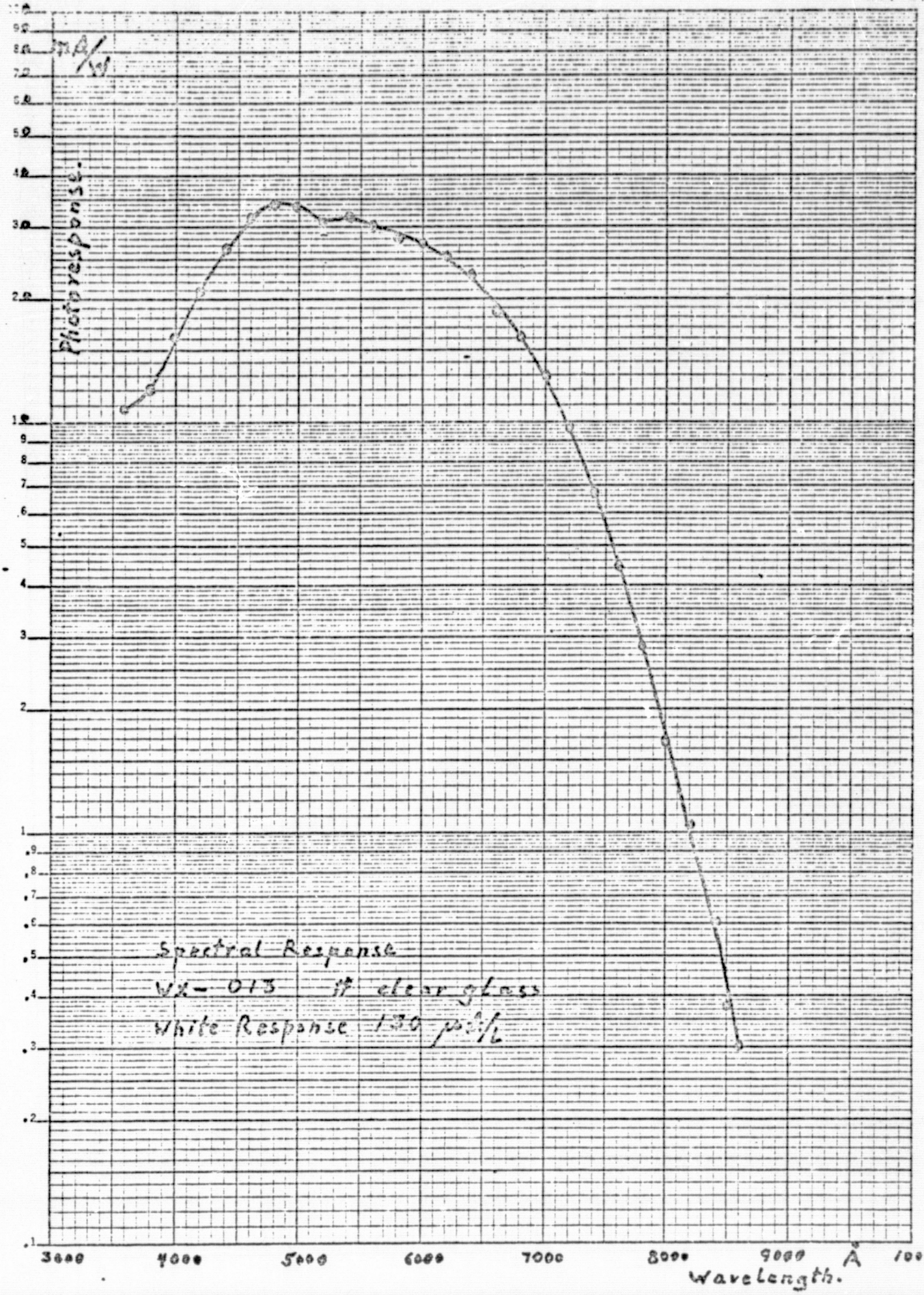
mA/w
Photoresponse.
10
9
8
7
6
5
4
3
2
1
.9
.8
.7
.6
.5
.4
.3
.2
.1
3000
4000
5000
6000
7000
8000
9000
Å
10000
Wavelength.
Spectral Response
VX-013 ¾" clear glass
White Response 130 μA/l

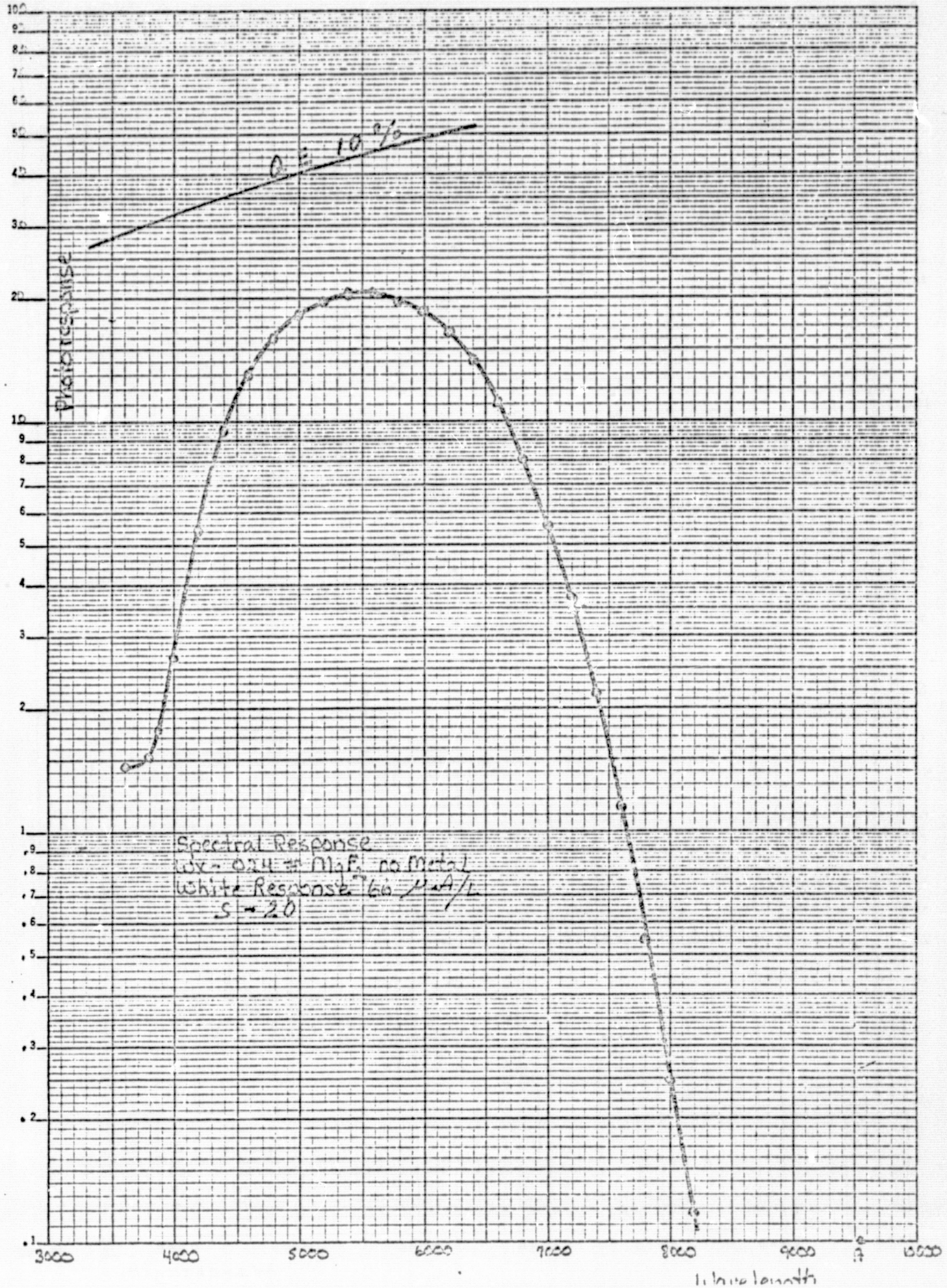

KEUFFEL & ESSER CO. MADE IN U.S.A.
3 CYCLES X 70 DIVISIONS

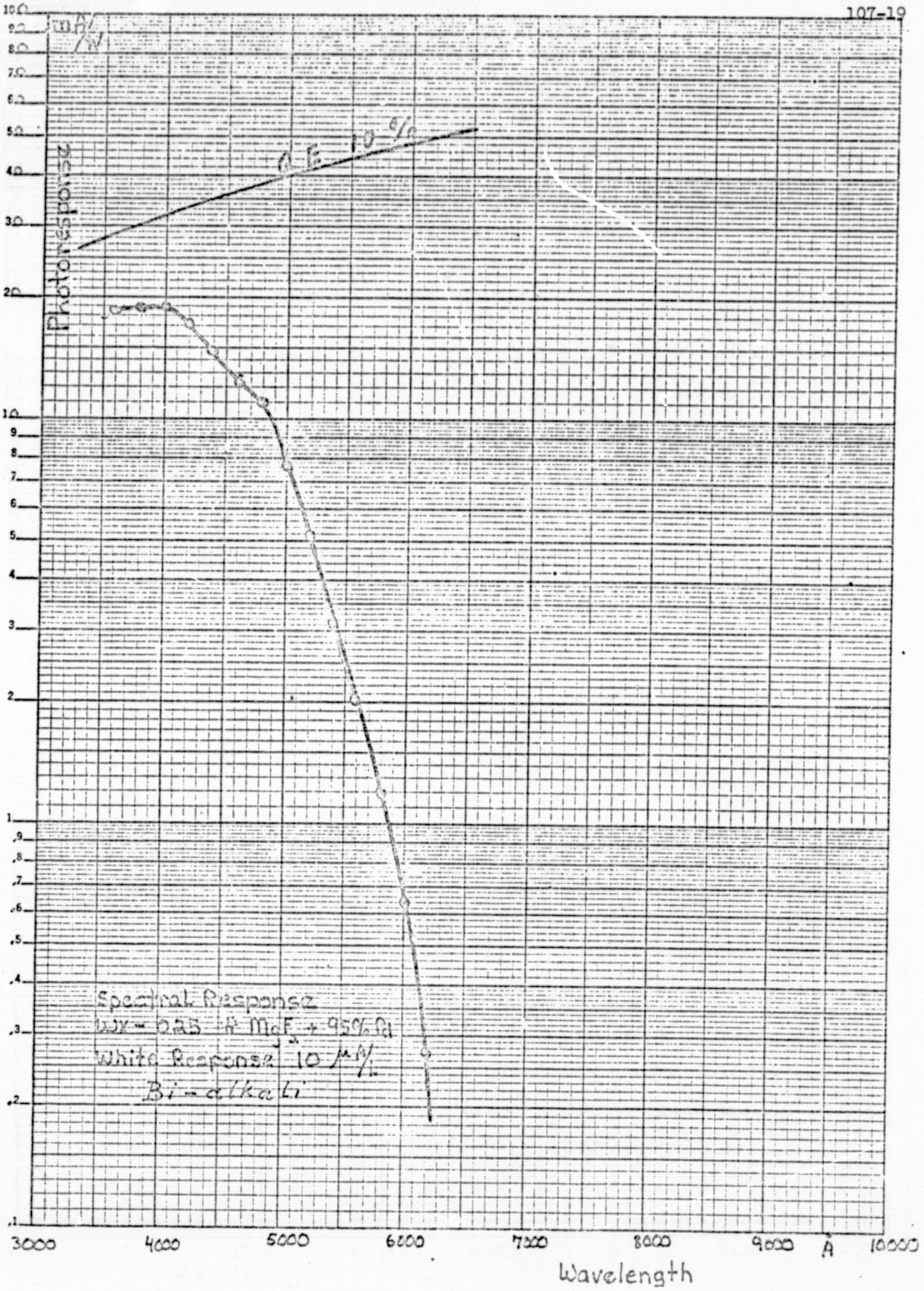

EMI 3 CYCLES X 70 DIVISIONS KEUFFEL & ESSER CO. MADE IN U.S.A.

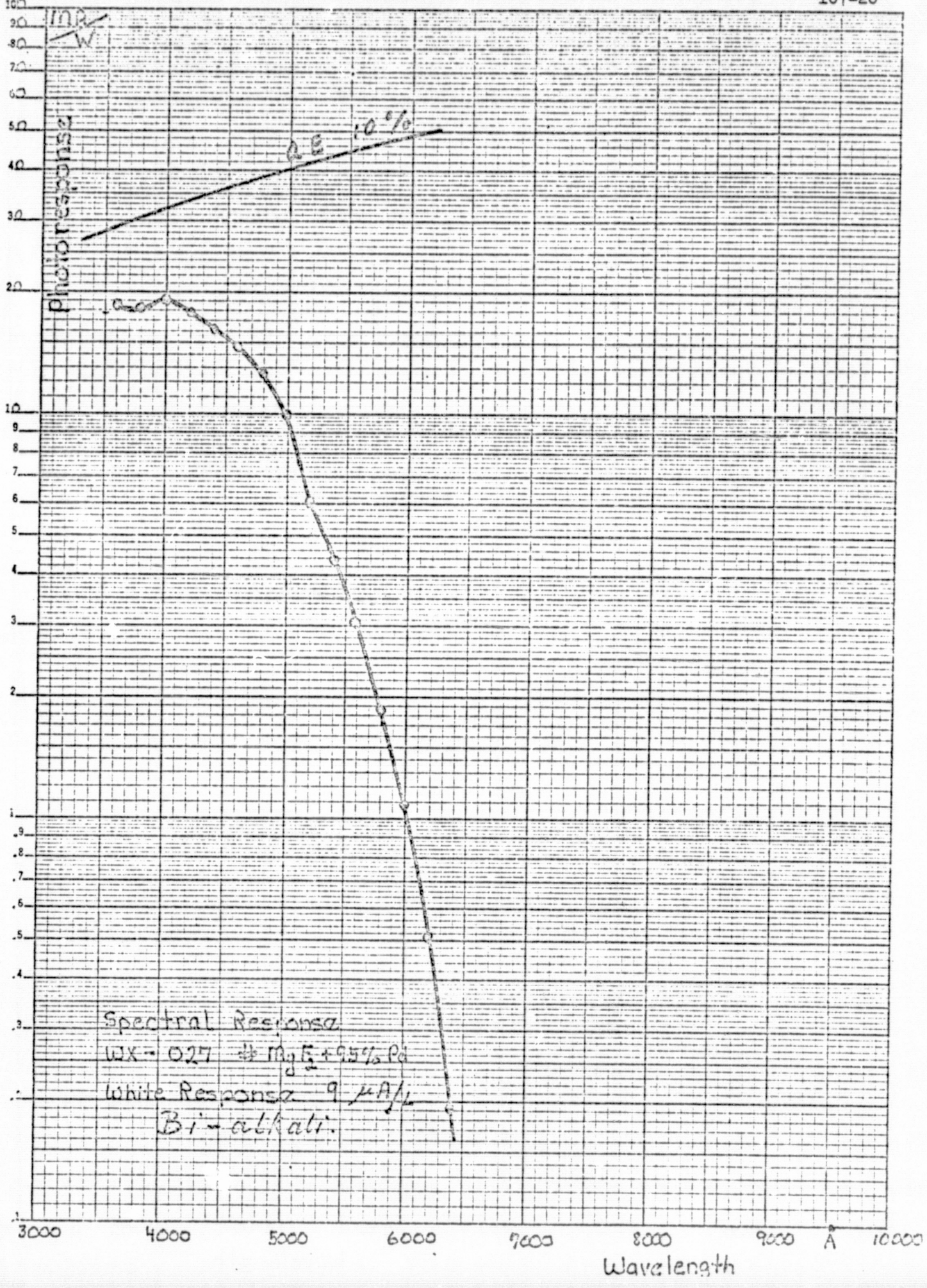

KEUFFEL & ESSER CO. MADE IN U.S.A.

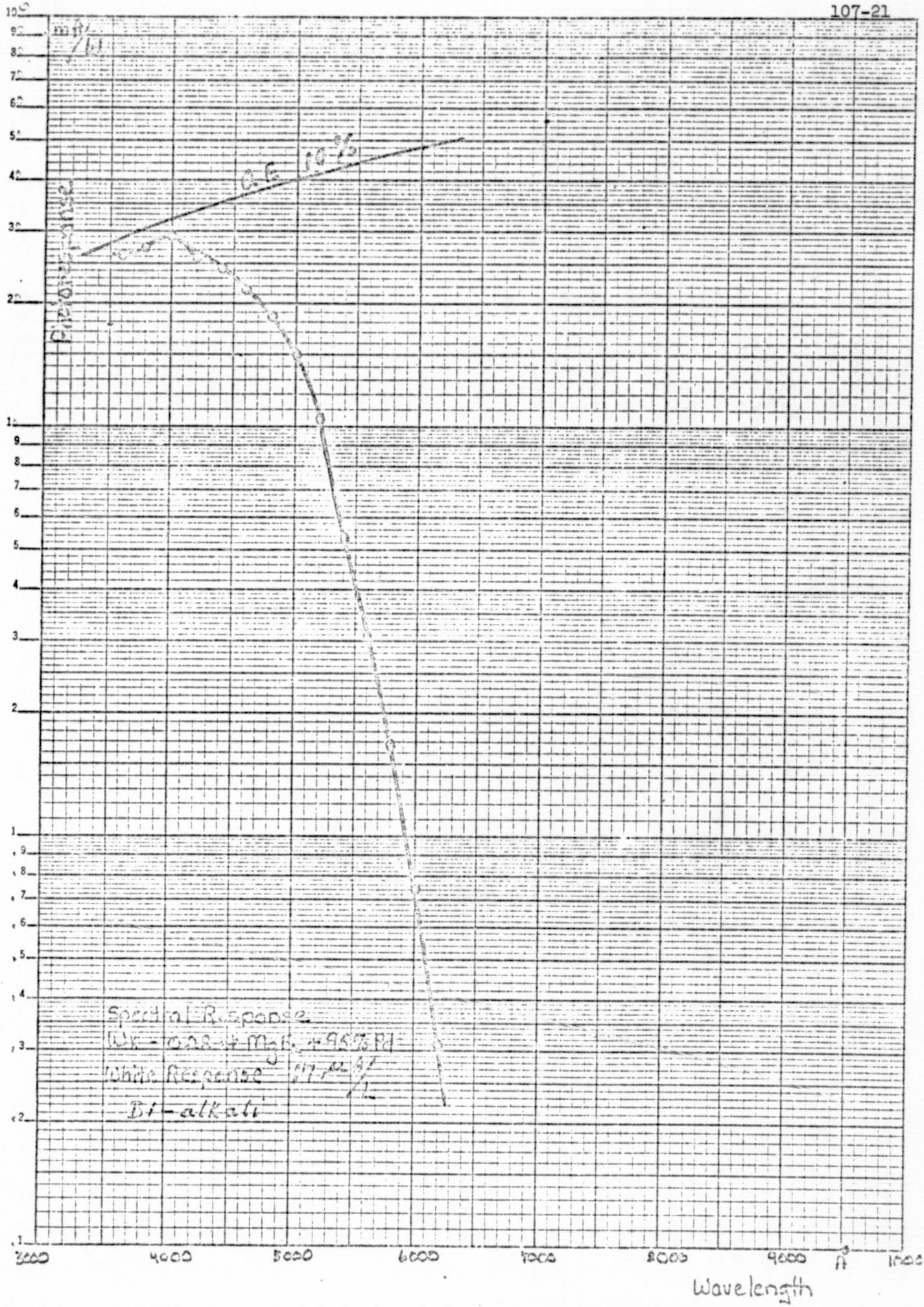

Spectral Response
Wavelength

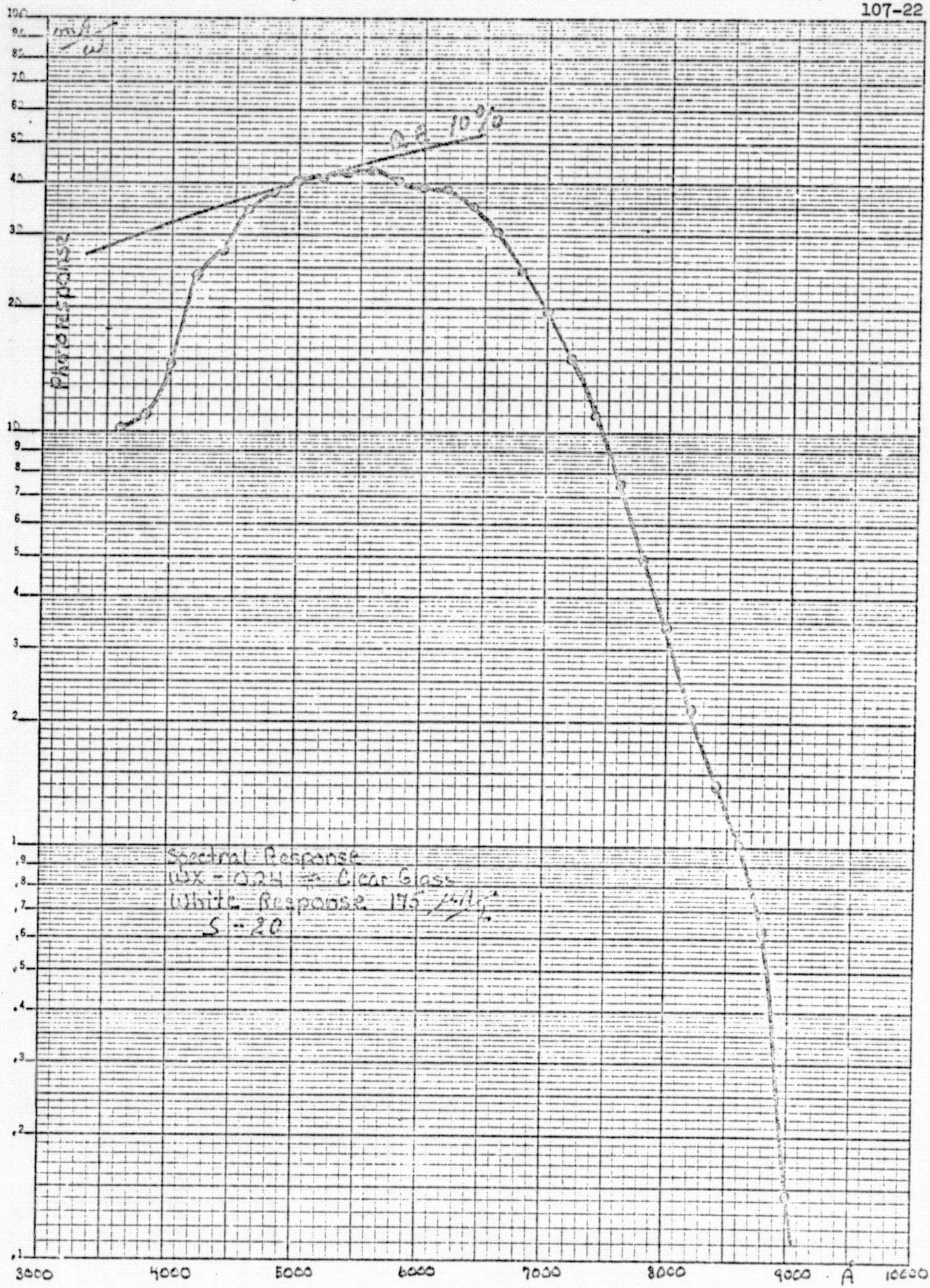

KEUFFEL & ESSER CO. MADE IN U.S.A.

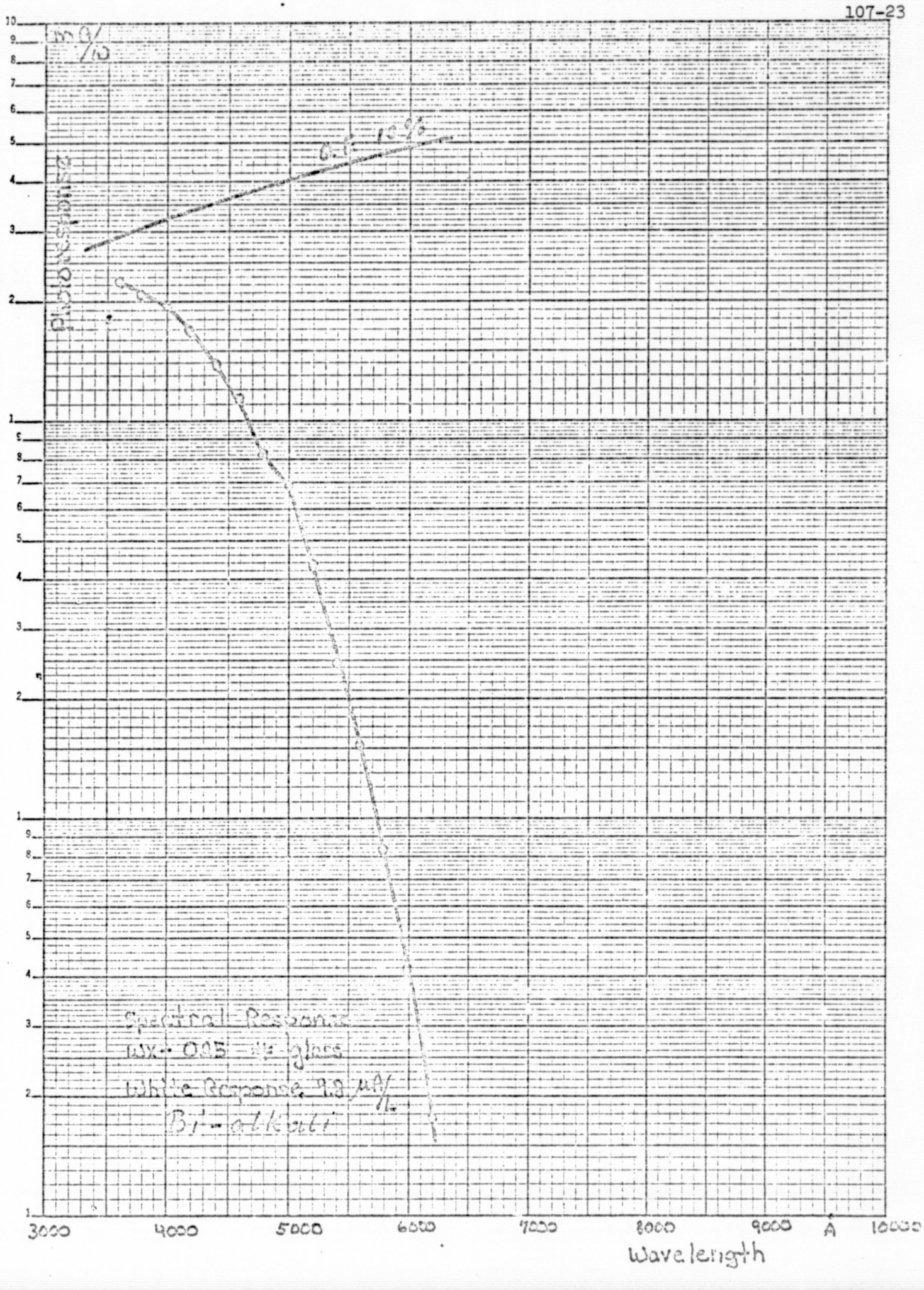

SEMI-LOG 3 CYCLES X 70 DIVISIONS
KEUFFEL & ESSER CO.
MADE IN U.S.A.

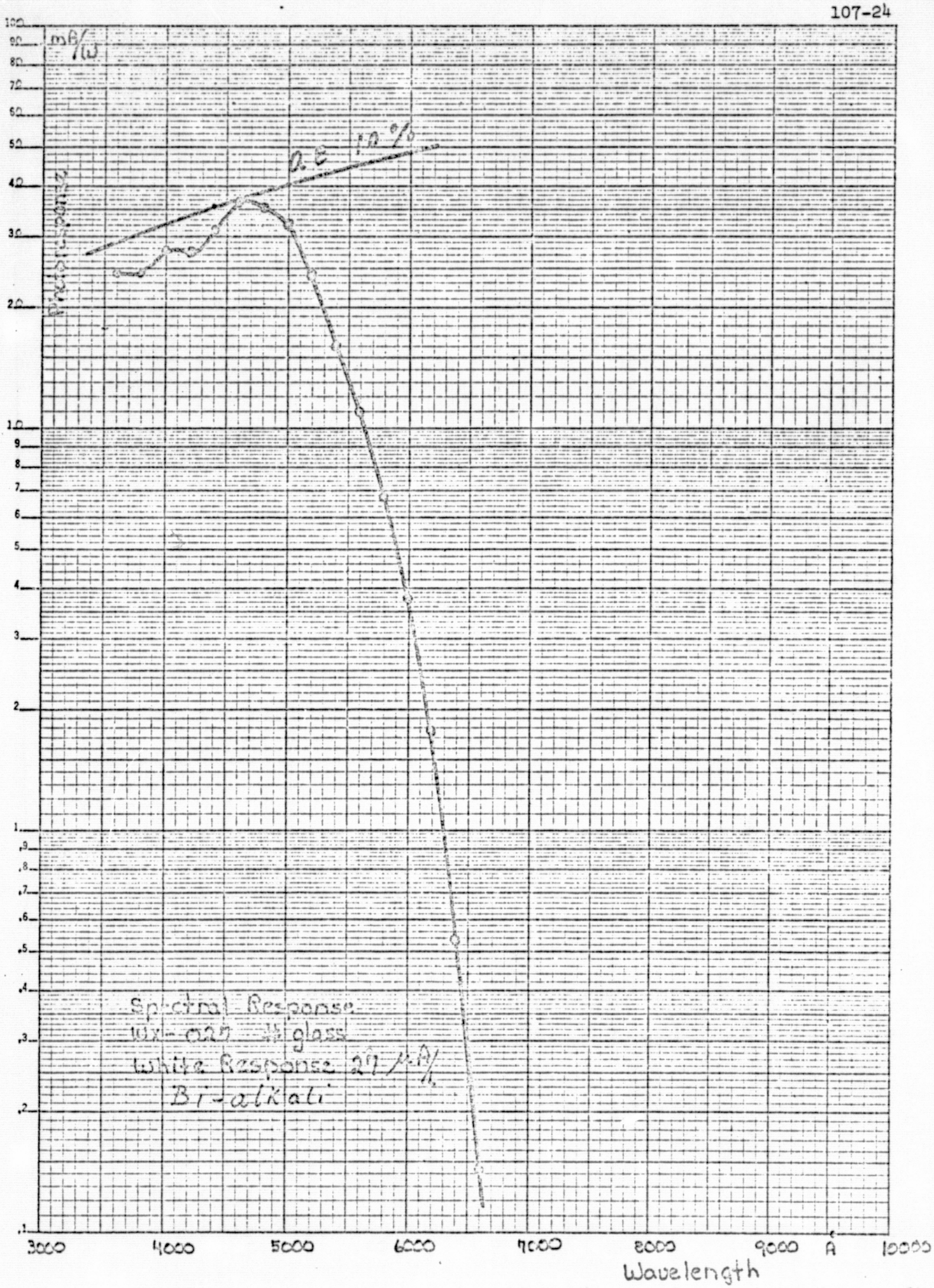

Spectral Response
WX-0227 ½ glass
White Response 27 μA/lm
Bi-alkali

KEUFFEL & ESSER CO. MADE IN U.S.A.

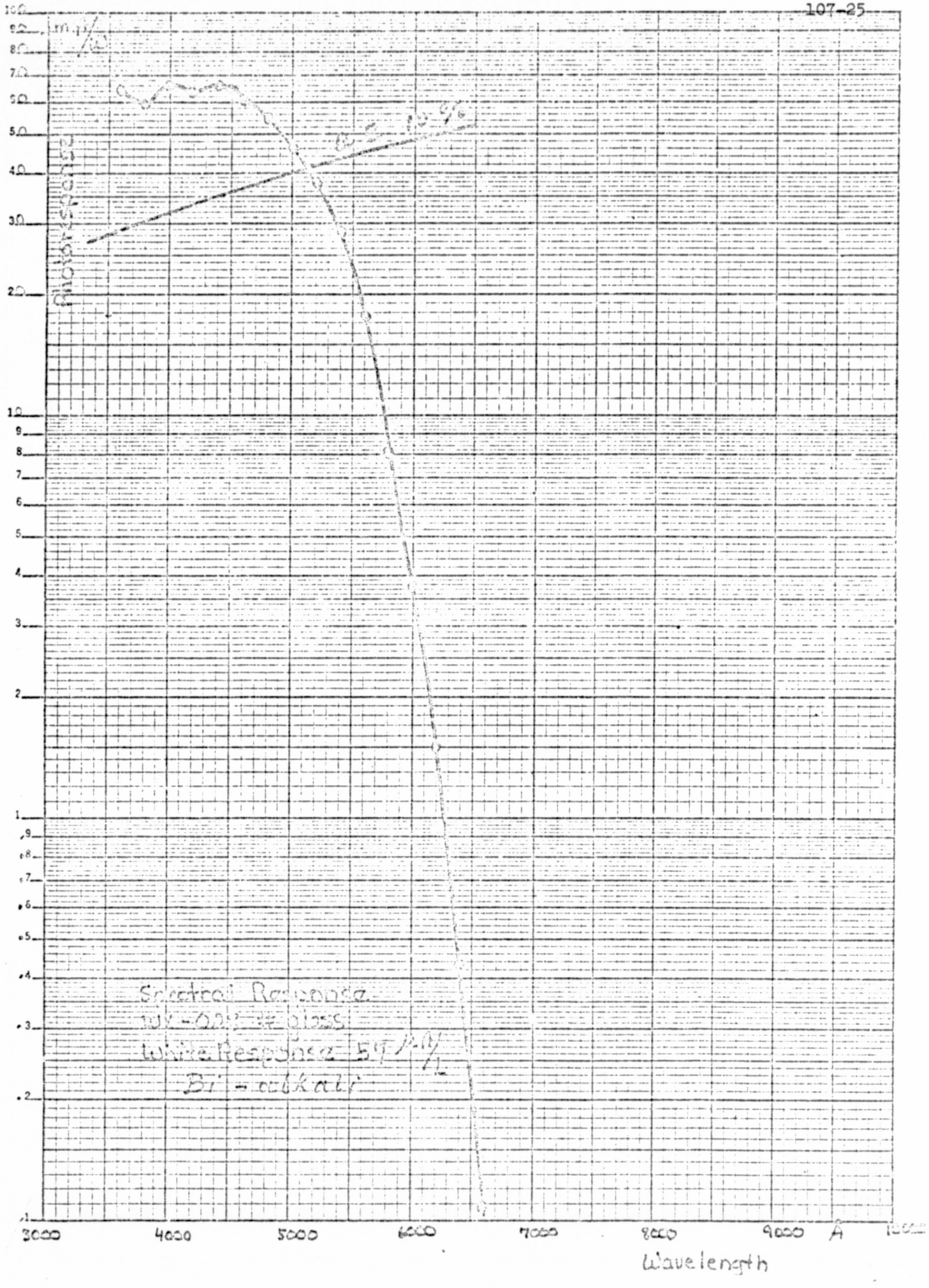
100
90
80
70
60
50
40
30
20
10
9
8
7
6
5
4
3
2
1
.9
.8
.7
.6
.5
.4
.3
.2
.1
3000
4000
5000
6000
7000
8000
9000
A
Wavelength
Spectral Response
Bi-alkali